UTSI REPORT 82/17
A FLIGHT TEST EVALUATION AND ANALYTICAL STUDY OF THE BALL-BARTOE JETWING PROPULSIVE LIFT CONCEPT WITHOUT EJECTOR

Completed For

NAVAL AIR SYSTEMS COMMAND
(AIR-03PA)

Under Contract
N00019-81-C-0506
30 September 81

by
Ralph D. Kimberlin
Uwe P. Solies
Atin K. Sinha

The University of Tennessee Space Institute

October 1, 1982

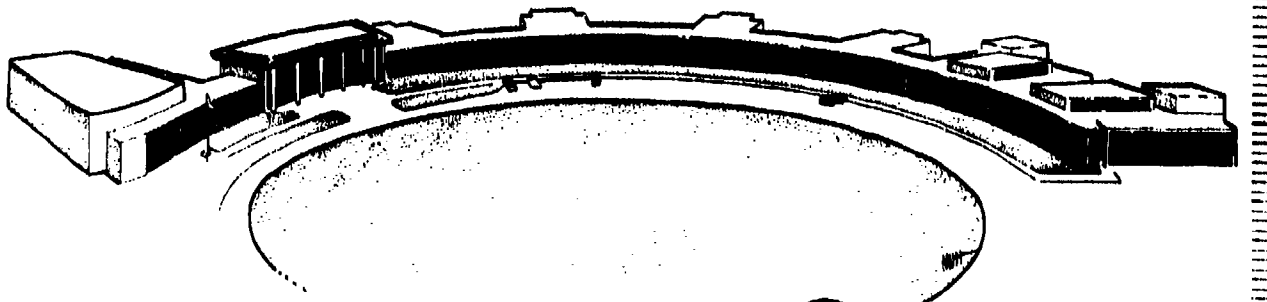

THE UNIVERSITY of TENNESSEE
SPACE INSTITUTE

Tullahoma, Tennessee

A FLIGHT TEST EVALUATION
AND
ANALYTICAL STUDY OF THE
BALL-BARTOE JETWING
PROPULSIVE LIFT CONCEPT
WITHOUT EJECTOR

BY

RALPH D. KIMBERLIN

UWE P. SOLIES

ATIN K. SINHA

THE UNIVERSITY OF TENNESSEE SPACE INSTITUTE

OCTOBER 1, 1982

FOREWORD

This program was performed by The University of Tennessee Space Institute for the Naval Air Systems Command Advanced Aircraft Development and Systems Objectives Office (AIR-03PA) under Naval Air Systems Command Contract N00019-81-C-0506, dated 30 September 1981. Active testing began on 30 October 1981 and was completed on 30 August 1982.

A total of 37.2 hours of flying time were flown in the performance of this task along with eleven months of analytical effort.

The following key personnel were primarily responsible for the conduct of this test, the analytical effort and/or the preparation of this report.

UTSI	
Principal Investigator and Project Test Pilot	Ralph D. Kimberlin, Associate Professor
Research Assistants	Uwe P. Solies Atin K. Sinha
Instrumentation Engineer	Robert Jones
Aircraft Maintenance	Donald Freeman
Support Groups	UTSI Aeroacoustics Division
NAVAL AIR SYSTEMS COMMAND	
Contract Monitor	Mr. W. T. Sparrow AIR-03PA3

TABLE OF CONTENTS

EXECUTIVE SUMMARY

The Ball-Bartoe "Jetwing" is a single engine upper surface blowing (USB) concept which achieves supercirculation lift, thrust, and a reduction in induced drag by ducting all engine air through the leading edge of the wing and ejecting it over the top surface through a slot nozzle. This nozzle is located at approximately 30 percent of the chord and extends along about 70 percent of the wing span. A Coanda flap of 55 degrees extension capability is mounted at the trailing edge of the blown portion of the wing. In addition to the main wing, a smaller wing panel is mounted above the slot nozzle. The air passage between the main wing and the smaller upper wing acts as an ejector to increase exhaust mass flow. The concept may be used with or without the upper wing. A thrust reversing method is also incorporated into the concept. The thrust is reversed by rotating the top of the slot nozzle so as to close the nozzle and open a reverse flow path.

The "Jetwing" concept has been incorporated into a research airplane. The Jetwing aircraft is a single seat, jet aircraft of conventional design powered by a Pratt and Whitney of Canada JT15D-1 turbofan engine of 2200 pounds static thrust. The aircraft has a wing span of 21.75 feet, a wing area of 105.6 square feet, and a maximum gross weight of 3750 pounds.

This report covers the results of a flight test program with the upper wing removed, a measurement of flyover noise with and without the upper wing, and the results of an analytical study into methods for predicting the Jetwing aerodynamic coefficients. A comprehensive flight test program with the upper wing installed was previously conducted under a separate effort. Both programs were conducted for Naval Air Systems Command by the University of Tennessee Space Institute. The purpose of these efforts was to validate the NASA Ames Research Center full scale wind tunnel data on the aircraft by flight test, develop methods for predicting aerodynamic coefficients for such a concept, and to obtain performance, stability, control, and noise data sufficient to evaluate the Jetwing concept for future application to other flight vehicles.

Test results show an excellent agreement between the flight test and wind tunnel in all items except lift coefficient versus angle of attack. The disagreement between wind tunnel and flight test on this item was most likely due to measurement inaccuracies in the flight test, and the round about data reduction method required to extract flight test data for comparison.

The test results also show significant differences between the performance and handling qualities of the aircraft with and without the upper wing. The configuration without the upper wing is superior from both the performance and handling qualities standpoint. The reason for these differences is not fully understood, but it is felt to be a function of both the zero lift drag increase and the increase in thickness of the USB jet with the upper wing installed. The question concerning USB jet thickness also has implications for USB configurations other than the Jetwing.

The flyover noise levels of the Jetwing airplane are very low with the aircraft noise disappearing into the background noise in a light wind. Aircraft configuration did not appear to have significant effect upon these levels. Such low noise levels has important significance for military airplanes, particularly those involved in ground attack.

Results of the analytical study showed that lift and excess thrust (or drag) coefficients could be predicted with reasonable accuracies using relatively simple methods. Pitching moment coefficient was more difficult to predict using simple methods, and will probably require use of the more complex, panel or vortex lattice, methods.

LIST OF FIGURES

LIST OF TABLES

LIST OF SYMBOLS AND ABBREVIATIONS

SYMBOL OR ABBREVIATION	DEFINITION
A	Aspect ratio
AGL	Above ground level
a_o	Lift curve slope of airfoil section
a_w	Lift curve slope of the wing
b	Wing span
B_o	Fourier coefficient for α dependent supercirculation lift term
c	Airfoil chord length
c'	Total equivalent airfoil chord length
c_f	Mechanical flap chord length projected on the airfoil chord
c'_f	Total equivalent flap chord length projected on the airfoil chord
c_{fj}	Equivalent jet flap length projected on the airfoil chord
c_t	Wing tip chord
c_r	Wing root chord
^oC	Degrees centigrade
C_D	Coefficient of drag
C_{Do}	Zero lift coefficient of drag
C_{Fex}	Coefficient of excess thrust
C_j	Jet blowing coefficient based on actual airfoil chord
C'_j	Jet blowing coefficient based on equivalent airfoil chord
C_J	Three-dimensional jet blowing coefficient

SYMBOL OR ABBREVIATION	DEFINITION
$\bar{c}$	Mean aerodynamic chord
C_ℓ	Two-dimensional lift coefficient
C_L	Three-dimensional lift coefficient
$C_{\ell a}$	Two-dimensional lift coefficient due to basic aerodynamic pressure lift
C_{LA}	Three-dimensional lift coefficient due to basic aerodynamic pressure lift
$C_{\ell j}$	Two-dimensional lift coefficient due to jet induced effects (supercirculation + jet momentum)
$C_{\ell\Gamma}$	Two-dimensional lift coefficient due to supercirculation
$C_{L\Gamma}$	Three-dimensional lift coefficient due to supercirculation
$C_{\ell\alpha}$	Derivative of two-dimensional lift coefficient with respect to α
$C_{\ell\delta}$	Derivative of two-dimensional lift coefficient with respect to δ_F
$C_{LA\alpha}$	Derivative of three-dimensional aerodynamic pressure lift coefficient with respect to α
$C_{LA\delta}$	Derivative of three-dimensional aerodynamic pressure lift coefficient with respect to δ_F
$C_{L\Gamma\alpha}$	Derivative of three-dimensional supercirculation lift coefficient with respect to α
$C_{L\Gamma\delta}$	Derivative of three-dimensional supercirculation lift coefficient with respect to δ_J
C_m	Pitching moment coefficient based on actual airfoil chord
C'_m	Pitching moment coefficient based on equivalent airfoil chord
C_M	Pitching moment coefficient

SYMBOL OR ABBREVIATION	DEFINITION
C_T	Thrust coefficient
c.g.	Aircraft center of gravity
CTOL	Conventional Takeoff and Landing
D_o	Fourier coefficient for δ dependent supercirculation lift term
dB	Decibel, unit for sound pressure level
$F(A, \eta C_j)$	Function for 3-D correction of 2-D formulae (Spence)
F_G	Gross thrust
F_{GS}	Standardized or weight corrected gross thrust
G	Subfunction of $F(A, \eta C_j)$
g	Acceleration due to gravity
$G(A, C_j)$	Function for 3-D correction of 2-D formulae (Williams)
H_P	Pressure altitude
H_z	Herz, cycles per second
ITT	Interstage turbine temperature of the turbofan engine
j	Jet momentum per unit span ($\dot{M}_j V_j$)
JT15D-1	The Pratt and Whitney of Canada designation for the turbofan engine installed in the JETWING aircraft
k	Factor to adjust nonideal induced drag term
KIAS	Knots indicated airspeed
KCAS	Knots calibrated airspeed
KTAS	Knots true airspeed
L_{fi}	Lift generated by two-dimensional jet flap alone

SYMBOL OR ABBREVIATION	DEFINITION
M	Pitching moment of an airfoil section
M_{FU}	Pitching moment of fuselage
$\dot{M}_j$	Rate of mass flow for the jet blowing on airfoil
M.A.C.	Mean aerodynamic chord
M S L	Mean sea level
N_1	Main rotor speed of the turbofan engine
N_2	Gas generator rotor speed of the turbofan engine
NASA	National Aeronautics and Space Administration
NBS	National Bureau of Standards
$O.A.T._i$	Indicated ambient air temperature
p	Ratio of z to c'
P_a	Ambient static pressure
P_{t8}	Total pressure at the engine exhaust nozzle
Δp	Differential pressure
q	Dynamic pressure
QSRA	NASA Quiet Shorthaul Research Aircraft
r	Factor to account for nonideal jet blowing
RD	Relative distance
S	Wing reference area
S'	Portion of wing reference area with blowing
SPL	Sound pressure level

SYMBOL OR ABBREVIATION	DEFINITION
STOL	Short Take-Off and Landing
t	Time
T_a	Observed ambient air temperature
T_s	The standard temperature at the test pressure altitude
t/c	Thickness to chord ratio of airfoil section
USB	Upper Surface Blowing
UTSI	The University of Tennessee Space Institute
V	Airspeed
V_c	Calibrated airspeed, or the indicated airspeed corrected for instrument and position error
V_E	Equivalent airspeed - the calibrated airspeed corrected for compressibility
V_{EW}	The equivalent airspeed corrected for nonstandard aircraft weight
V_i	Indicated airspeed
V_I	Indicated airspeed corrected for instrument error
V_j	Jet blowing velocity at any spanwise station
V_T	True airspeed - the equivalent airspeed corrected for air density
W	Aircraft weight
W_E	The aircraft empty weight
W_S	The aircraft standard weight - 3600 lbs. for the JETWING

SYMBOL OR ABBREVIATION	DEFINITION
W_T	The aircraft weight at the time of the test data point
x	Distance from the leading edge along airfoil chord
y	$\cos \psi_1$
YC-14	Boeing prototype Advanced Medium Shorthaul Transport aircraft
z	Distance of the leading edge of airfoil section from the datum line about which pitching moment is desired
α	Geometric angle of attack (includes zero lift angle of attack in Prediction Methods 1 and 3)
α_e	Effective angle of attack of airfoil section
α_i	Induced angle of attack for airfoil section
γ	Flight path angle, or angle of climb or descent (Also, circulation on chordwise elements of airfoil section in Prediction Method 3)
γ_s	Flight path angle corrected to sea level conditions and standard weight
δ	Flap (and/or jet) deflection angle with respect to airfoil chord line
δ_a	The aileron deflection angle
δ_e	Elevator deflection angle
δ_F	Flap deflection angle with respect to airfoil chord line
δ_J	Jet deflection angle with respect to airfoil chord line

SYMBOL OR ABBREVIATION	DEFINITION
δ_j	Jet deflection angle with respect to flap chord line
δ_n	Leading edge flap deflection angle with respect to airfoil chord line
δ_r	Rudder deflection angle
δ_{rev}	Position of thrust reverser
δ_s	The horizontal stabilizer deflection angle
ΔC_{DP}	Drag increment due to non-elliptic spanwise lift distribution
θ	Aircraft pitch angle: angle between longitudinal reference axis and the horizon
ψ	Angular coordinate for elements of airfoil including mechanical and jet flap
ψ_1	Trailing edge coordinate of trailing edge mechanical flap
ψ_0	Hinge line coordinate of trailing edge mechanical flap
ψ_n	Hinge line coordinate of leading edge flap
κ	Factor for adjustment of induced drag difference
λ	Factor for adjustment of partial span blowing for δ dependent terms
ν	Factor for adjustment of partial span blowing for α dependent terms
π	Quadrature constant (3.1415927)
σ	Subfunction of $G(A, C_j)$ (Williams) or $F(A, \eta C_j)$ (Wertz)

SYMBOL OR ABBREVIATION	DEFINITION
η	Turning efficiency factor
ς	Subfunction of σ
χ	Function of flap to wing chord ratio

INTRODUCTION

This report covers the results of a two part research effort on the Ball-Bartoe "Jetwing" propulsive lift concept. This effort was conducted by the University of Tennessee Space Institute, Tullahoma, Tennessee for the Advanced Aircraft Development and Systems Objectives Office (AIR-03PA) of Naval Air Systems Command under Contract Number N00019-81-C-0506.

The first part of the effort, which is covered in Part I of this report, was a follow on to a previous effort conducted under Naval Air Systems Command Contract Number N00019-80-C-0126 and reported in UTSI Report 81-1 [1]. The effort reported herein consisted of a performance flight test with the upper wing (ejector wing) removed, and flyover noise measurements with and without the upper wing. Performance, Stability and Control flight test with the upper wing installed were a part of the previous effort.

The second part of the effort consisted of an analytical study to develop a method, or methods, to predict the aerodynamic coefficients of a "Jetwing" configured aircraft. These coefficients would be of sufficient accuracy for use in preliminary design studies. The results of this analytical effort are reported in Part II of this report.

Results of both the flight test and analytical effort are compared to full scale test results of the research aircraft in the NASA Ames Research Center 40' x 80' wind tunnel with the aim of evaluating the Jetwing concept for applications to future flight vehicles.

PART I

FLIGHT TEST REPORT

SECTION I

INTRODUCTION

This section of the report covers the flight testing of the Ball-Bartoe "Jetwing" Research Aircraft with the upper wing removed. The purpose of these tests was to evaluate the Jetwing powered lift concept for future application to other flight vehicles by:

1. Obtaining performance and C_L vs. α data with the upper wing removed sufficient to validate the NASA Ames Research Center 40′ x 80′ wind tunnel data for this configuration.

2. Obtaining flyover noise data in several configurations of gear, flaps and power setting with and without the upper wing installed.

Flight tests were started on October 30, 1981 and completed on August 30, 1982. A total of 52 flights were flown for 37.2 flying hours to accomplish the test objectives. All test objectives were met and the results are given in Section V of this part of the report.

Flight testing of the aircraft with the upper wing installed was conducted under Naval Air Systems Command Contract N00019-80-C-0126 and reported in [1].

SECTION II

DESCRIPTION OF THE TEST ARTICLE

DESCRIPTION

The Jetwing STOL research aircraft is a single engine, single seat, upper surface blowing (USB) powered lift, jet aircraft with conventional landing gear (Figures 1 and 2). Figure 3 is a three view drawing of the aircraft showing its general arrangement. Table [1] lists other pertinent design features and dimensions.

The powered lift concept used on the Jetwing aircraft allows upper surface blowing (USB) from a single jet engine. Upper surface blowing has previously been limited to multi-engine configurations such as Boeing YC-14 and NASA Quiet Shorthaul Research Aircraft (QSRA). In the "Jetwing" concept USB is achieved from a single engine by ducting all engine air (both from by-pass and core exhaust) to a slot nozzle on the upper surface of the wing. The nozzle is located at approximately 30-40 percent of the wing chord and extends along approximately 70 percent of the wing span. The fan by-pass air is ducted to the outboard portion of the wing while the core exhaust is ducted to the inboard portion of the wing as is shown in Figure 4. Located above the nozzle is a separate, and much smaller wing surface. The purpose of this surface is to act as an ejector or thrust augumentor. A Coanda type, single element flap is located at the trailing edge of the wing along the portion of the wing span covered by the nozzle. A two-dimensional sketch of the arrangement is shown in Figure 5.

The concept may be used with, or without, the smaller upper wing surface which wind tunnel tests have shown to have negligible effect on powered lift capabilities (See Figures 6 and 7). All testing reported herein was conducted with the upper wing removed as shown in Figure 1.

Incorporated into the fan by-pass air nozzle is a thrust reverser which is operated as is shown in Figure 8.

Since the USB covers such a large portion of the wing span, a separate bleed air system for the ailerons is not required.

FIGURE 1

SIDE VIEW JETWING RESEARCH AIRCRAFT
(WITH UPPER WING REMOVED)

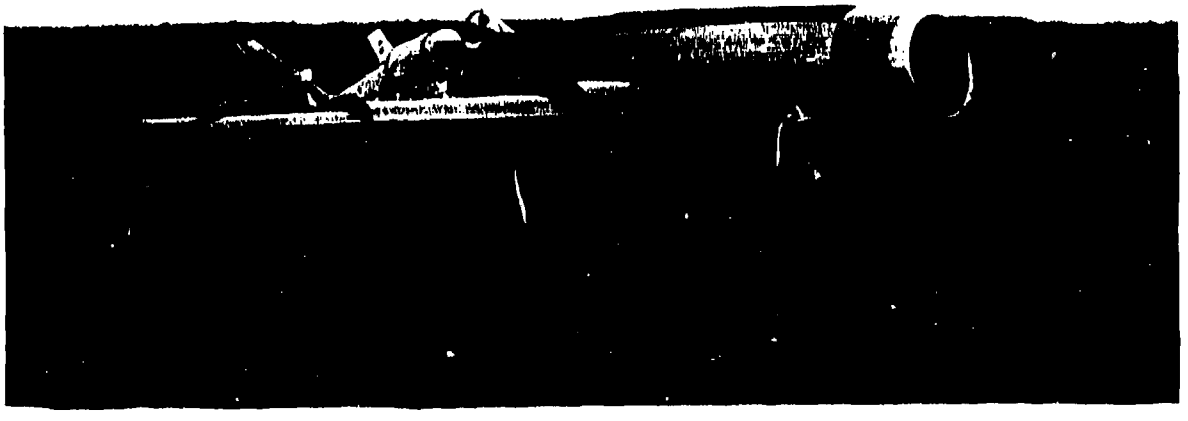

FIGURE 2

THREE QUARTER FRONT VIEW JETWING RESEARCH AIRCRAFT
(WITH UPPER WING REMOVED)

TABLE I

JETWING PHYSICAL DESCRIPTION

Powerplant	Pratt & Whitney JT15D-1 Turbofan
Rated Takeoff Thrust	2200 LB. Static Thrust @ Sea Level Standard Conditions (Uninstalled)
Rated Maximum Continuous Thrust	2050 LB. Static Thrust @ Sea Level Standard Conditions (Uninstalled)
Maximum Continuous Thrust as Installed in Jetwing Aircraft	1750 LB. Static Thrust @ Sea Level Standard Conditions
Fuel Capacity	106 Gal.
Maximum Takeoff Gross Weight	3750 LB.
Empty Weight	2330 LB. Without Ballast
Ballast	412 LB.
Center of Gravity Location with Ballast, Pilot and Full Fuel	35.5% M.A.C.
Wing Airfoil Section	NACA 23020 Modified at Root NACA 23015 at Tip
Wing Span	21.75 FT
Wing Area	105.6 FT^2
Aspect Ratio	4.48
Mean Aerodynamic Chord	5.08 FT
Taper Ratio	0.46
Wing Incidence	0° Root 0° Tip

Upper Wing Airfoil Section	Clark Y-12% Thickness
Upper Wing Span	15.1 FT
Upper Wing Area	23.16 FT^2
*Upper Wing Vertical Position Relative to Main Wing Measured at Trailing Edge of Upper Wing at the Inboard Support Fairing	
**Position #1	5.437 IN
Position #2	7.625 IN
Position #3	6.531 IN
Incidence Angle With Lower Wing Chord	Approximately 5^o
Aileron Type	Setback Hinge
Aileron Span	35.75 IN Each
Aileron Area	3.44 FT^2 Each
Aileron Deflection	$\pm$ 25^o
Flap Type	Coanda Single Element
Flap Span	69 IN Each
Flap Area	10.6 FT^2 Each
Flap Deflection	0^o to 55^o
Horizontal Tail Airfoil Section	8% Thick Symmetrical
Horizontal Tail Span	9.33 FT

*See Reference [1] for Internal Dimension of Ejector and Area Ratios

**Position Used for the Flight Tests Reported in Reference [1]

Horizontal Tail Area	27.5 FT^2
Horizontal Tail Aspect Ratio	3.16
Horizontal Tail Volume ($\bar{V}_H$)	0.74
Elevator Area	13.25 FT^2
Elevator Deflection	$+29^\circ$ to -25°
Horizontal Stabilizer Trim Deflection	$+20^\circ$ to -2°
Vertical Tail Airfoil Section	8% Thick Symmetrical
Vertical Tail Span	5.67 FT
Vertical Tail Area	18.33 FT^2
Vertical Tail Aspect Ratio	1.75
Vertical Tail Volume ($\bar{V}_V$)	0.115
Rudder Area	8.06 FT^2
Rudder Deflection	$\pm 20^\circ$
Engine Exhaust Nozzle Area (at top surface of wing)	
Fan Duct Total	156.2 IN^2
Gas Generator Duct Total	96.3 IN^2
Aircraft Length	28.6 FT
Aircraft Height	6.1 FT
Construction	
Fuselage	Welded Steel Tube Truss Covered With Titanium and Aluminum
Wing	Built up Aluminum and Titanium
Tail	Built up Aluminum

Landing Gear	Conventional, Retractable
Egress System	None
Longitudinal Control System	Reversible With Pushrod Linkage to Elevator
Longitudinal Trim	Electrically Actuated Trimmable Stabilizer
Directional Control System	Reversible With Cable Linkage to Rudder
Lateral Control System	Reversible With Pushrod Linkage to Ailerons
Moments of Inertia and Component Weights	See Reference [1]

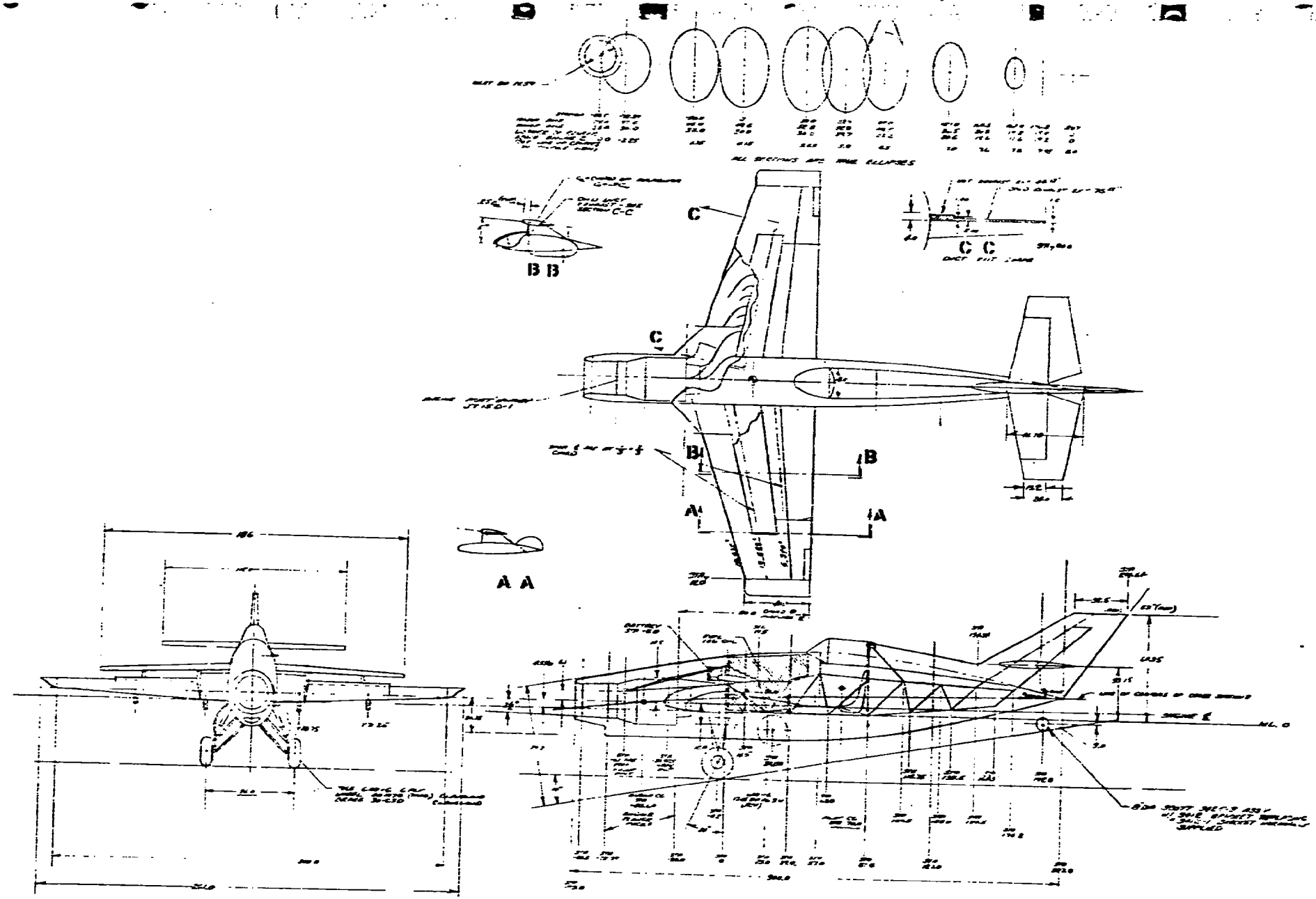

FIGURE 3
GENERAL ARRANGEMENT DRAWING OF JETWING RESEARCH AIRPLANE

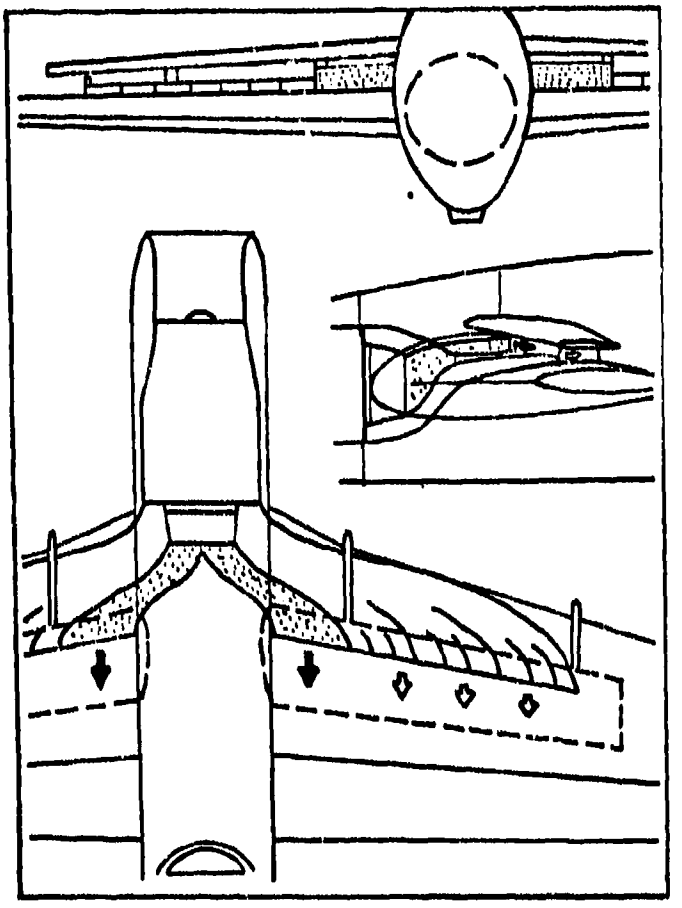

FIGURE 4 JETWING DUCTING ARRANGEMENT
(FROM REFERENCE 2)

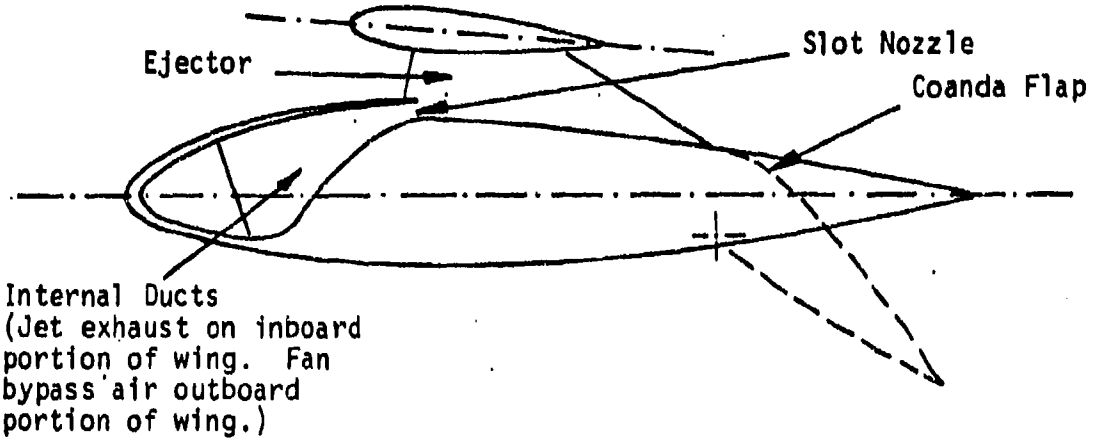

FIGURE 5 TWO-DIMENSIONAL VIEW OF JETWING CONCEPT

T-498
Gear Down, $\delta_F = 15$, $\delta_a = 0$, $\delta_e = 0$, $\delta_s = 0$
$\delta_r = 0$, Upper Wing @ #1, $\delta_{rev} = 0$, c.g. @ $.33\bar{c}$

Run	C_J	q
26 ▽	0	9.7
25 ⬡	.75	16.6
29 △	2.53	4.9

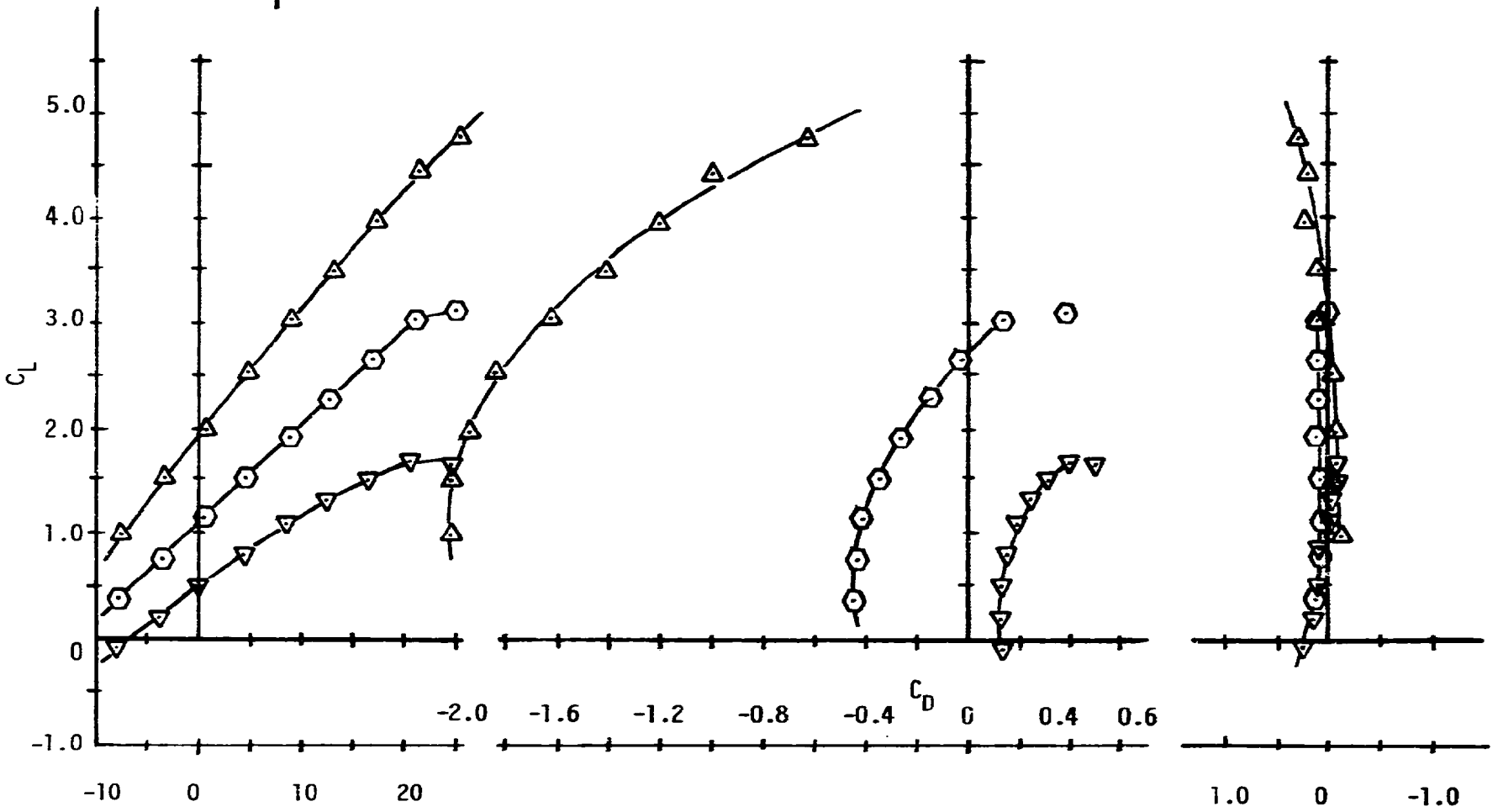

FIGURE 6
WIND TUNNEL DATA WITH UPPER WING INSTALLED

T-498

Gear Down, $\delta_F = 15$, $\delta_a = 0$, $\delta_e = 0$, $\delta_s = 0$

$\delta_r = 0$, Upper Wing Off, $\delta_{rev} = 0$, c.g. @ $33\bar{c}$

Run		C_J	q
9	▽	0	25.3
8	○	.49	25.2
7	⬡	.75	16.5
6	□	1.40	8.8
5	△	2.52	4.9

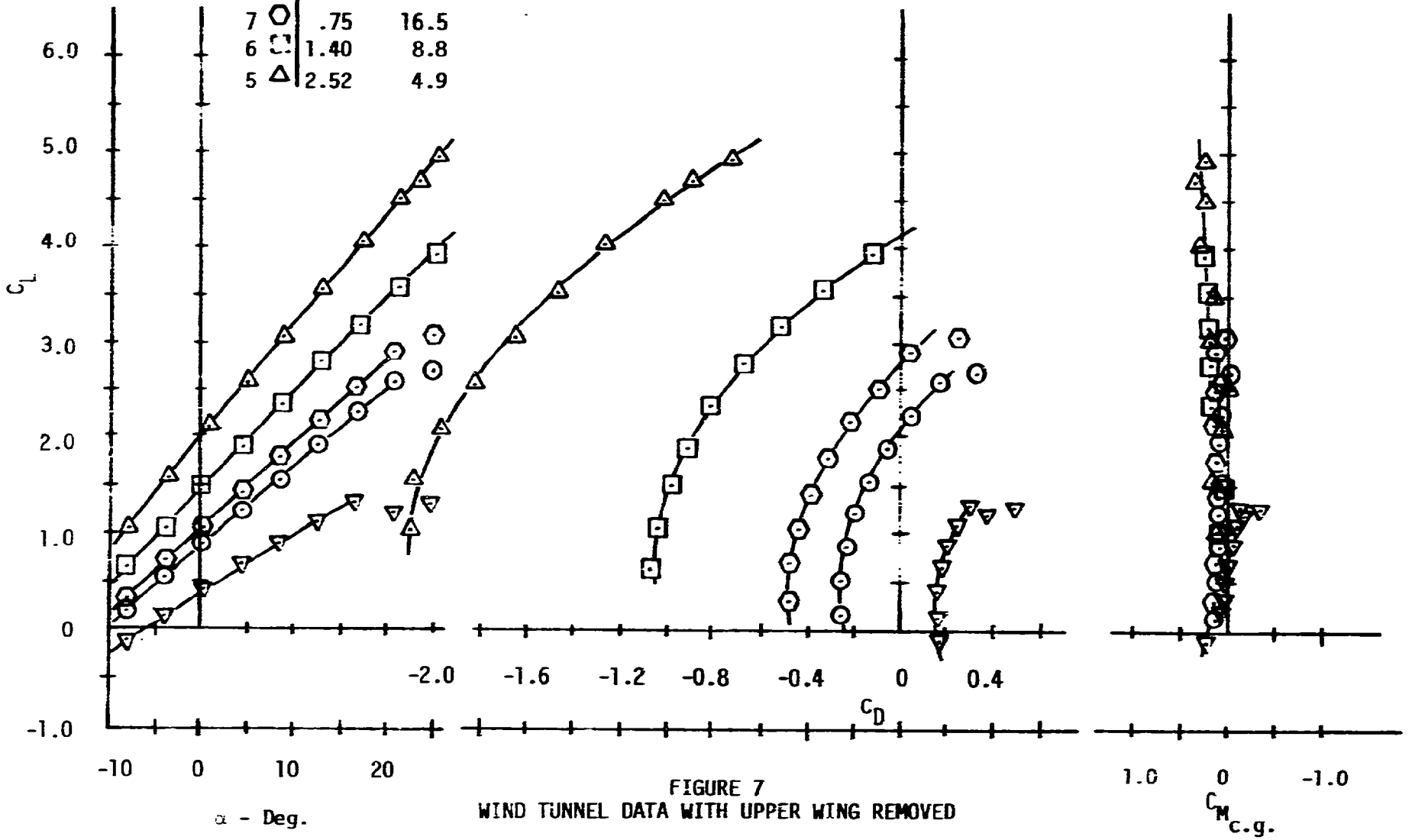

FIGURE 7
WIND TUNNEL DATA WITH UPPER WING REMOVED

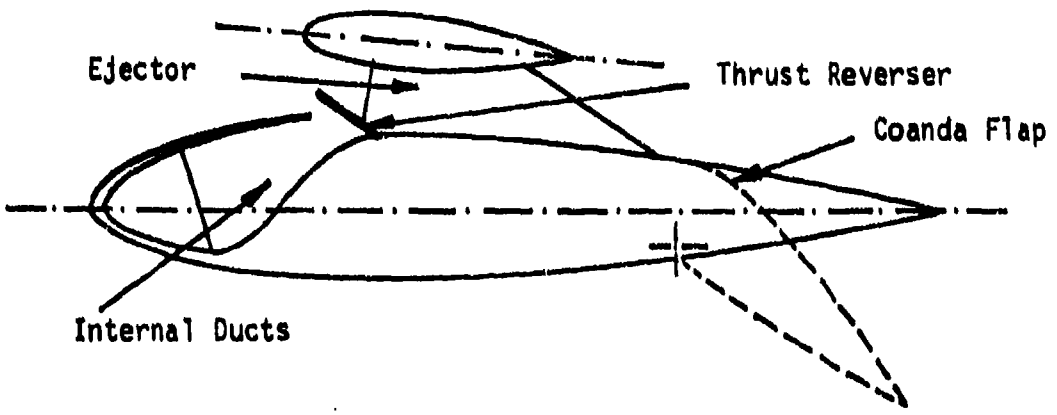

FIGURE 8 TWO-DIMENSIONAL VIEW OF JETWING CONCEPT WITH THRUST REVERSER DEPLOYED

SECTION III

TEST PROCEDURES

The test procedure used to accomplish this effort followed standard flight test practice except as required to account for flight safety and test vehicle limitation.

The aircraft's aerodynamic configuration during these tests was the same as that tested in the wind tunnel at Ames Research Center (upper wing removed) except for changes necessary to install flight test instrumentation.

Prior to collecting flight test data the aircraft configuration was defined in detail. During testing a configuration log was maintained which recorded all changes made to the aircraft configuration including instrumentation and flight trim adjustments. This log was cross-referenced with aircraft flight number so that it was possible to determine the exact configuration during any test flight.

For performance testing the aircraft loading was 3691 lbs. gross weight with the center of gravity at 35.17 percent M.A.C. This loading is equidistant between the two c.g.'s tested in the wind tunnel.

Prior to the start of testing the actual aircraft weight and c.g. was determined by weighing the aircraft with pilot, fuel load and ballast on board. This weight and c.g. was used as a basis for calculation of test weight and c.g. position for data reduction.

PERFORMANCE FLIGHT TESTS. The test procedures used for measuring the performance of the Jetwing with the upper wing removed were essentially the same as those used during testing under contract N00019-81-C-0126 and reported in [1]. This procedure was to perform sawtooth climbs, and descents, at various airspeeds and power settings in order to develop a map of flight path angle (γ) and equivalent airspeed (V_E) which defined the aircrafts performance envelope for a given configuration. Sawtooth climbs or descents were performed in 10 to 15 knots increments in the following speed range and configuration.

SPEED RANGE	CONFIGURATION
1. 80-170 knots	Gear and Flaps up
2. 70-120 knots	Gear down ,Flaps 15°
3. 50-120 knots	Gear down, Flaps 30°

Each speed range was repeated at four power settings, when practical, which approximated the following values of gross thrust:

1. Maximum Available thrust
2. 1000 lbs.
3. 500 lbs.
4. Idle Thrust

Test altitude was varied depending upon the thrust level required. Maximum available thrust testing began at approximately 2000 ft. pressure altitude. Since the data reduction method reduced all data to a sea level standard condition, test altitude was not critical except for obtaining maximum thrust.

Two climbs, or power idle descents, were done crosswind in opposite directions for each data point. An average of the two climbs was used in determining the data point to reduce wind created errors. During each climb the following data were recorded at 30 second intervals:

1. Fuel Remaining, for determination of test weight (W_T)
2. Indicated Airspeed (V_i)
3. Gross Thrust indication ($N_1, P_{t8}/P_a, N_2$, ITT).
4. Angle of attack (α)
5. Pitch angle (θ)
6. Pressure altitude (H_p)
7. Time (t)
8. Outside air temperature (T_a)
9. Aircraft configuration

These data were plotted and values of rate of climb or descent determined for use in determining flight path angle. These data were reduced to standard values of flight path angle (γ), equivalent airspeed (V_E), and gross thrust (F_{GS}), and plotted in the V - γ map as described in [1]. Further reduction to values of lift coefficient (C_L), and excess thrust coefficient ($C_{F_{ex}}$), or drag coefficient (C_D), was also performed as outlined in [1]. Geometric angle of attack was determined by recording the pitch angle at the same time that flight path angle data were being taken. Geometric angle of attack was then calculated by subtracting flight path angle from pitch angle.

FLYOVER NOISE TESTING. The flyover noise tests were conducted on the Tullahoma Municipal Airport in an area of flat terrain having no excessive sound absorption characteristics. The noise measuring microphone was located so that there were no obstructions, which might influence the sound field from the airplane, within a conical space above the microphones. This conical space was defined by an axis normal to the ground plane, and by a half angle 75 degrees from this axis.

The testing was carried out under the following conditions:

1. Clear Air

2. Relaltive Humidity between 90 and 30 percent.

3. Ambient temperature between 86 and 41° F at 33 feet above the ground.

4. Wind not in excess of 10 knots at 33 feet above the ground.

5. There were no temperature inversions or wind conditions which would significantly alter the noise level of the airplane when the noise level was recorded,.

The flyovers included at lenst six level flights over the measuring station for each configuration tested. These flyovers were t a height of 1000 feet ± 30 feet above the station, and were within ± 10 degrees of the zenith when passing overhead.

The configurations tested included:

	UPPER WING	FLAPS	GEAR	AIRSPEED	POWER
(1)	ON	UP	UP	165 KCAS	FOR LVL FLT
(2)	ON	15°	UP	110 KCAS	FOR LVL FLT
(3)	ON	30°	UP	75 KCAS	FOR LVL FLT
(4)	OFF	UP	UP	165 KCAS	FOR LVL FLT
(5)	OFF	15°	UP	110 KCAS	FOR LVL FLT
(6)	OFF	30°	UP	75 KCAS	FOR LVL FLT

The noise measuring microphone was mounted upon a tripod approximately four (4) feet above the ground so as to minimize interference with the sound being measured. The noise measured by that microphone was recorded on a strip recorder. This system for measuring and recording the sound complied with the recommended characteristics in International Electrotechnical Commission Publication No. 179, entitled "Precision Sound Level Meters" [3] and with Federal Air Regulation 36 Appendix A paragraph A36.2 [4]. These publications also cover the calibration of such equipment. Immediately prior to and after each test a recorded acoustic calibration of the system was made with an acoustic calibrator for the purposes of checking system sensitivity and providing an acoustic reference level for analysis of the sound level data. In addition, prior to each series of tests the ambient noise, including both acoustical background and electrical noise of the measurement systems, was recorded in the test area with the system gains set at levels used for aircraft noise measurements.

The following data were recorded for each test run:

1. Ambient air temperature and humidity at 33 feet above the surface.

2. Maximum, minimum, and average wind velocities at 33 feet above the surface.

3. Aircraft noise level.

4. Test aircraft airspeed in knots.

5. Test aircraft engine power setting.

6. Aircraft height in feet.

Flight data parameters were corrected to standard conditions. Noise data were not corrected if the ambient temperature was within a range of 68°F $\pm$ 9°F, and the relative humidity was above 40 percent but not exceeding 90 percent. When conditions did not fall within the specified range, the data were corrected to 77°F and 70 percent relative humidity using an approved method.

SECTION IV

INSTRUMENTATION

The on board instrumentation used in these tests was the same instrumentation as used on the previous test reported in [1]. It was functionally checked out and recalibrated prior to the start of testing.

The types of instrumentation required for this program may be placed in groups which relate to the type of data being collected. These groups of instrumentation are:

1. Air Data Instrumentation

2. Engine Thrust Instrumentation

3. Pitch and Angle of Attack Instrumentation

4. Noise Measurement Instrumentation

AIR DATA INSTRUMENTATION. The instrumentation installed on the test aircraft which collected air data included:

1. Sensitive Airspeed Indicator calibrated in knots.

2. Sensitive Altimeter calibrated in feet.

3. Ambient Air Temperature Gauge calibrated in degrees Centrigrade.

The airspeed indicator and altimeter were panel mounted as shown in Figure 9 and connected to a wingtip mounted, swivel pitot static boom shown in Figure 10. These instruments were calibrated through the airspeed and altitude ranges of interest using water and mercury manometers with traceability to the National Bureau of Standards (NBS).

The ambient air temperature gauge was calibrated from $0 - 40°C$ in a water bath using a laboratory thermometer which was also traceable to NBS.

Similar calibrated instrumentation was installed on the Cessna 310 and DHC-3 Otter which were used as pace aircraft during the Airspeed Calibration portion of the prior flight test program.

ENGINE THRUST INSTRUMENTATION. Instrumentation installed in the test aircraft which gave an indication of engine thrust included.

1. Main Rotor Speed Tachometer (N_1) calibrated in percent RPM.

2. Gas Generator Speed Tachometer (N_2) calibrated in percent RPM.

3. Interstage Turbine Temperature gauge (ITT) calibrated in °C.

4. Pressure Gauge calibrated in inches of water which mensured the differential pressure between the total pressure in the hot or cold duct and the outside ambient static pressure. This was a single gauge which operated through a pressure switch in order to read hot or cold duct differential pressure.

FIGURE 9

PICTURE OF PILOT'S INSTRUMENT PANEL SHOWING
AIR DATA AND ENGINE THRUST INSTRUMENTATION

FIGURE 10 FULL SWIVEL PITOT-STATIC BOOM MOUNTED
ON LEFT WINGTIP, 32 INCHES FORWARD OF WING LEADING EDGE

5. SDI Hoskins Fuel Flow and Fuel Quantity Instrumentation which consists of two panel mounted instruments which contain an integral computer. Fuel flow calibration is in either gallons or pounds per hour.

All of the engine instrumentation and air data instrumentation was panel mounted for visual readout by the pilot as is shown in Figure 9.

All of the engine instrumentation listed above except for the fuel flow instrumentation was calibrated using standards traceable to NBS. The fuel flow instrumentation was calibrated at the manufacturer and guaranteed to maintain two percent accuracy in normal use. Periodic spot checks during the test program confirmed this level of accuracy.

In addition to the engine related thrust instrumentation one other piece of instrumentation was required during the thrust calibration. This instrument, a Dillon Dynamometer is shown inFigure 11 as it was installed in the thrust measuring apparatus. This instrument was readout in pounds of force and had received a traceable calibration by its manufacturer.

PITCH AND ANGLE OF ATTACK. The instrumentation required to measure pitch and angle of attack consisted of:

1. Angle of Attack Sensors

2. Vertical Gyro for Pitch Angle

Angle of attack information was obtained from the sensors shown in Figure 12. The angle of attack vane drives a rotary potentiometer which is connected electrically through a 12 position rotary switch to the milliammeter of Figure 13. Calibration was accomplished by measuring vane deflection angles and obtaining corresponding milliammeter readings. Zero reference was the aircraft waterline.

A vertical gyro mounted near the center of gravity and above the exhaust ducting, as shown in Figure 14, was used to determine pitch angles. Prior to installation, this device was calibrated with the instrumentation package on a calibration bench. This device was also wired to provide a visual readout through the milliammeter.

All instrument readings which could be displayed on the milliammeter could also be recorded, three at a time versus a time basis, on a cassette magnetic tape recorder. These data could then be played back on an oscillograph or strip recorder after the flight. The cassette recorder was located just aft of the pilot's seat.

Before being displayed on the milliammeter or recorded on the cassette recorder all data signals were amplified and conditioned in an instrumentation amplifier and signal conditioner located near the vertical gyro as is shown in Figure 15. Power for the electrical instrumentation was connected through an instrumentation master switch located next to the rotary selector switch.

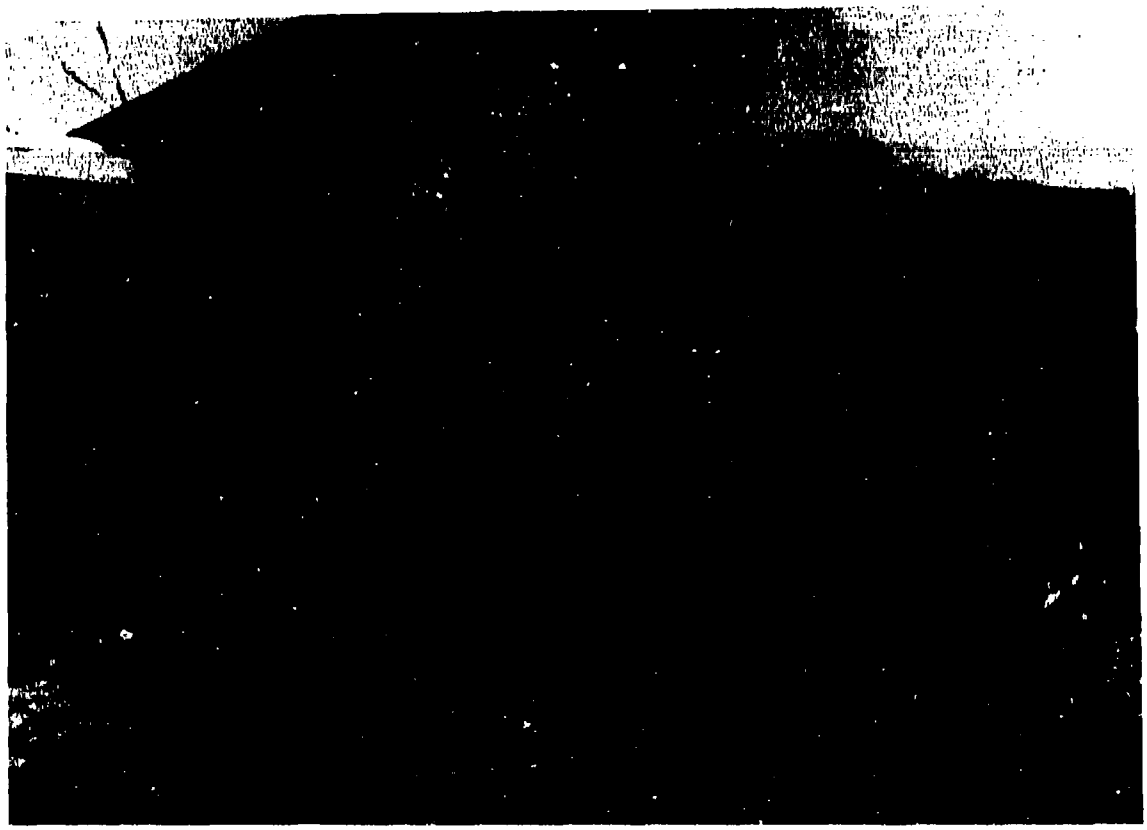

FIGURE 11

PICTURE OF DILLON DYNAMOMETER AS INSTALLED
IN THRUST MEASURING APPARATUS

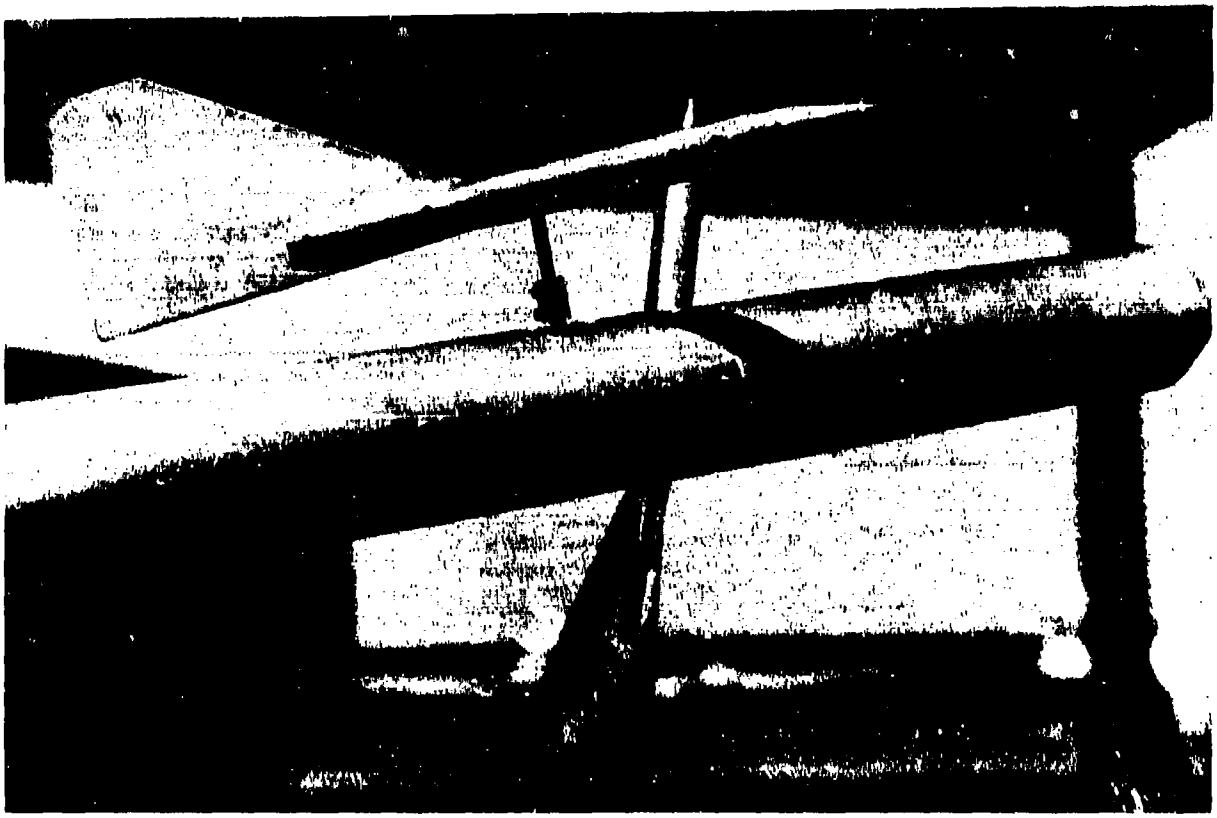

FIGURE 12

WINGTIP BOOM WITH ANGLE OF ATTACK AND SIDESLIP SENSORS MOUNTED ON RIGHT WING TIP, 52 INCHES FORWARD OF THE WING LEADING EDGE

FIGURE 13

MILLIAMMETER USED FOR READOUT OF STABILITY
AND CONTROL PARAMETERS (CENTER)

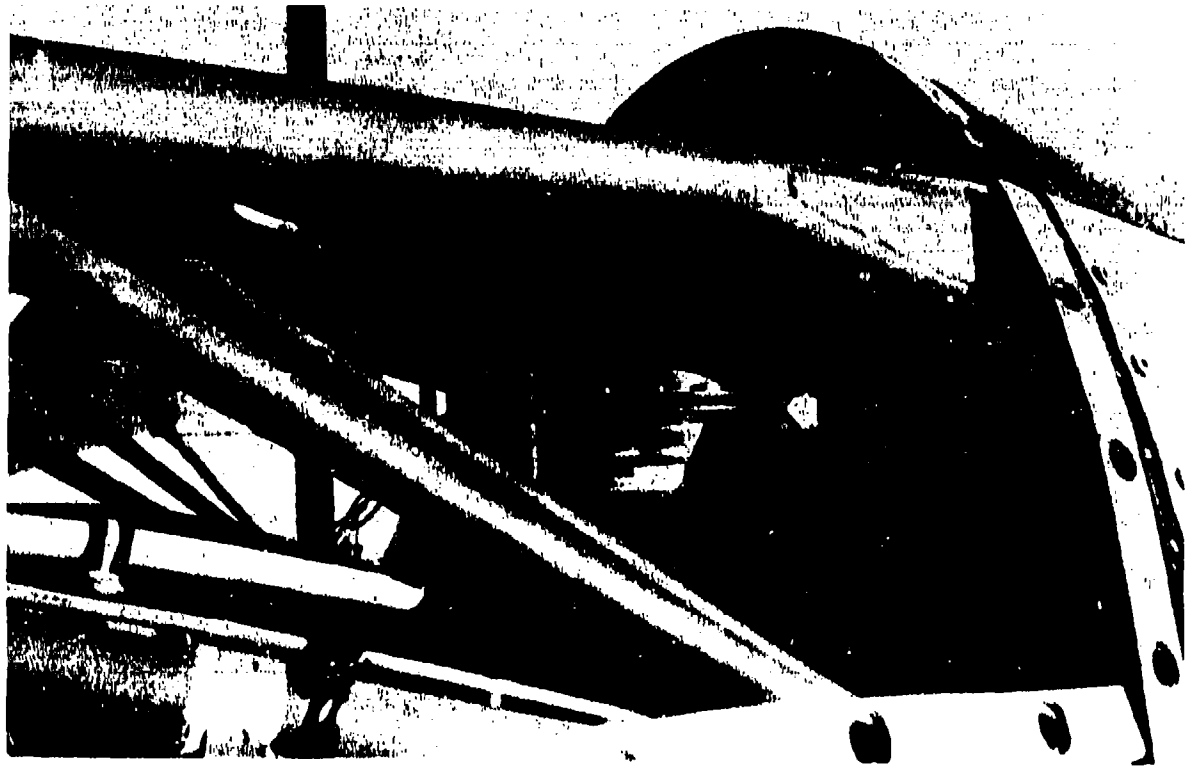

FIGURE 14

MOUNTING ARRANGEMENT OF VERTICAL GYRO

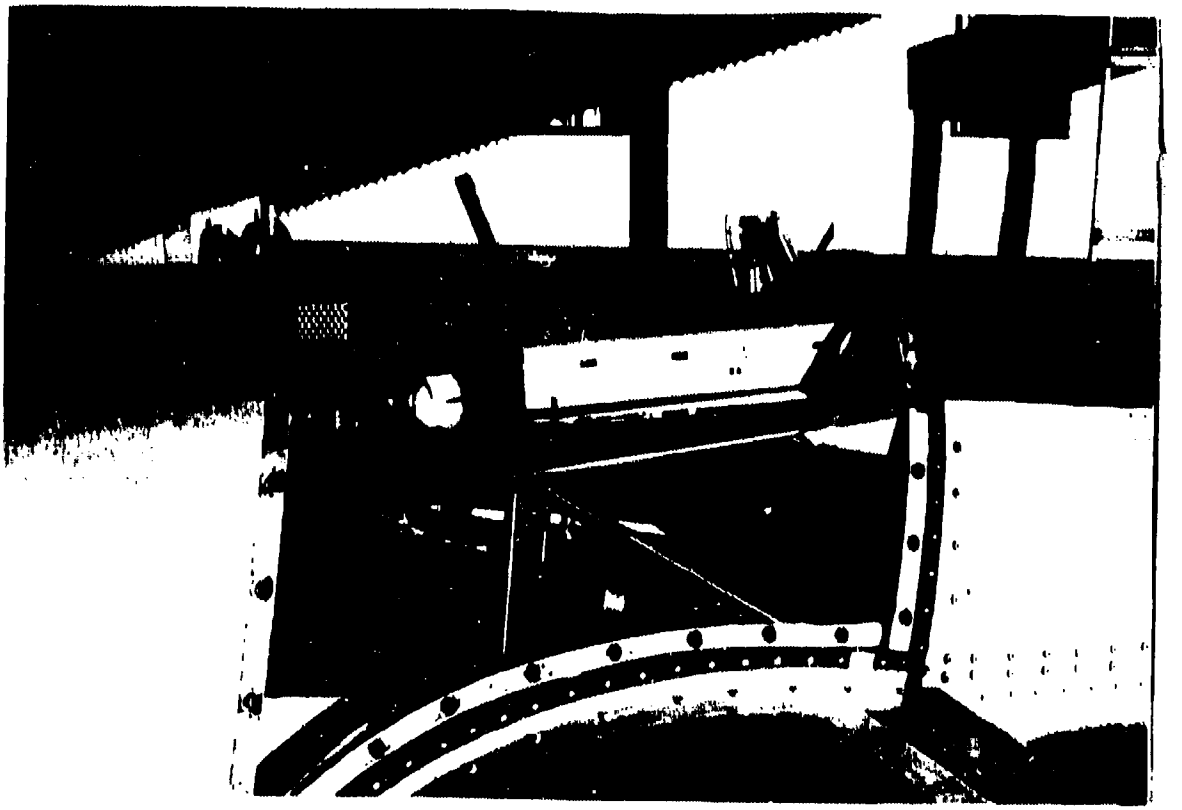

FIGURE 15

INSTRUMENTATION AMPLIFIER AND SIGNAL CONDITIONER (ARROW)

NOISE MEASUREMENT INSTRUMENTATION. For the measurement of the flyover noise level a Bruel & Kjaer type 4133 one half inch condenser microphone was used (Figure 16). This microphone was oriented at an angle of 90 degrees (grazing incidence) with respect to the aircraft flight path. This orientation corresponds to the optimum frequency response for this microphone.

The output from the microphone was input into a Bruel & Kjaer type 2112 Audio Frequency Spectrometer (Figure 17) which provided three recording modes - Octave, 1/3 Octave, and Linear. For these measurements the 1/3 Octave filters ranging from 25HZ to 40 KHZ were employed for the on-ground frequency distribution analysis of the aircraft while the Linear setting was used to record the instantaneous overall sound pressure level during the 1000 ft. flyover noise measurements.

The output of the Audio Frequency Spectrometer was fed into a Bruel & Kjaer type 2305 Graphic Level Recorder (Figure 17). This instrument supplied an amplitude (dB) versus frequency graph when utilizing the Audio Frequency Spectrometer as a 1/3 Octave analyzer, and an amplitude versus time plot when the Linear mode of the Audio Frequency Spectrometer was used.

Relative humidity during the tests was determined by use of a Sling Psychrometer and Psychrometric Charts, while wind direction and velocity were determined with the simple instruments shown in Figure 18.

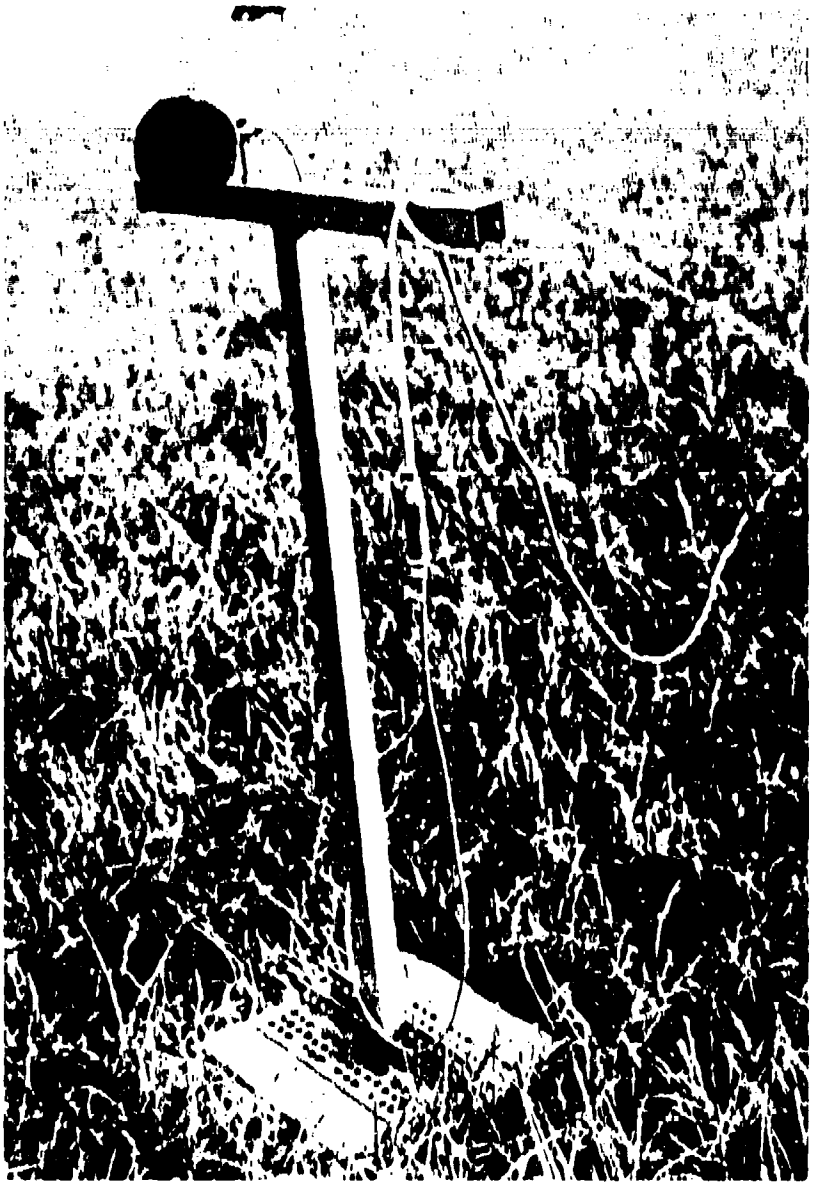

FIGURE 16

NOISE MEASUREMENT MICROPHONE

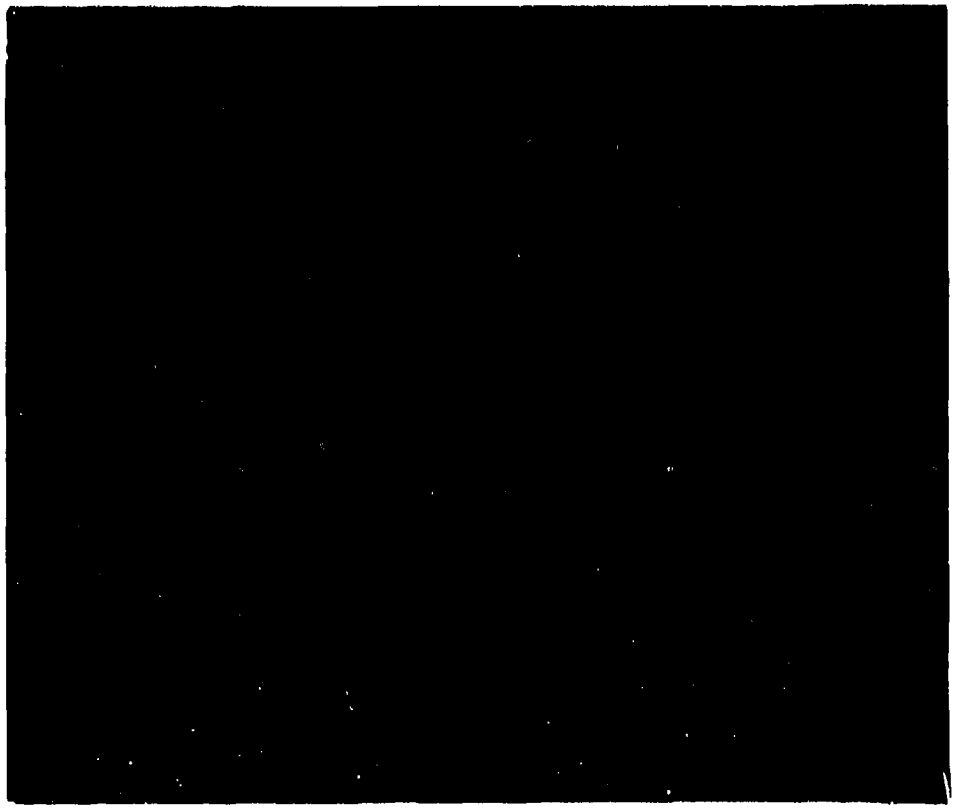

FIGURE 17

AUDIO FREQUENCY SPECTROMETER (LEFT)
AND GRAPHIC SOUND LEVEL RECORDER

FIGURE 18

WIND INSTRUMENTS

SECTION V

RESULTS AND DISCUSSION

INFLIGHT PERFORMANCE

As described in the test procedures, inflight performance was determined with the upper wing removed in three configurations of landing gear and flap setting:

1. Gear and Flaps Up

2. Gear Down and 15° Flap Deflection

3. Gear Down and 30° Flap Deflection

Results of performance tests in these configurations are shown in Figures 19, 20 and 21 as weight and air density corrected plots of flight path angle (γ_s) and equivalent airspeed (V_{EW}) for various thrust settings. As may be seen from these figures the extreme low speed end of the performance envelope was not investigated. The reason for not continuing the investigation into this region was the reduced longitudinal stability level and tail stall potential discussed in [1]. The aircraft was flown to speeds as low as 55 knots calibrated airspeed in level flight, or a slight climb, but performance data were not recorded.

Sufficient performance data were obtained to make comparisons with the NASA Ames Research Center 40' x 80' wind tunnel data at two separate values of blowing coefficient (C_J). These comparisons are shown in Figures 22 through 27 as plots of lift coefficient (C_L) versus excess thrust coefficient ($C_{F_{ex}}$). The agreement between the flight test and wind tunnel data for these configurations is excellent and exceeds the good agreement obtained for the same configurations with the upper wind installed as reported in [1]. This data agreement also speaks well for the simple and inexpensive flight test method used to obtain the flight test data.

LIFT COEFFICIENT VERSUS ANGLE OF ATTACK

At the same time that the flight path angle versus airspeed data of Figures 19 thru 21 was being obtained, the aircraft pitch angle was recorded. By subtracting the flight path angle (γ) from the pitch angle (θ) the geometric angle of attack (α) can be obtained. However, one problem arises when trying to compare these data with that obtained in a wind tunnel.

The problem is that for a powered lift airplane like the Jetwing the lift coefficient is a function of both angle of attack and blowing coefficient.

$$C_L = f(\alpha, C_J) \qquad (1-1)$$

In a wind tunnel the angle of attack and blowing coefficient can be varied independently. This is accomplished by holding tunnel airspeed and airplane gross thrust constant (C_J constant) while varying angle of attack.

In free flight, airspeed, gross thrust, blowing coefficient, and angle of attack are all interrelated, and can not be varied independently. As a result, the classic C_L versus α plots at a constant blowing

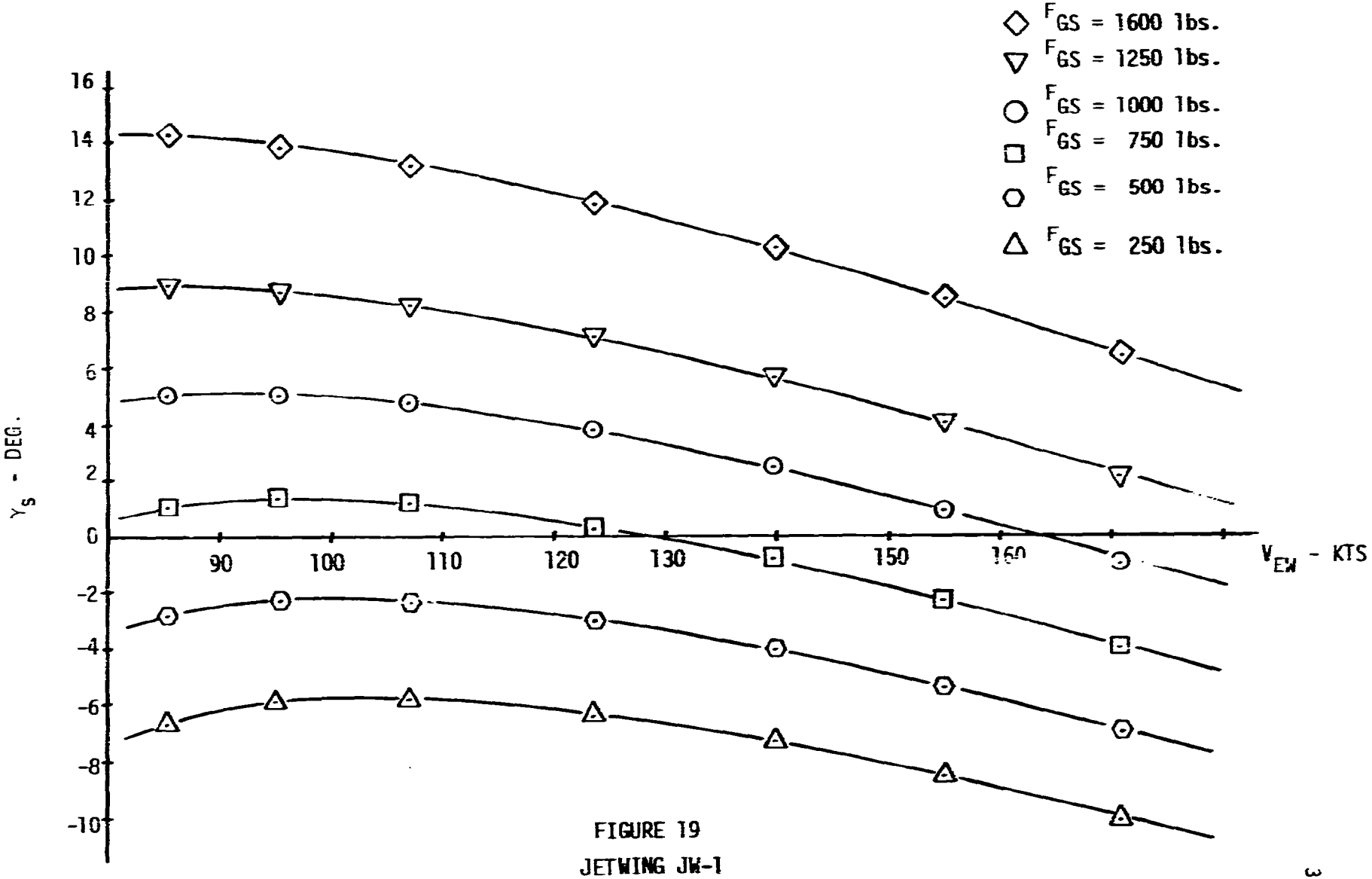

FIGURE 19

JETWING JW-1

γ_s VS. V_{EW}

UPPER WING REMOVED, GEAR AND FLAPS UP

W_S = 3600 lbs.

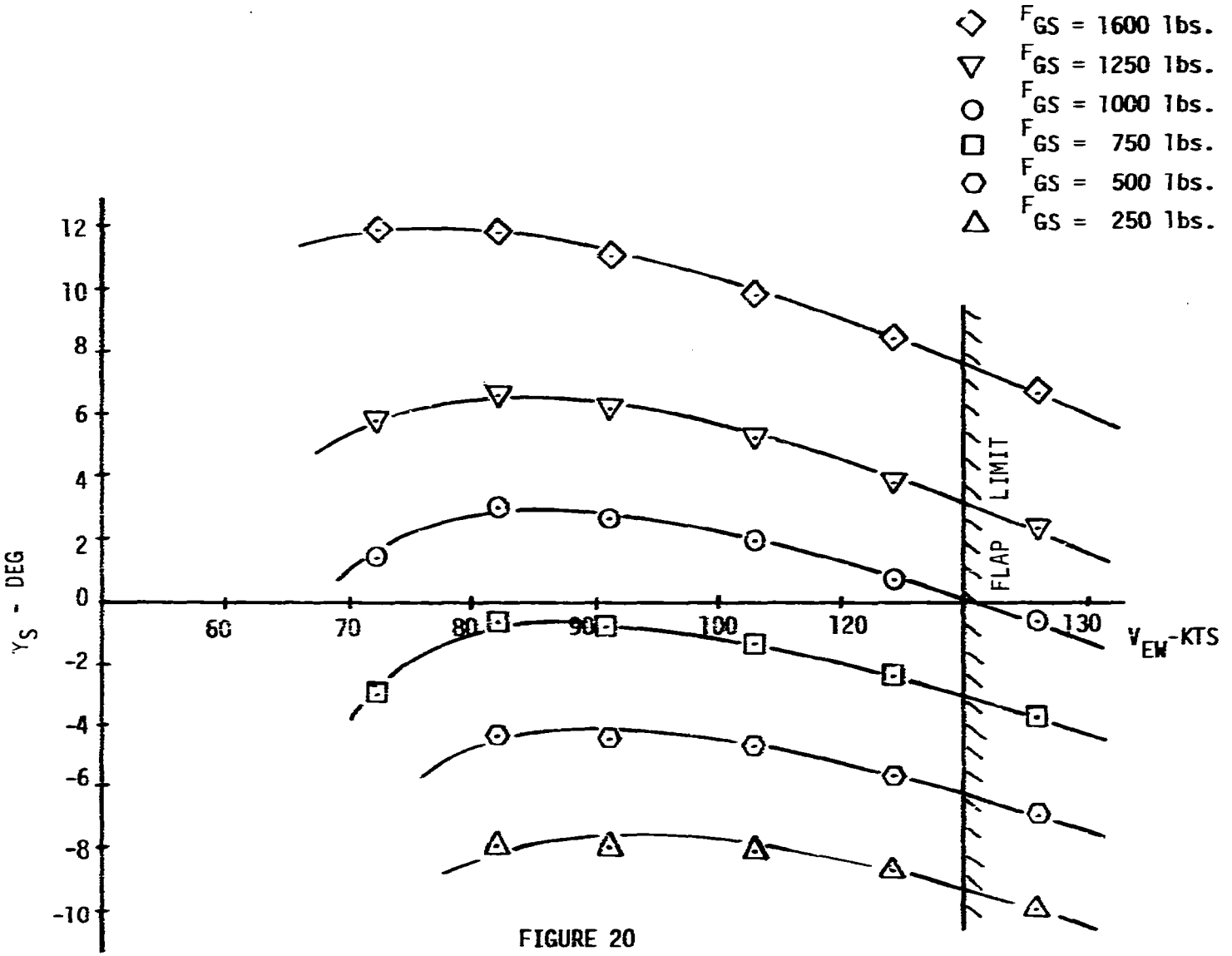

FIGURE 20

JETWING JW-1

γ_S VS. V_{EW}

UPPER WING REMOVED, GEAR DOWN, FLAPS 15°

W_c = 3600 lbs.

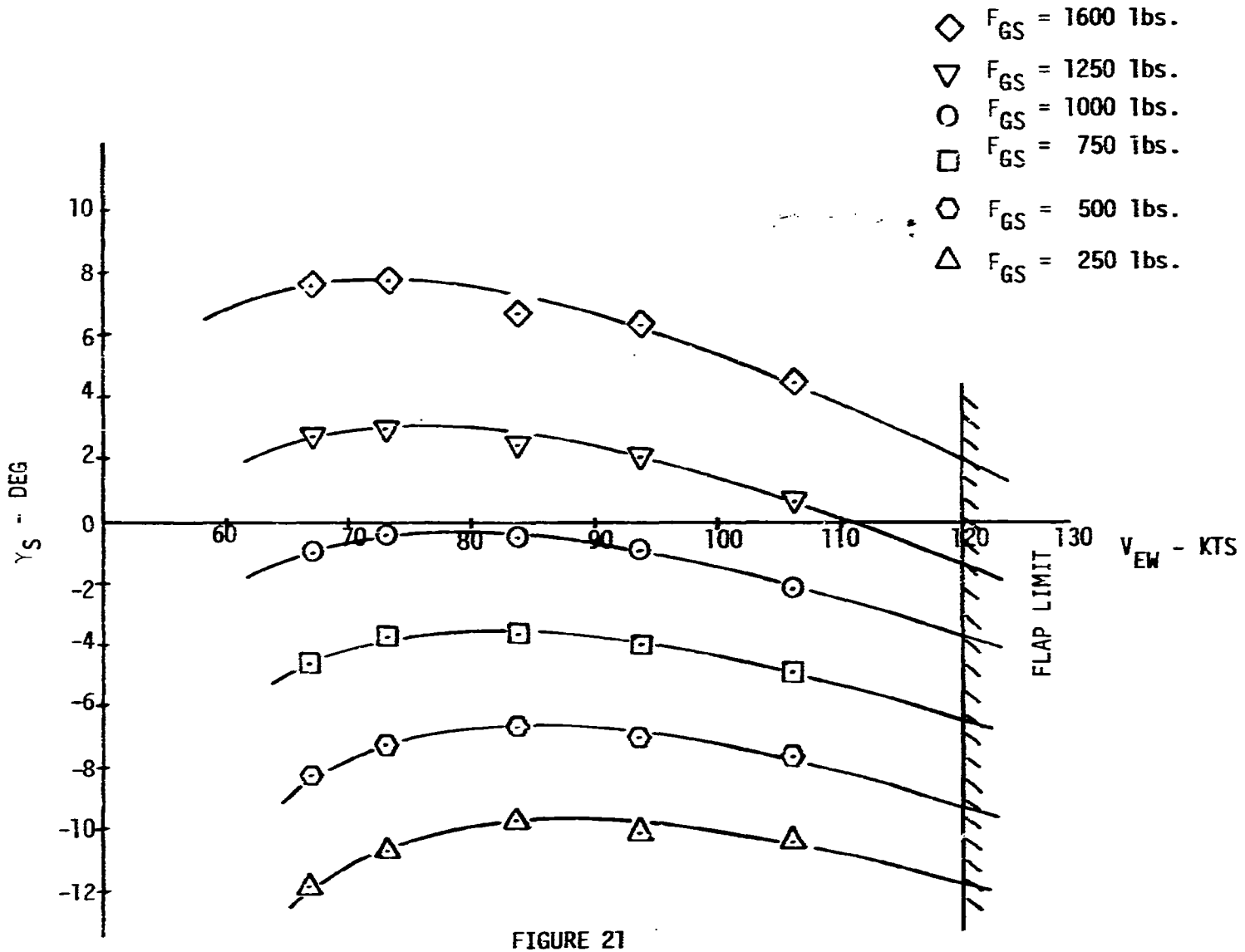

FIGURE 21

JETWING JW-1

γ_S VS. V_{EW}

UPPER WING REMOVED, GEAR DOWN, FLAPS 30°

FIGURE 22

JETWING JW-1

C_L vs. C_{Fex}

GEAR UP, FLAPS UP

C_J = 0.26

UPPER WING REMOVED

WIND TUNNEL
Run #4

FLIGHT TEST

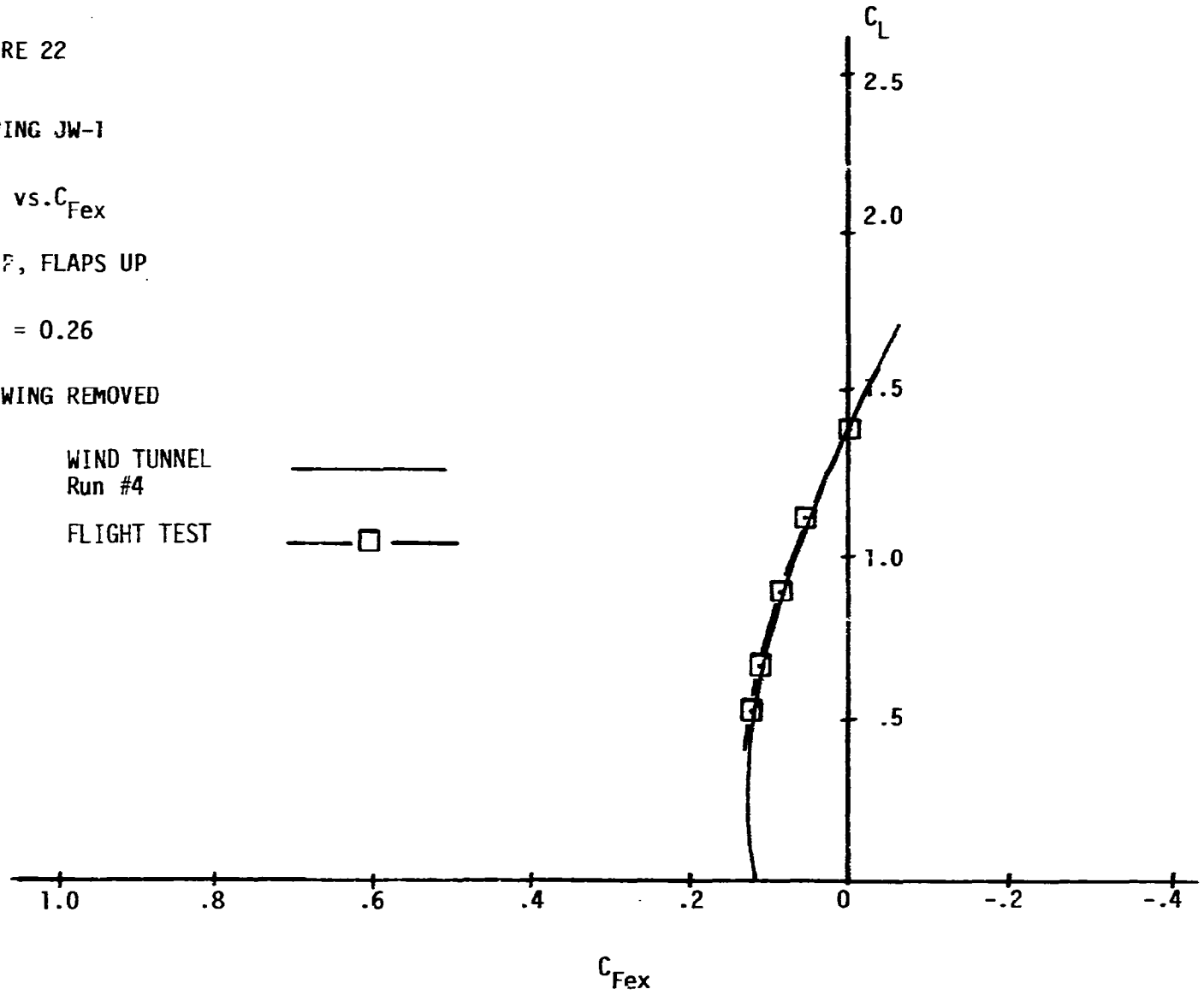

FIGURE 23

JETWING JW-1

C_L vs. C_{Fex}

GEAR UP, FLAPS UP

C_J = 0.43

UPPER WING REMOVED

WIND TUNNEL
Run #2

FLIGHT TEST

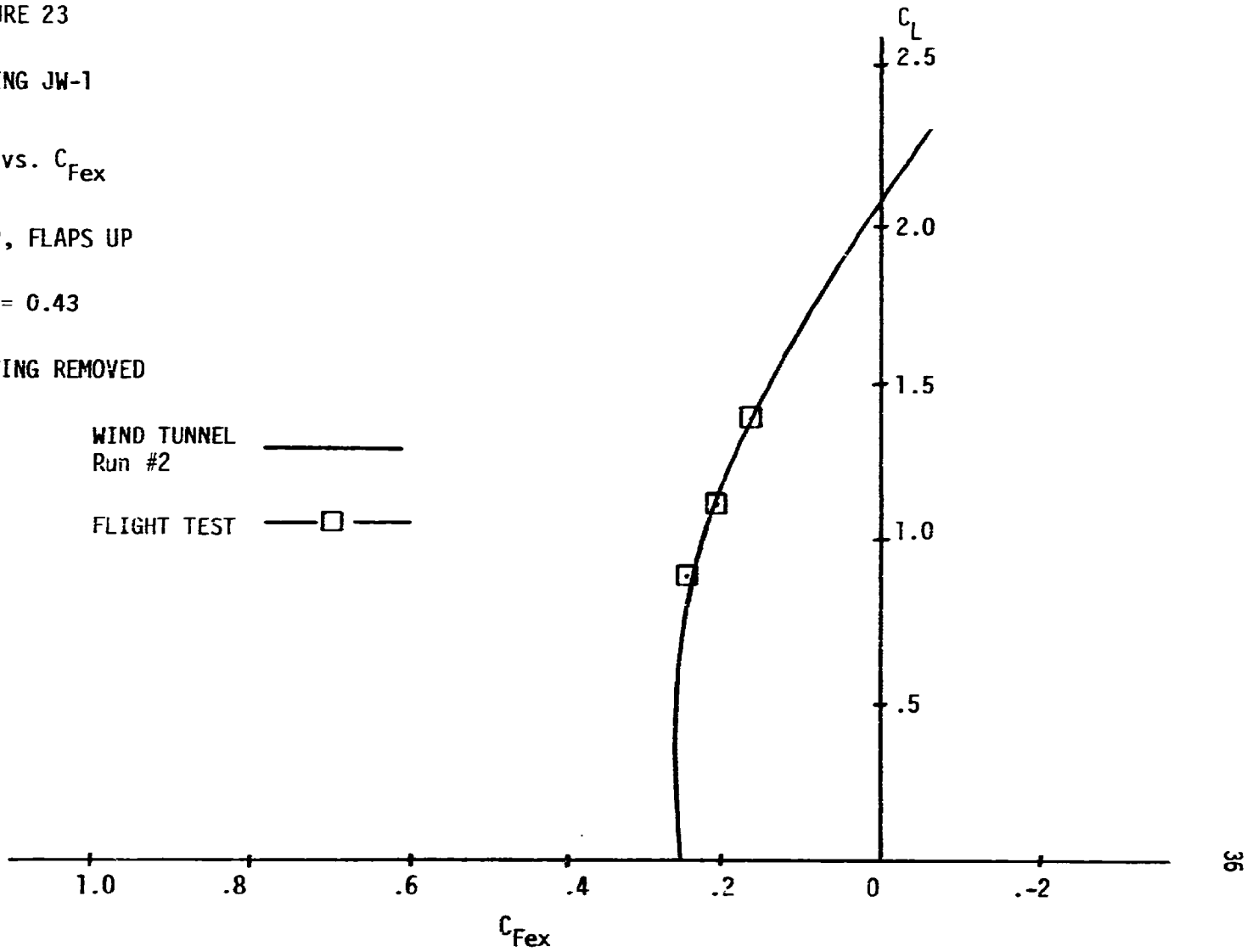

FIGURE 24

JETWING JW-1

C_L vs C_{Fex}

GEAR DOWN, FLAPS 15°

C_J = 0.49

UPPER WING REMOVED

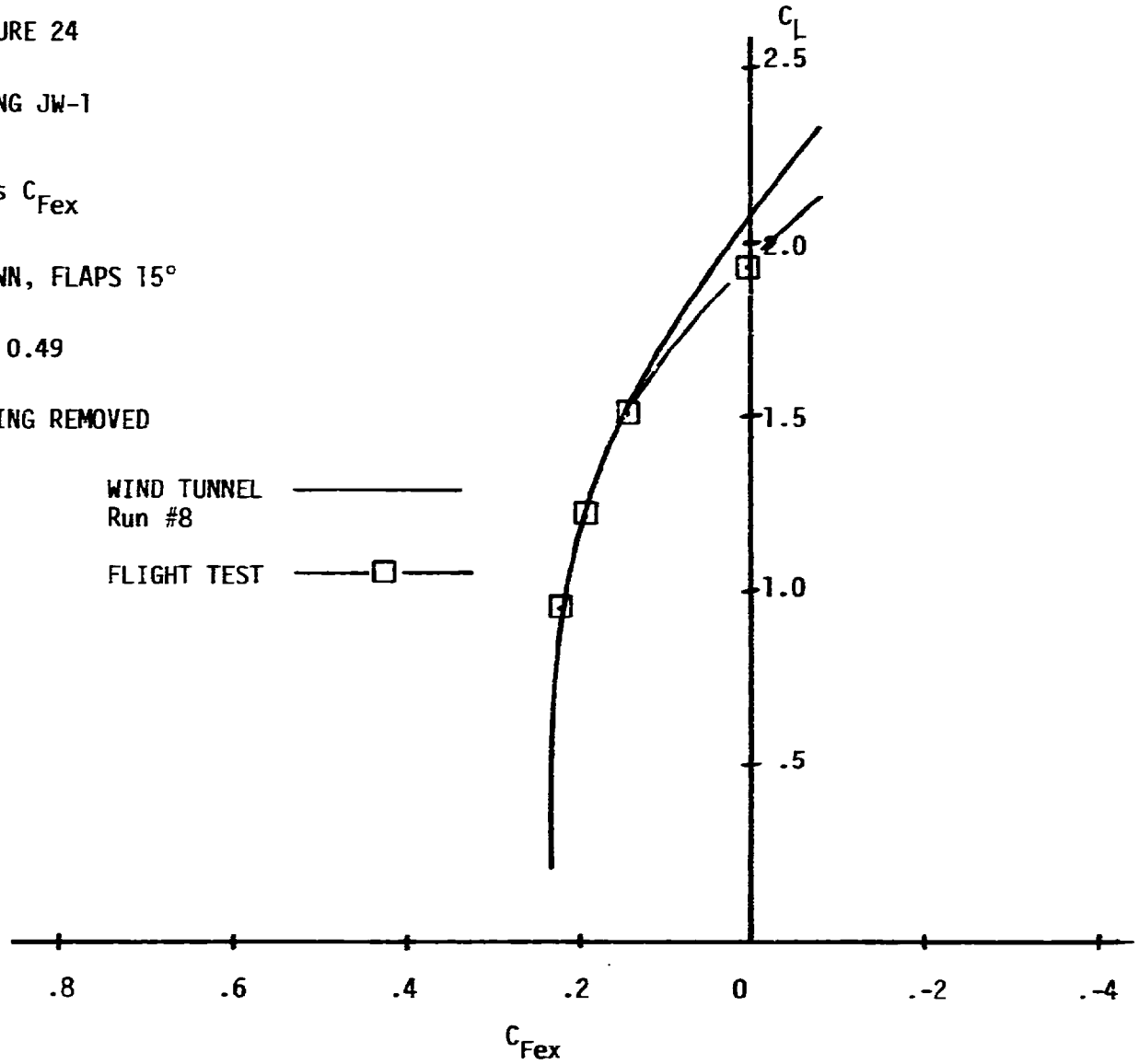

FIGURE 25

JETWING JW-1

C_L vs C_{Fex}

GEAR DOWN, FLAPS 15°

C_J = 0.75

UPPER WING REMOVED

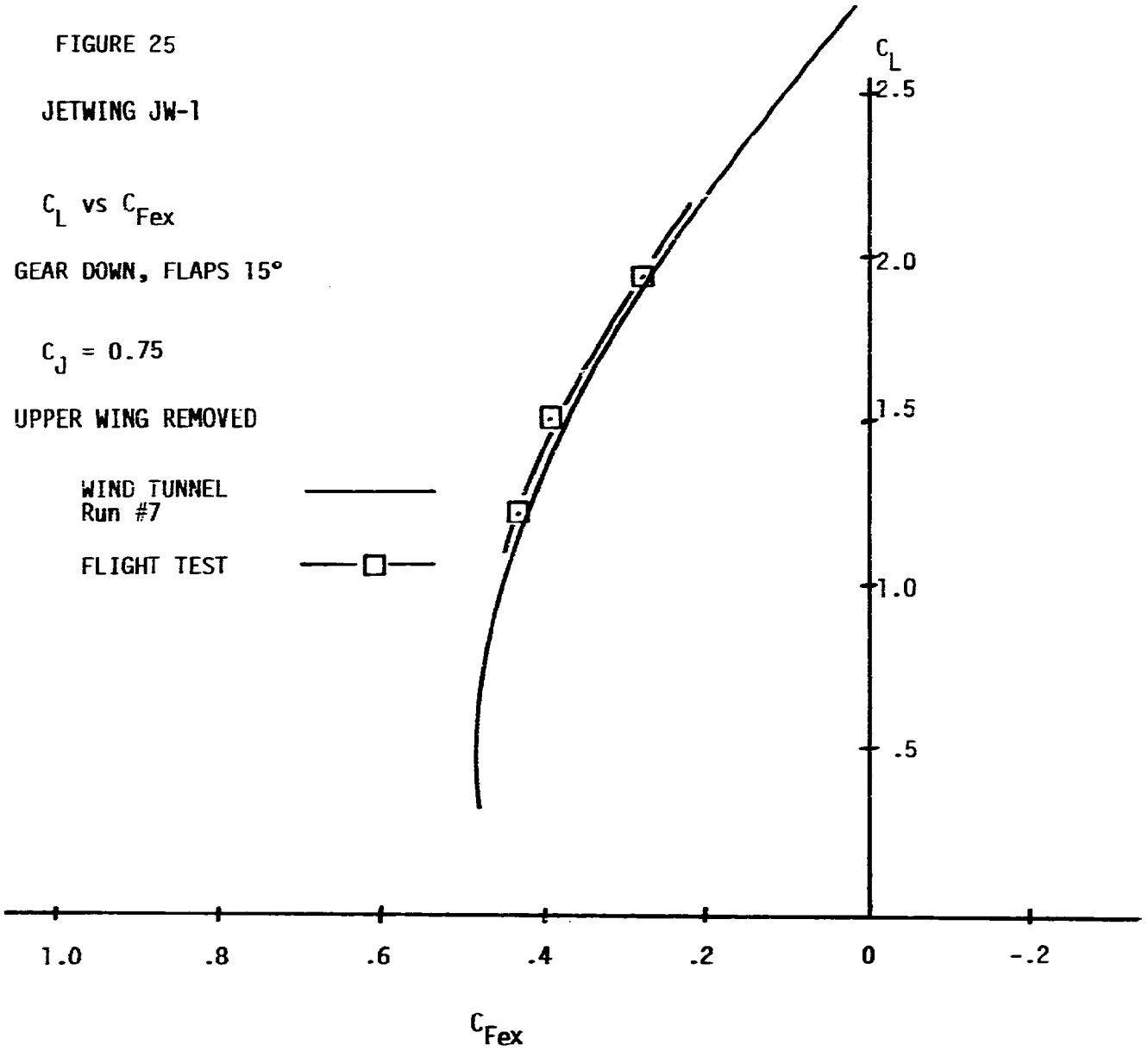

FIGURE 26
JETWING JW-1

C_L vs C_{Fex}

GEAR DOWN, FLAPS 30°

C_J = 0.49

UPPER WING REMOVED

WIND TUNNEL
Run #34

FLIGHT TEST

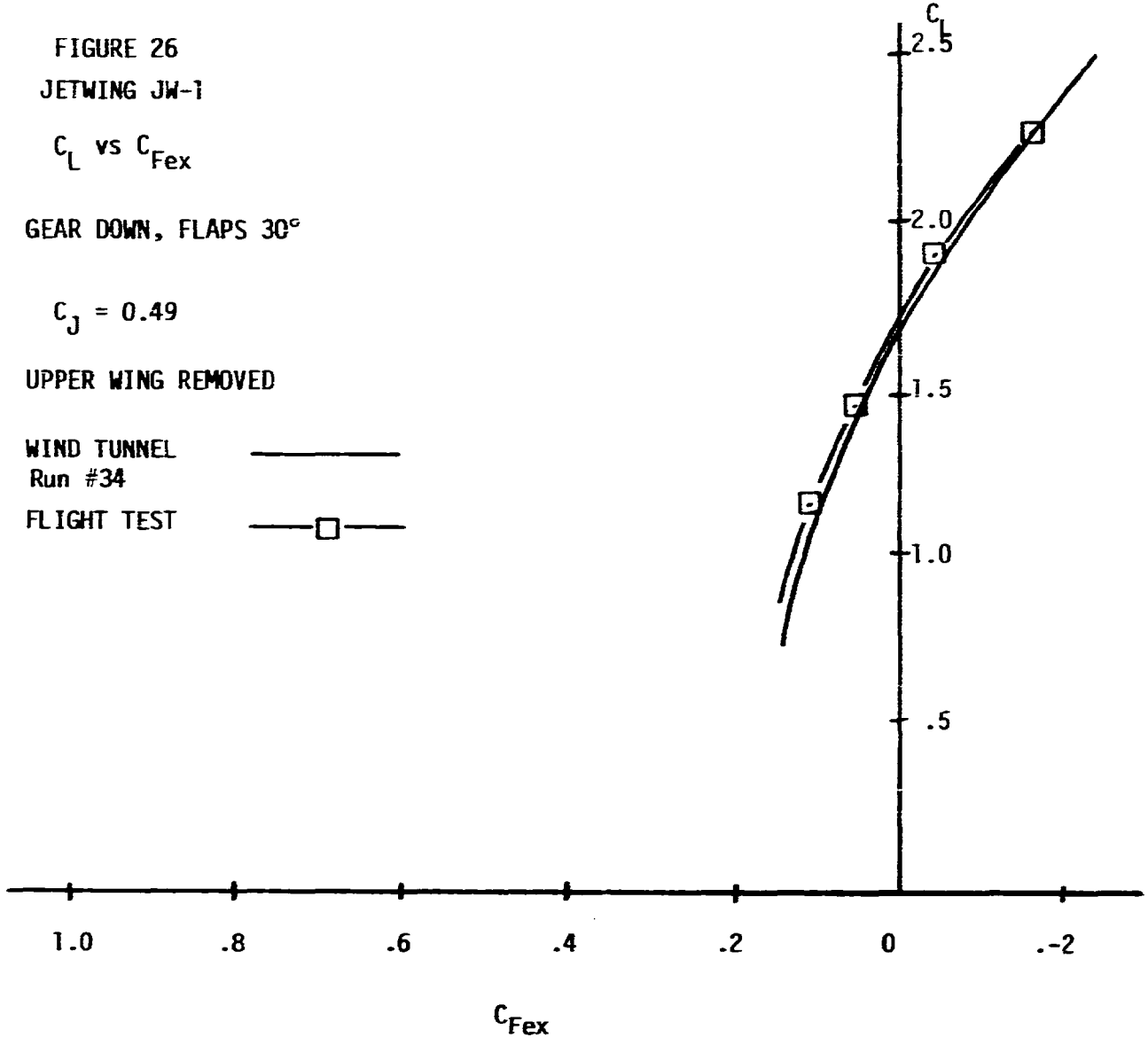

FIGURE 27

JETWING JW-1

C_L vs C_{Fex}

GEAR DOWN, FLAPS 30°

C_J = 0.74

UPPER WING REMOVED

WIND TUNNEL
Run #12

FLIGHT TEST

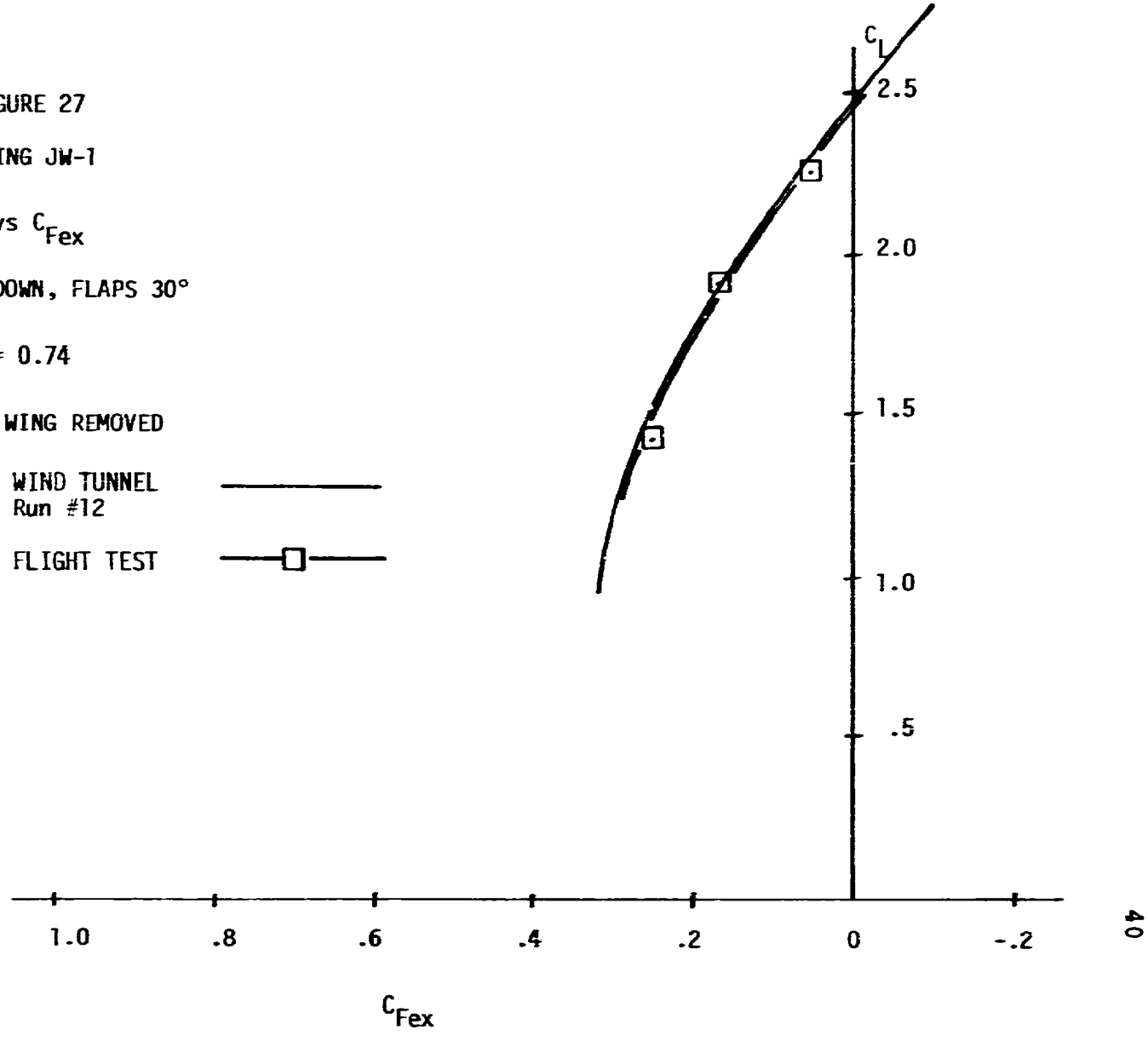

coefficient cannot be obtained directly by flight test.

To attempt to overcome this problem, and compare the flight test and wind tunnel results, the flight test data must be crossplotted on a plot of C_L versus C_J for various α such as is shown in Figures 28 through 30. Since the lines of constant angle of attack must be estimated from the angle of attack of individual data points, considerable error may be introduced by this plot. This error is compounded by the error involved in measuring aircraft pitch angle.

The results of such a comparison for the Jetwing with the upper wing removed are shown in Figures 31 through 36. These results do not compare as well as the excess thrust data shown in Figures 22 through 27. In light of the past discussion this descrepancy might be expected. Most of the difference is probably due to the measurement and crossplotting errors just discussed. However, there may be some error in the tunnel data due to wall effects which has not been accounted for. Such an error might help to explain the consistent difference in lift curve slope shown between the flight test and wind tunnel data.

COMPARISON WITH UPPER WING INSTALLED DATA

Figures 37, 38 and 39 show the results of performance tests reduced to sea level standard conditions with and without the mini-wing installed. These results show two interesting features.

First, for all configurations the airspeed at which best angle of climb occurs decreases with an increase in gross thrust or blowing coefficient. This change indicates a reduction in induced drag with thrust (or blowing coefficient) increase as is indicated by the theory [1]. Such a drag reduction has interesting applications for air-combat maneuvering, and means that in order to fly steep approaches at low airspeeds additional zero lift drag is needed.

The second interesting feature of these figures is that at every thrust setting and flap configuration the airplane with the upper wing installed is out performed by the airplane without the upper wing. This difference in performance generally increases with an increase in thrust setting, particularly in the case with 30 degrees flap deflection. Although, most of this difference in performance may be explained by the fact that with the upper wing installed the airplane has more zero lift drag, it may not be the complete story. If the increase in C_{D_0} were totally responsible for the performance difference, there should be an increase in the performance difference with an increase in airspeed. However, this does not appear to be true in all cases. In fact, the difference appears to decrease at higher airspeeds when the flaps are deflected. In addition, static thrust calibrations [1] showed a slight increase in static thrust with the upper wing installed. This thrust difference should tend to reduce the performance difference at the lower speeds. It then appears that the performance difference may be a function of induced drag in addition to the difference in C_{D_0}.

One item which may affect induced drag is the thickness of the USB jet. With the upper wing installed the jet is greater than twice as thick as with the upper wing removed. Recent wind tunnel studies [5] have shown that high aspect ratio nozzles (thin blowing jet) provide better USB performance than those with low aspect ratio (thick blowing jet). An analysis of wind tunnel results of Jetwing configurations showed that the supercirculation portion of the total lift was from 5 to 7 percent higher when the upper wing was off. These results are shown in Figure 40. It is difficult to determine if USB jet thickness is a significant factor in the performance difference shown in Figures 37, 38 and 39 but it does appear to beg further investigation.

FIGURE 28

JETWING JW-1

C_L vs C_J

For Various α

GEAR UP, FLAPS UP

UPPER WING REMOVED

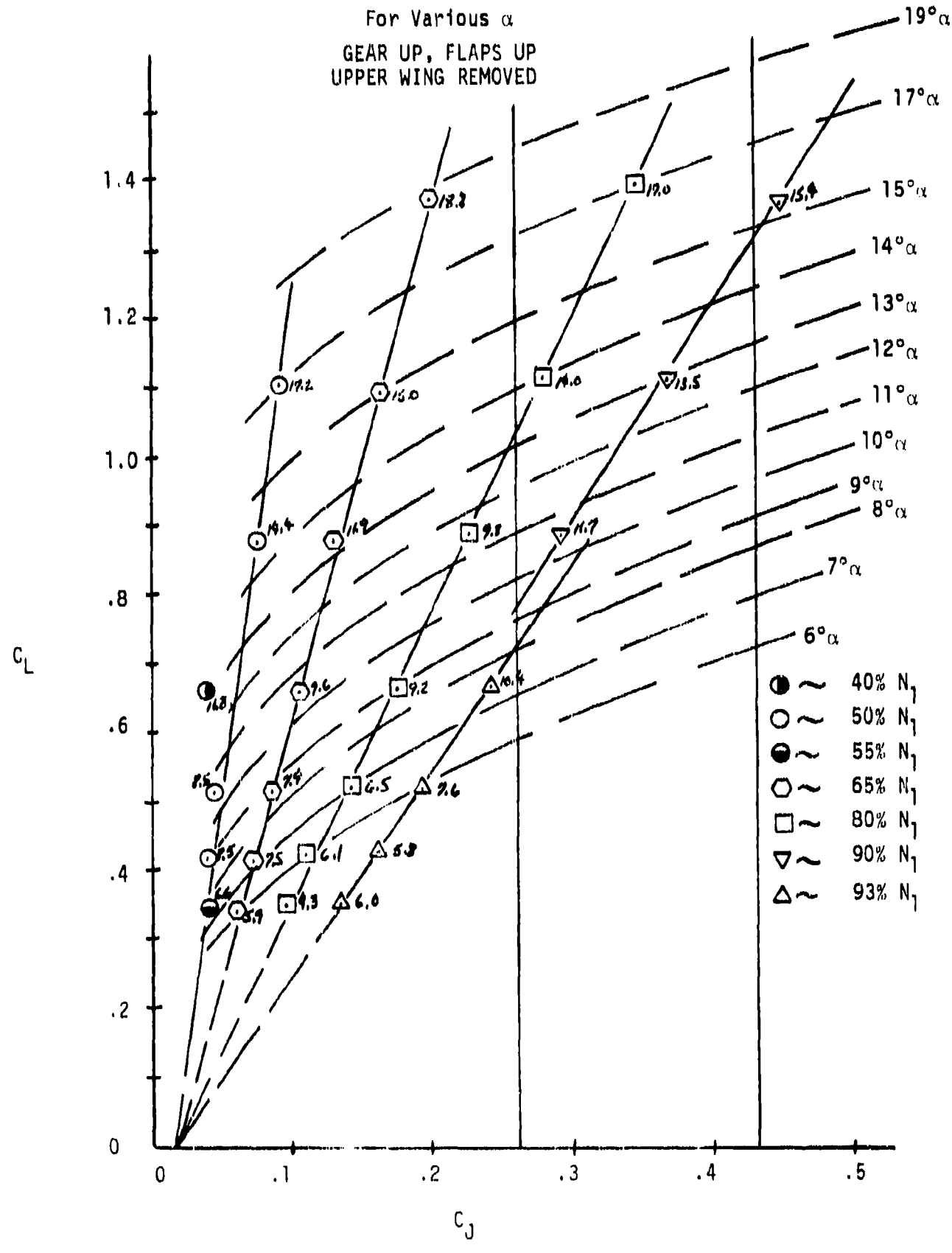

FIGURE 29
JETWING JW-1
C_L vs C_J
For Various α
GEAR DOWN, FLAPS 15°
UPPER WING REMOVED

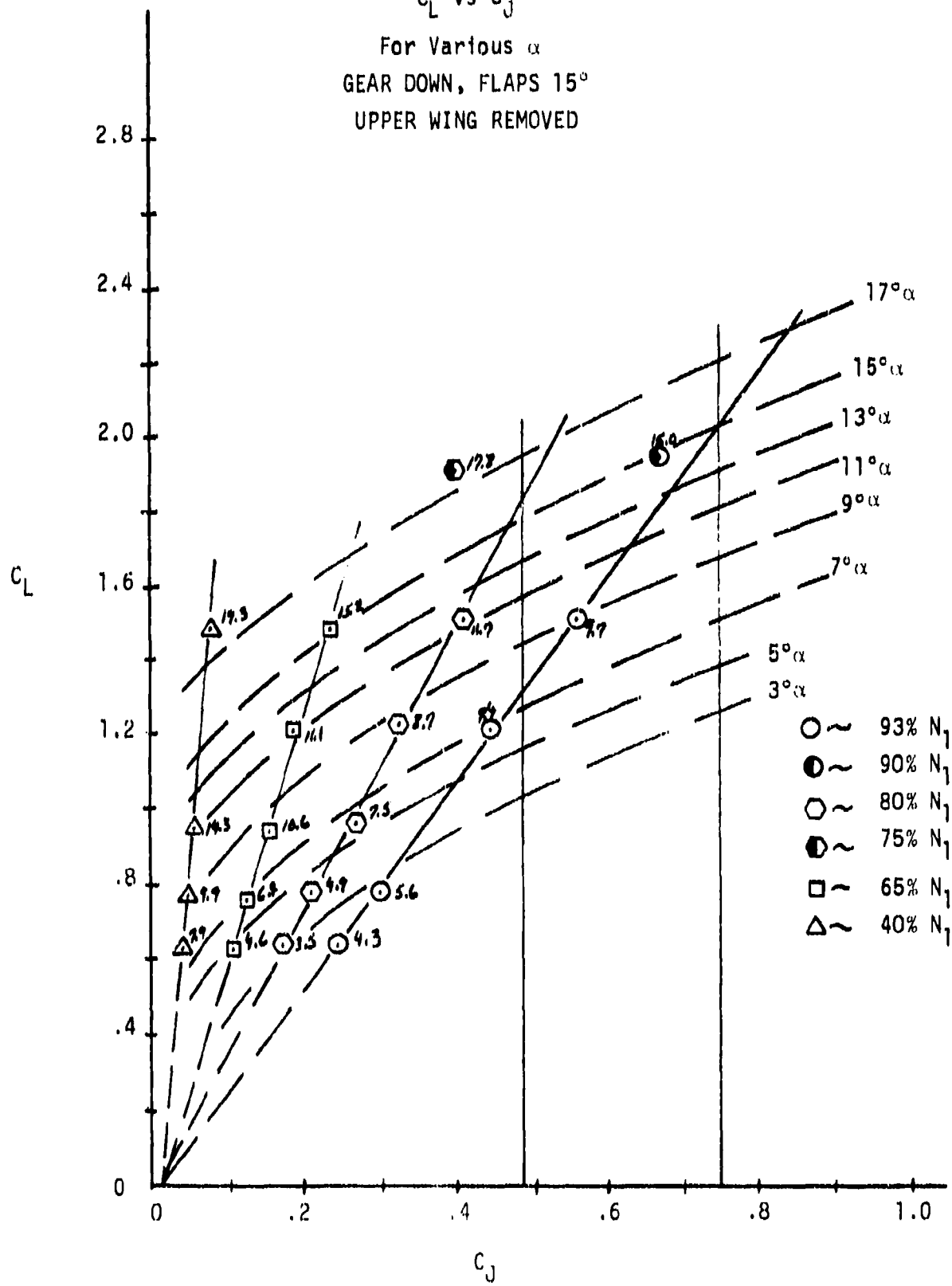

FIGURE 30

JETWING JW-1

C_L vs C_J

For Various α

GEAR DOWN, FLAPS 30°

UPPER WING REMOVED

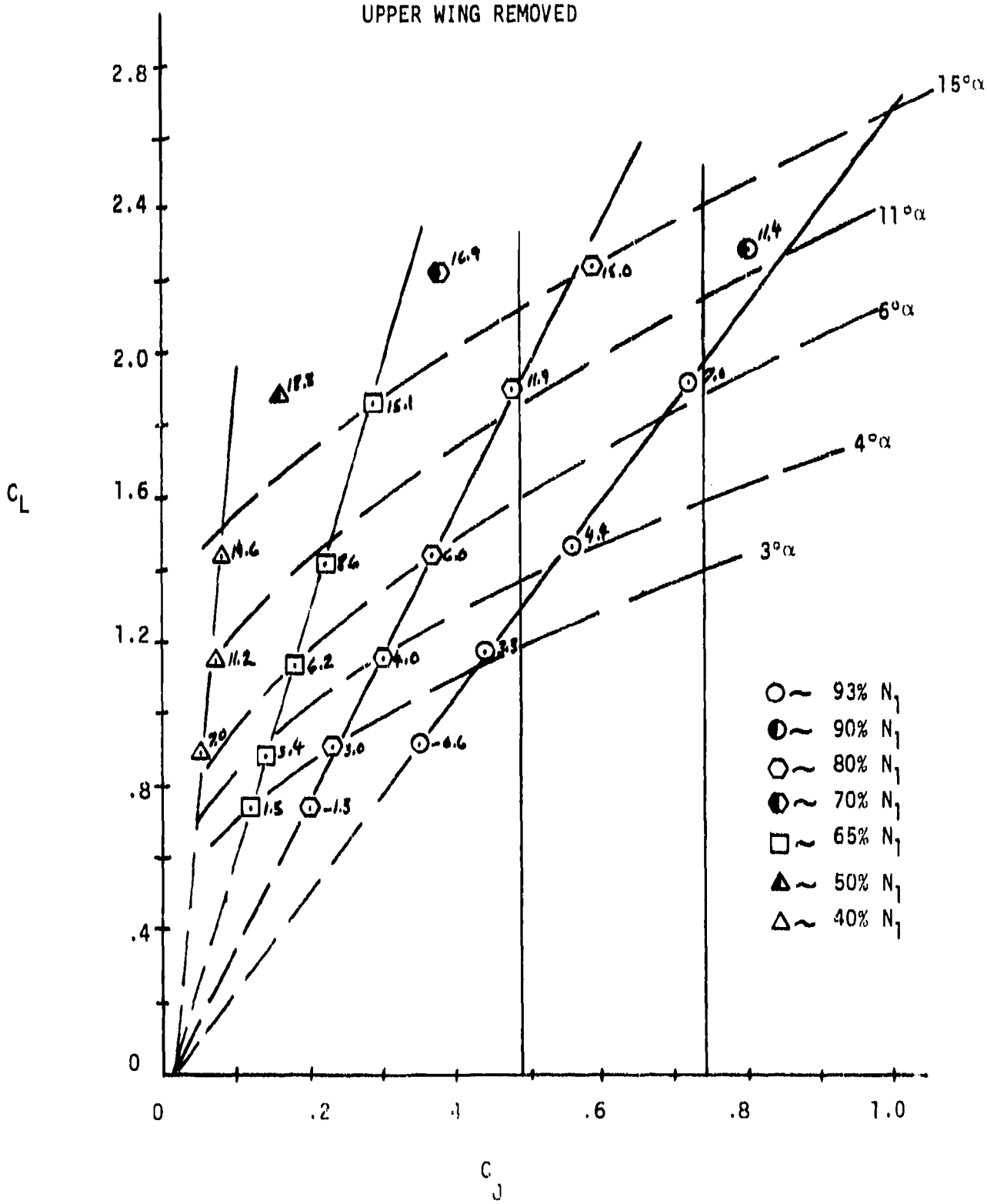

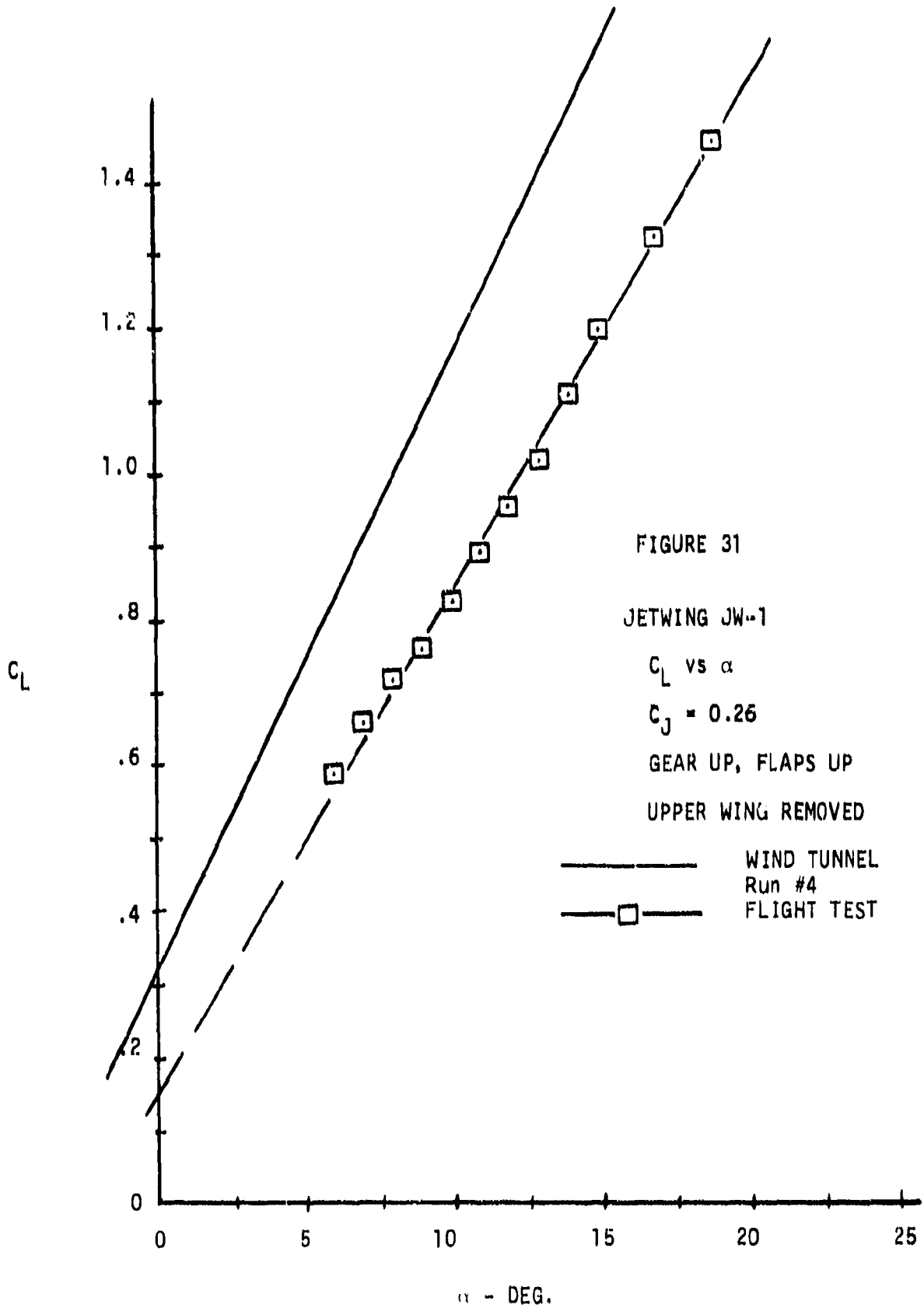
1.4
1.2
1.0
.8
.6
.4
.2
0
C_L
0
5
10
15
20
25
α - DEG.
FIGURE 31
JETWING JW-1
C_L vs α
C_J = 0.26
GEAR UP, FLAPS UP
UPPER WING REMOVED
WIND TUNNEL
Run #4
FLIGHT TEST

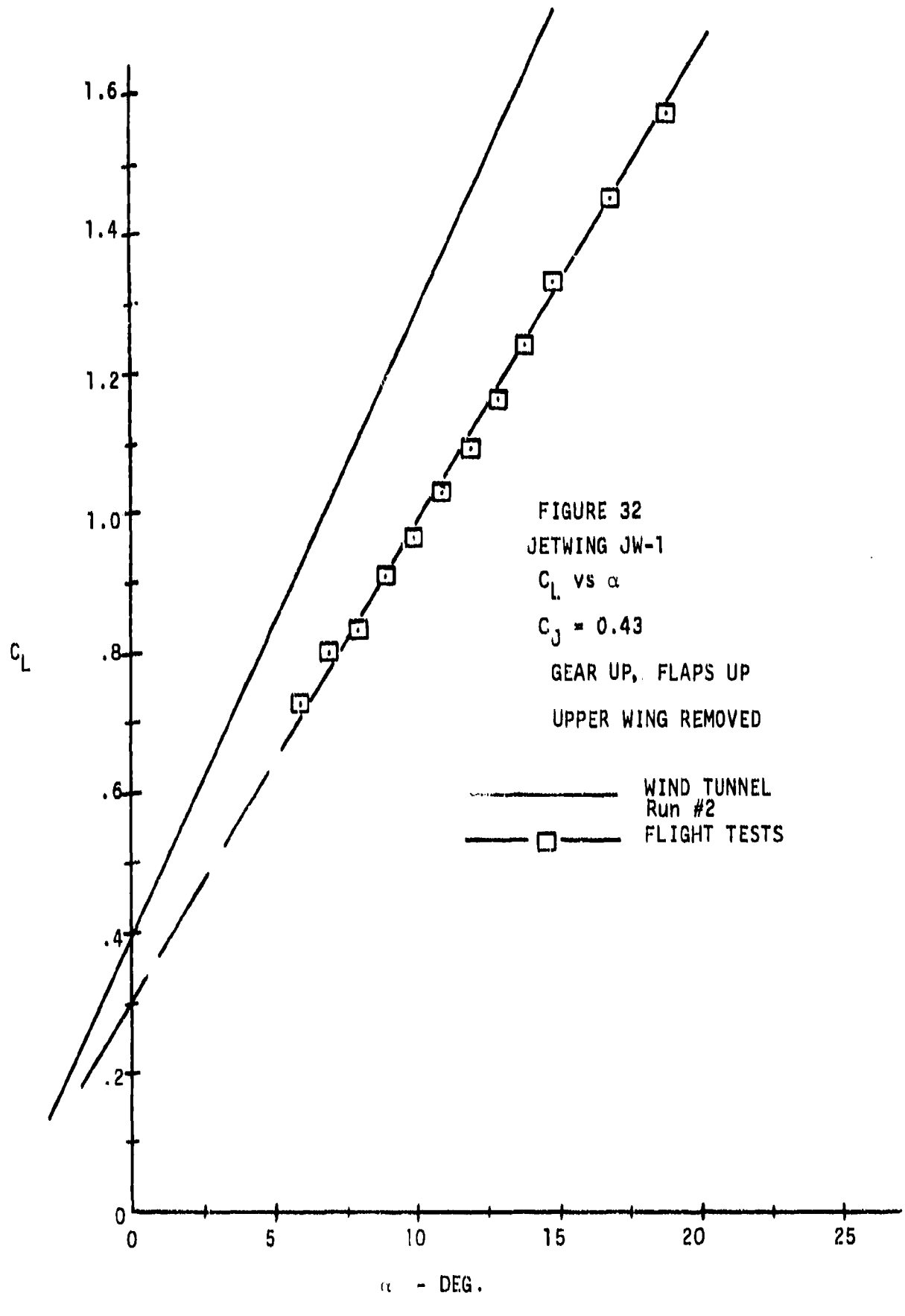
1.6
1.4
1.2
1.0
.8
.6
.4
.2
0
C_L
0
5
10
15
20
25
α - DEG.
FIGURE 32
JETWING JW-1
C_L vs α
C_J = 0.43
GEAR UP, FLAPS UP
UPPER WING REMOVED
WIND TUNNEL
Run #2
FLIGHT TESTS

FIGURE 33
JETWING JW-1
C_L vs α
GEAR DOWN
FLAPS 15°
UPPER WING REMOVED
C_J = 0.49

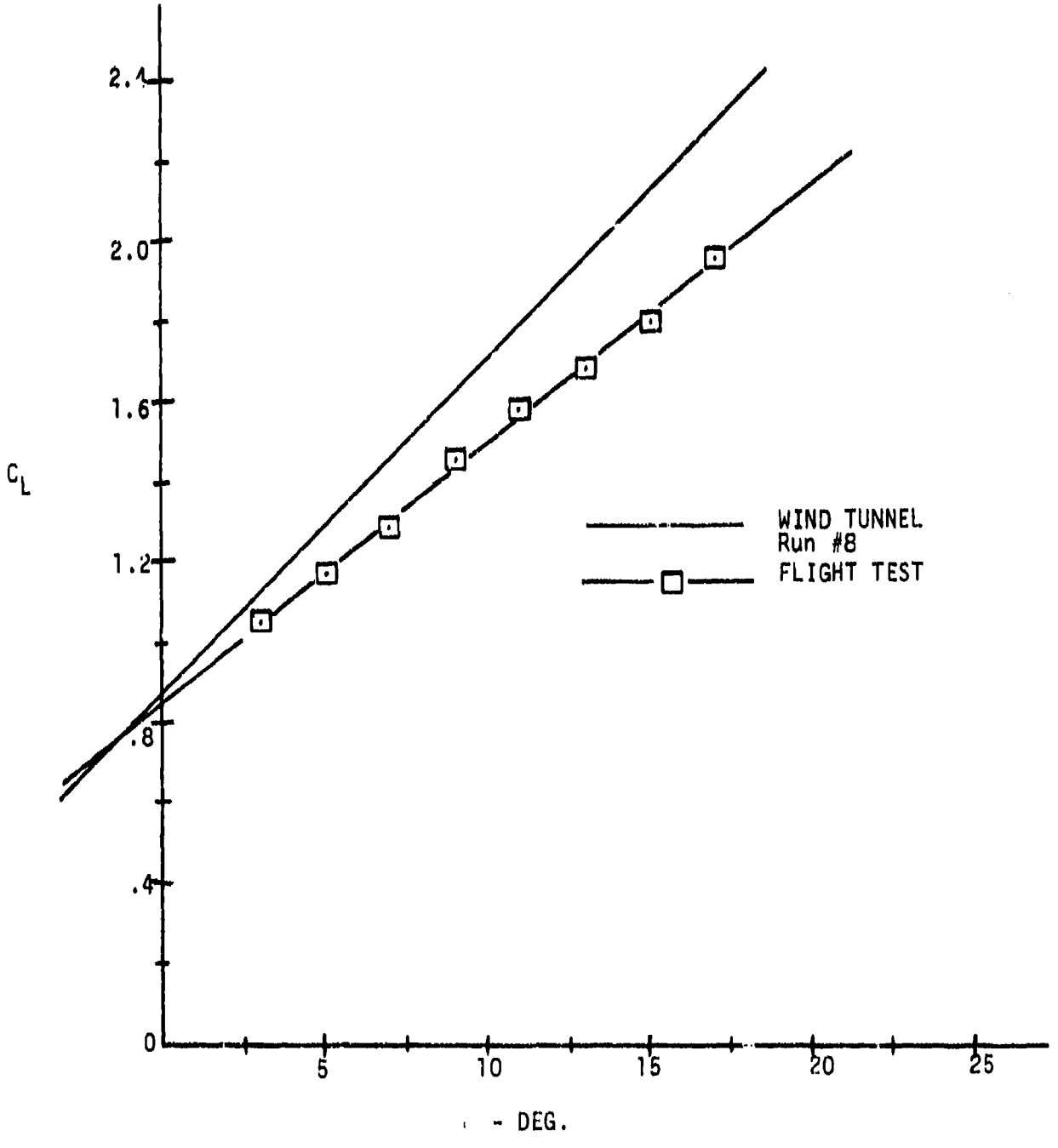

FIGURE 34
JETWING JW-1
C_L vs α
GEAR DOWN
FLAPS 15°
UPPER WING REMOVED
C_J = 0.75

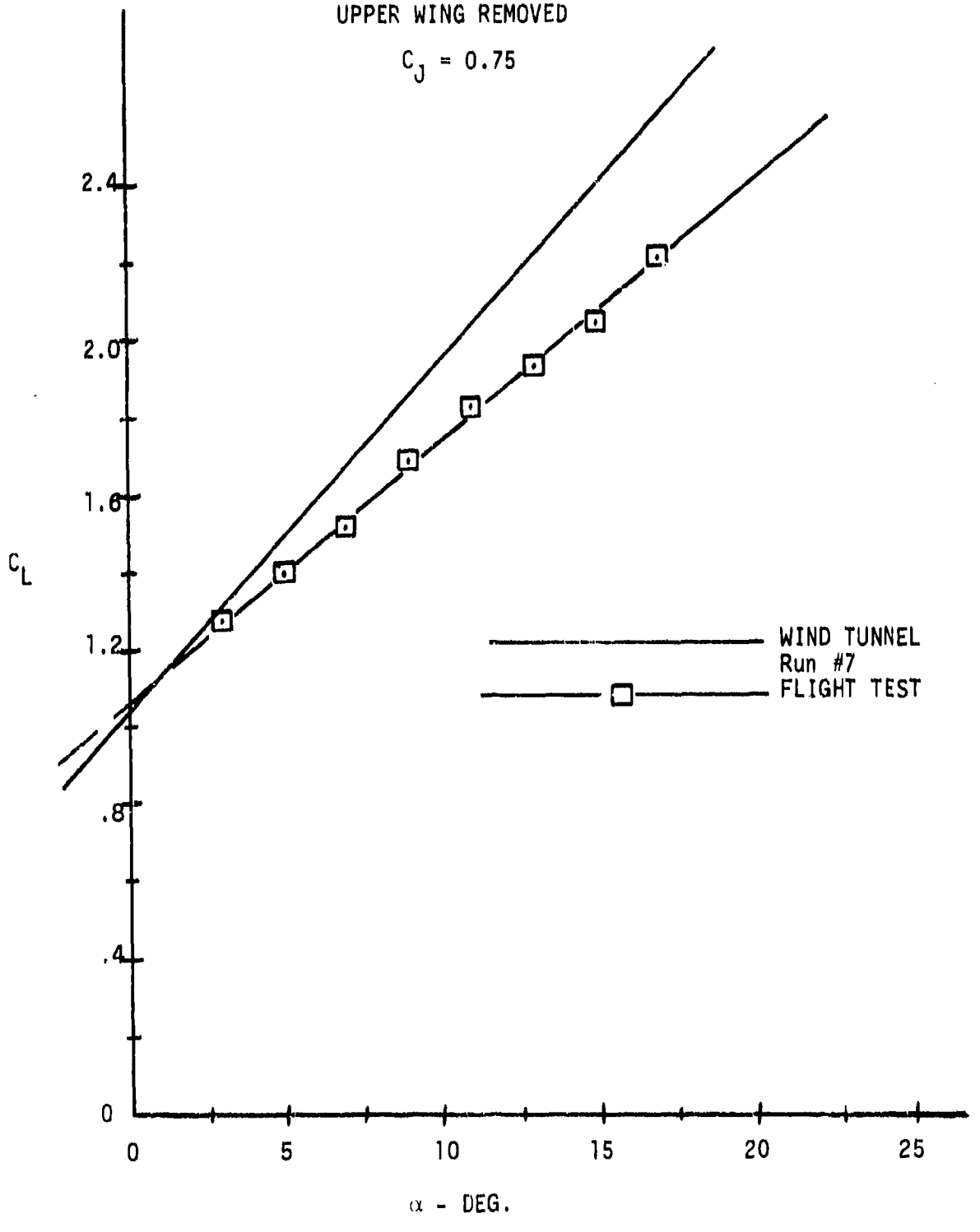

FIGURE 35

JETWING JW-1

C_L vs α

C_J = 0.49

GEAR DOWN

FLAPS 30°

UPPER WING REMOVED

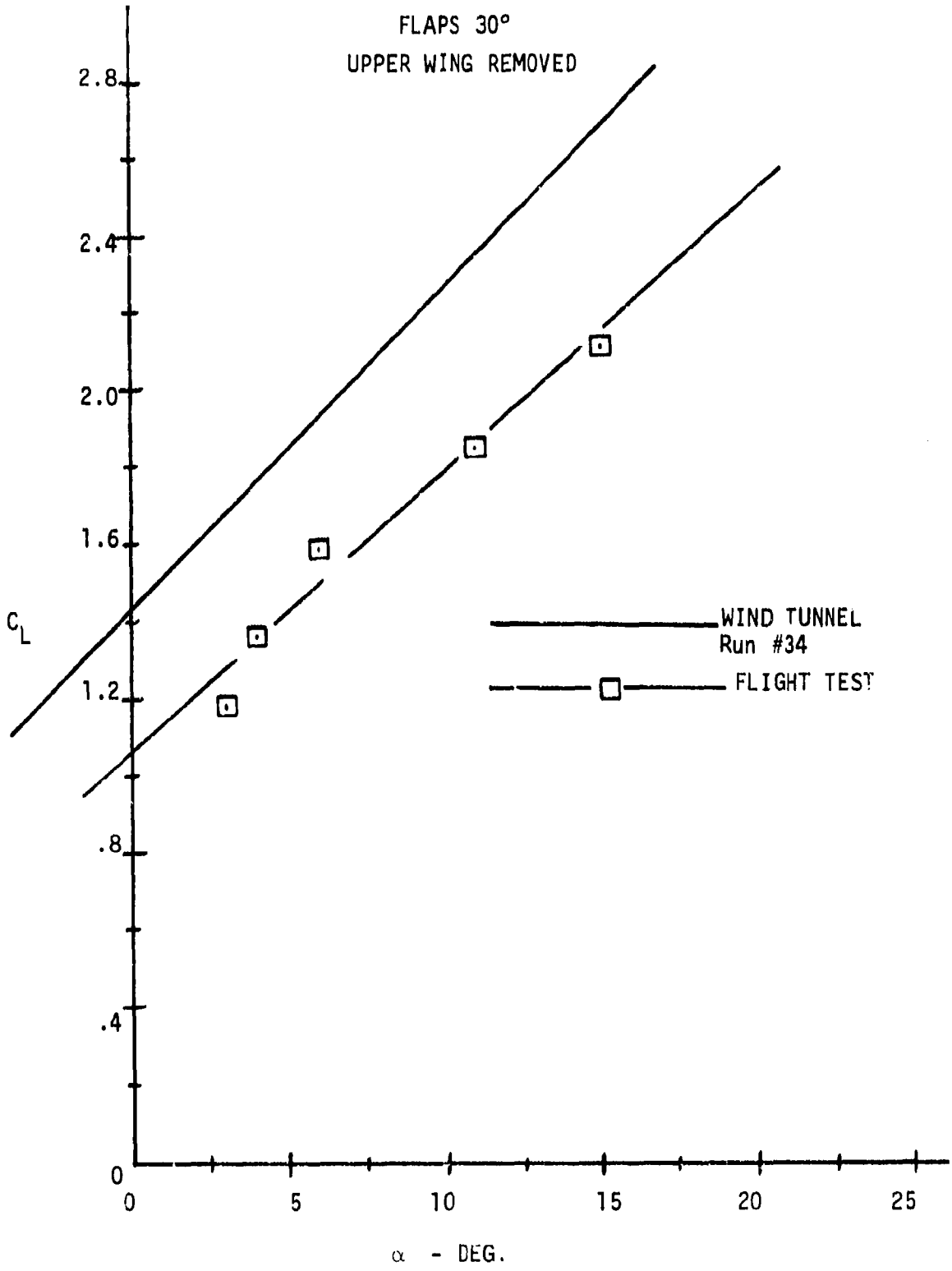

FIGURE 36

JETWING JW-1

C_L vs. α

C_J = 0.75

GEAR DOWN

FLAPS 30°

UPPER WING REMOVED

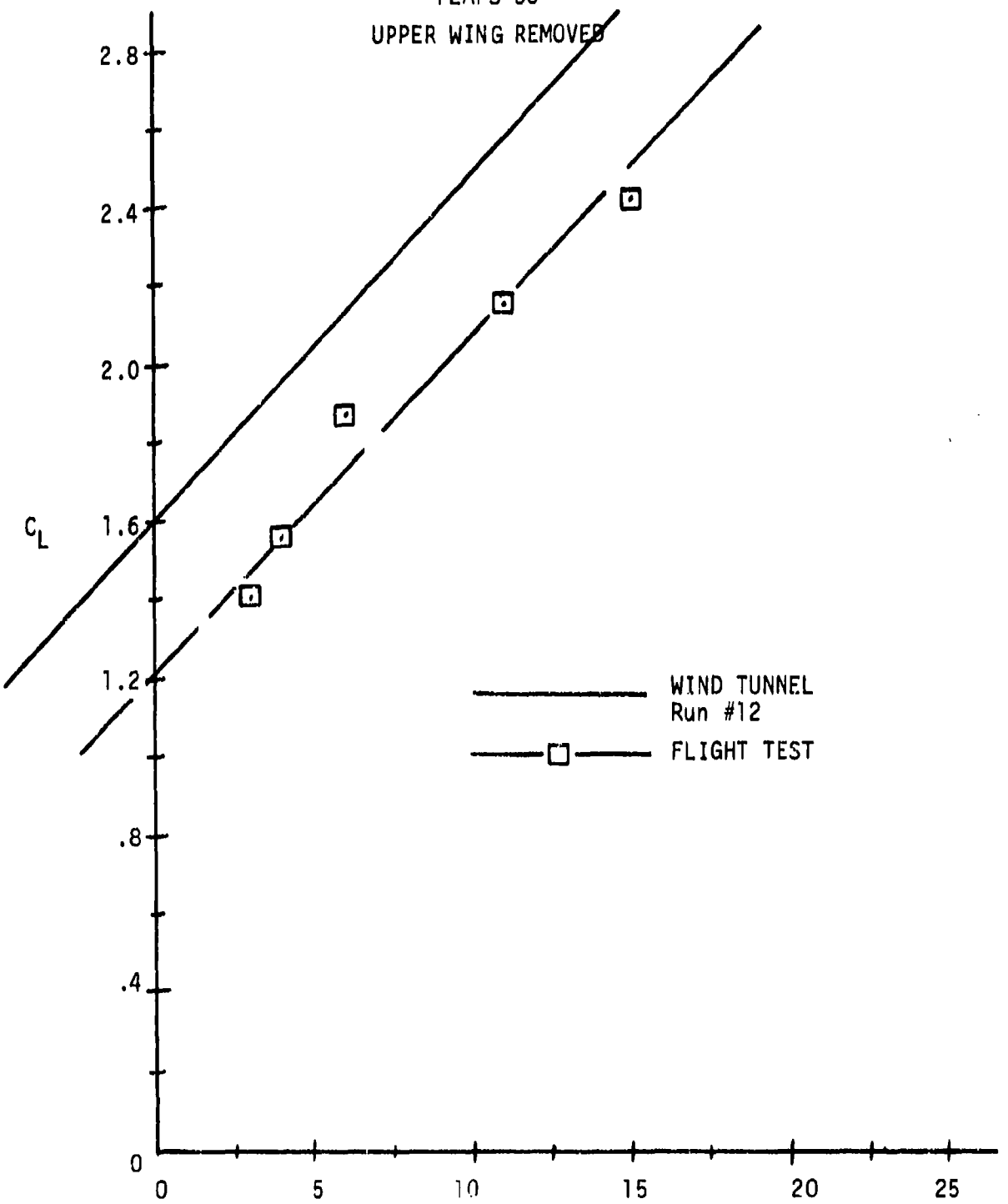

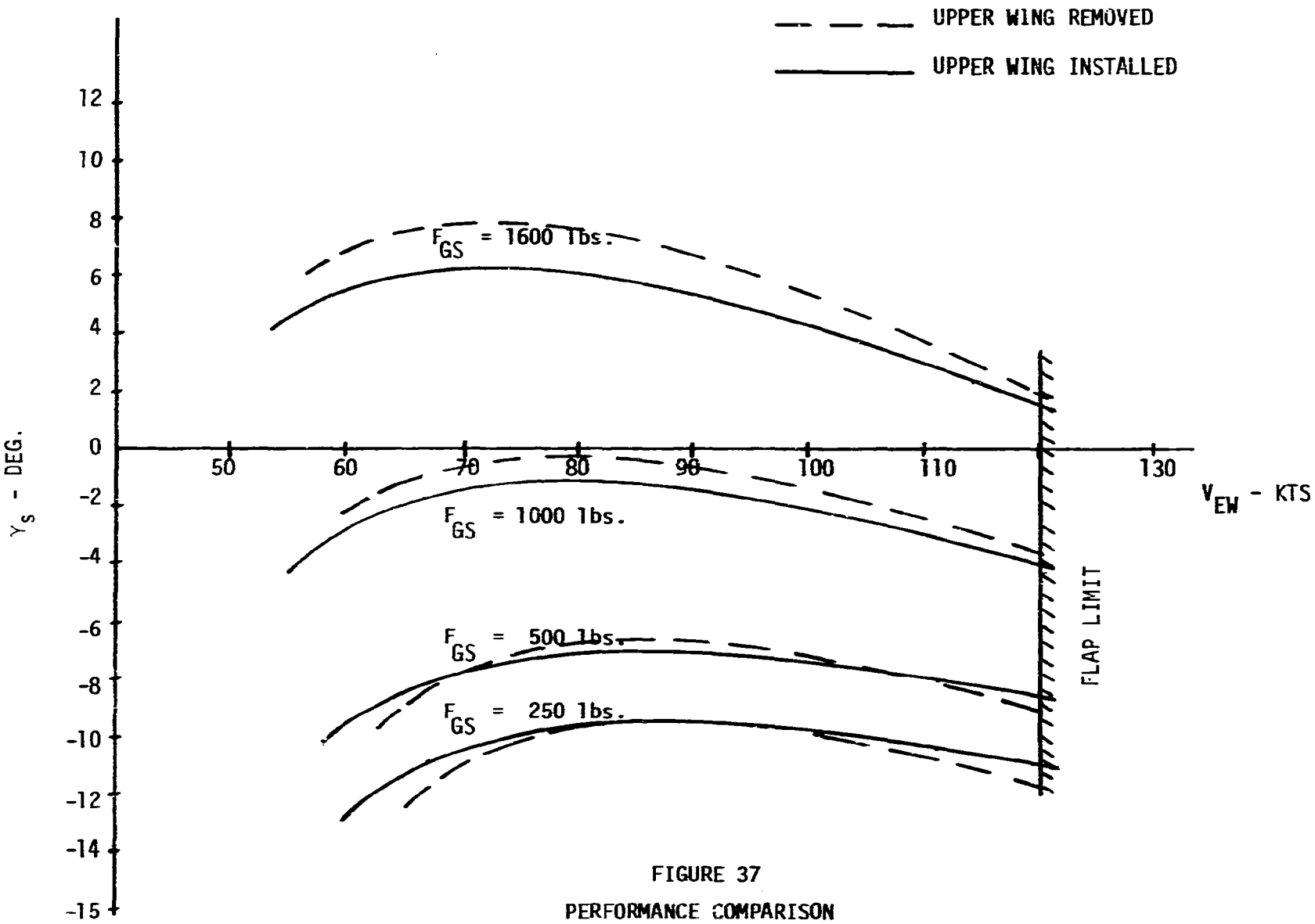

FIGURE 37

PERFORMANCE COMPARISON
JETWING JW-1
WITH AND WITHOUT UPPER WING
GEAR DOWN FLAPS 30°

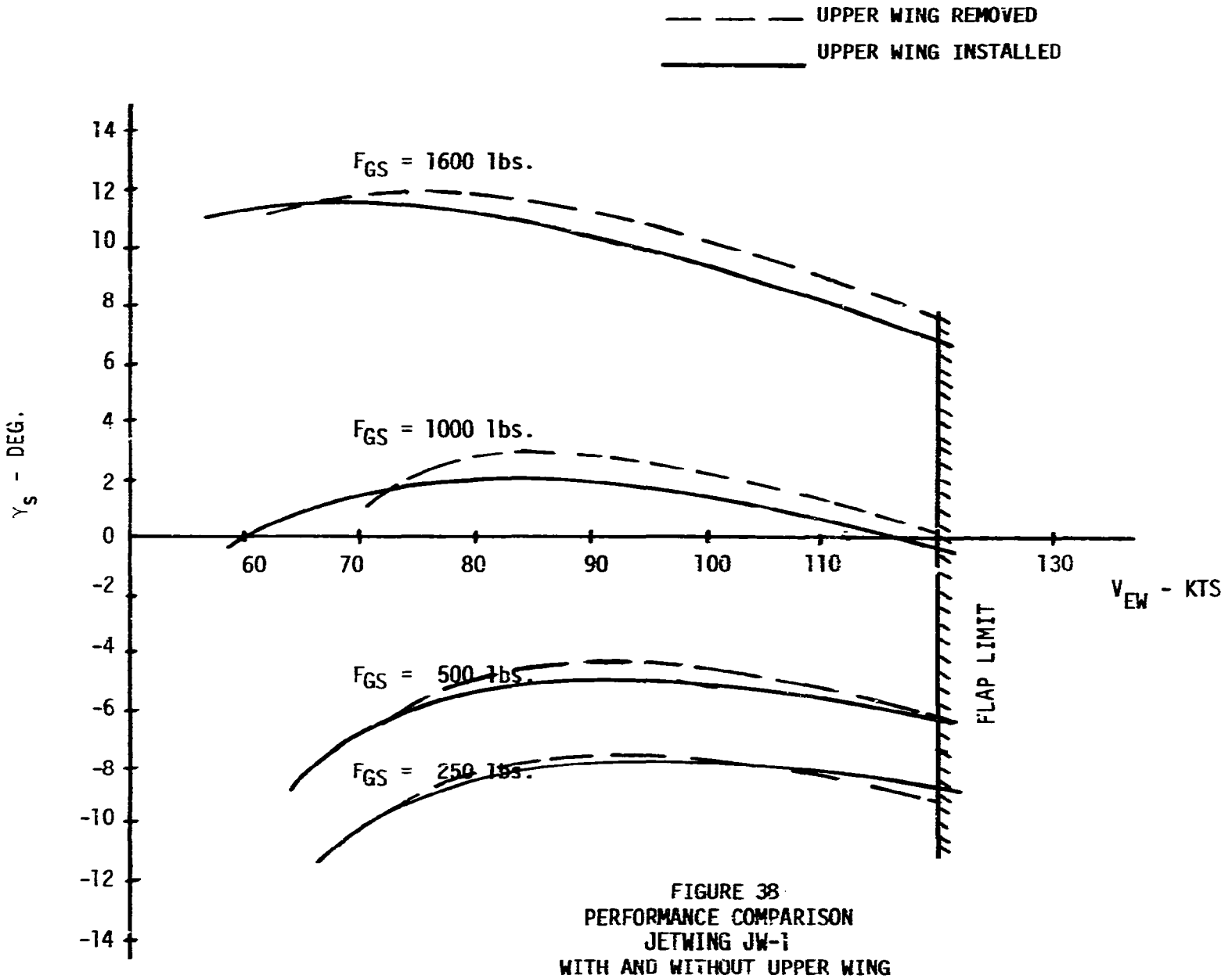

FIGURE 38
PERFORMANCE COMPARISON
JETWING JW-1
WITH AND WITHOUT UPPER WING
GEAR DOWN, FLAPS 15°

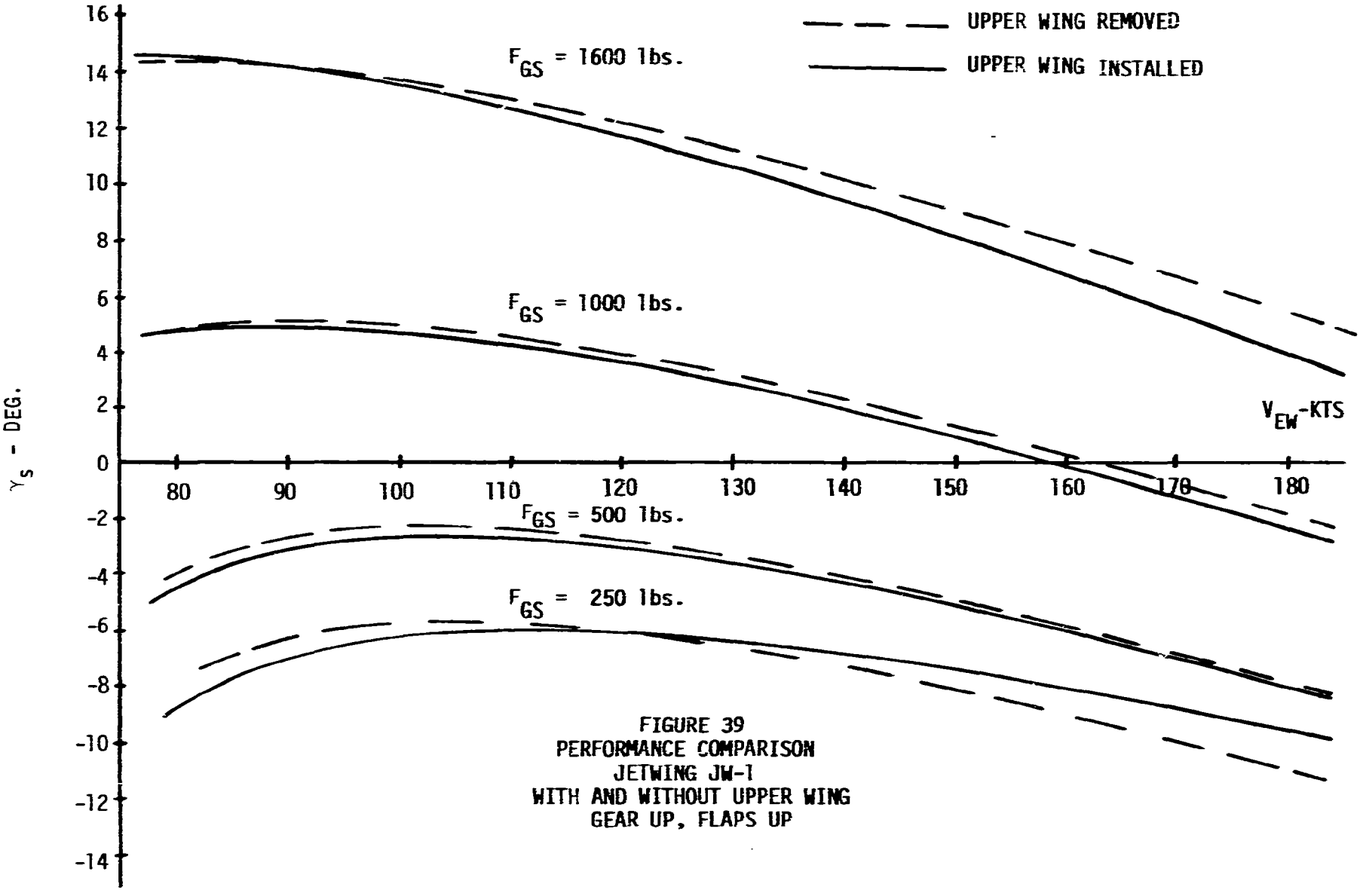

FIGURE 39
PERFORMANCE COMPARISON
JETWING JW-1
WITH AND WITHOUT UPPER WING
GEAR UP, FLAPS UP

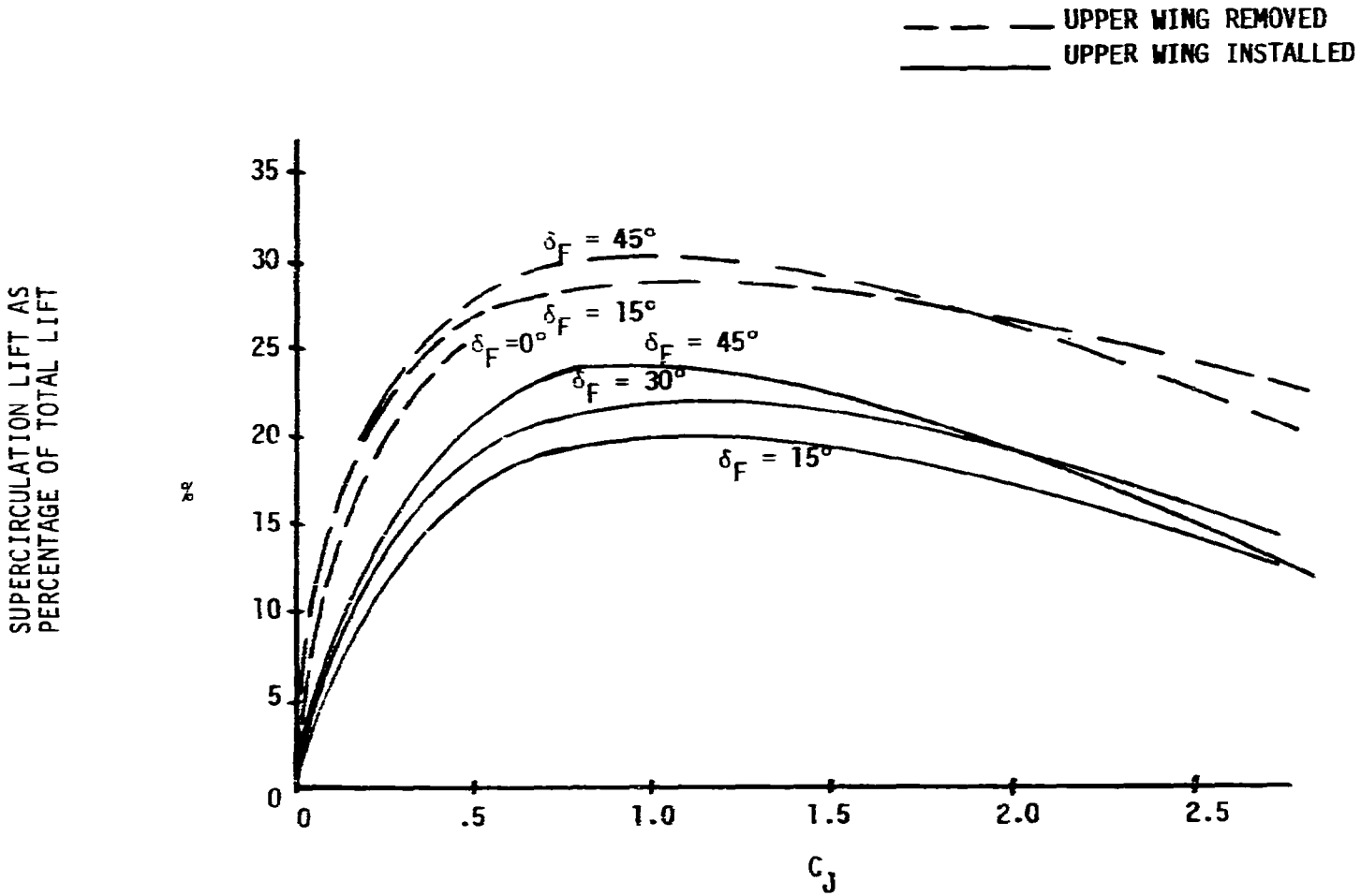

FIGURE 40
COMPARISON OF SUPERCIRCULATION LIFT AS A PERCENTAGE
OF TOTAL LIFT VERSUS BLOWING COEFFICIENT FOR JETWING JW-1
WITH AND WITHOUT UPPER WING INSTALLED EXTRACTED FROM FULL SCALE TUNNEL DATA
AT α = 0°

HANDLING QUALITIES

A complete quantitative handling qualities evaluation of the aircraft was previously conducted with the upper wing installed and reported on in [1]. With the upper wing removed, handling qualities were qualitatively evaluated and compared with the upper wing installed configuration. This was done because changes in handling qualities due to the configuration change were thought to be small. In addition, the same test pilot would fly both series of tests.

Differences in handling qualities between the two aircraft configurations were confined to the longitudinal motions. One of the most noticeable changes was in longitudinal static stability. With the upper wing installed the aircraft had static margins of from 0 to −3% depending upon flap position and power settings. With the upper wing removed the aircraft's static margins became less negative and for some cases became slightly positive. The reason for this phenomenon has not been determined and further investigation appears warranted.

Another difference in longitudinal handling qualities occurred at low power setting. With the upper wing removed a light to moderate airframe buffet occurred anytime the power setting was reduced to values below 50%N_1. The power setting where the onset of this buffet occurred appeared to be a function of airspeed and flap position with the highest power setting for buffet onset occurring at airspeeds above 150 knots with the flaps up. Although the source of this buffet was not positively determined, the most likely source is a turbulent shear layer which develops between the blowing jet and the free stream flow whenever the speed of the jet drops below that of the free stream. This buffet was not observed with the upper wing installed.

NOISE MEASUREMENT

The Graphic Level Recorder provided two kinds of data: 1. Sound pressure level (SPL) (amplitude) versus time (t) plots from the 1000 ft flyover measurements and; 2. Sound pressure level (SPL) versus frequency (F) from the static ground measurements.

The flyover data were crossplotted as sound pressure level (SPL) versus relative distance (RD). Relative distance was determined by correlating the airspeed from the flight data with the time intervals on the amplitude versus time graph. At the point where the noise of the approaching aircraft started to rise above the background noise level, the relative distance was set to zero.

Marks were put on the graph when the JETWING crossed overhead the microphone. From this mark the approximate position of the microphone on the SPL vs. RD plot could be determined.

Representative plots for a take-off and three flyovers with different configurations are shown in figures 41 and 42.

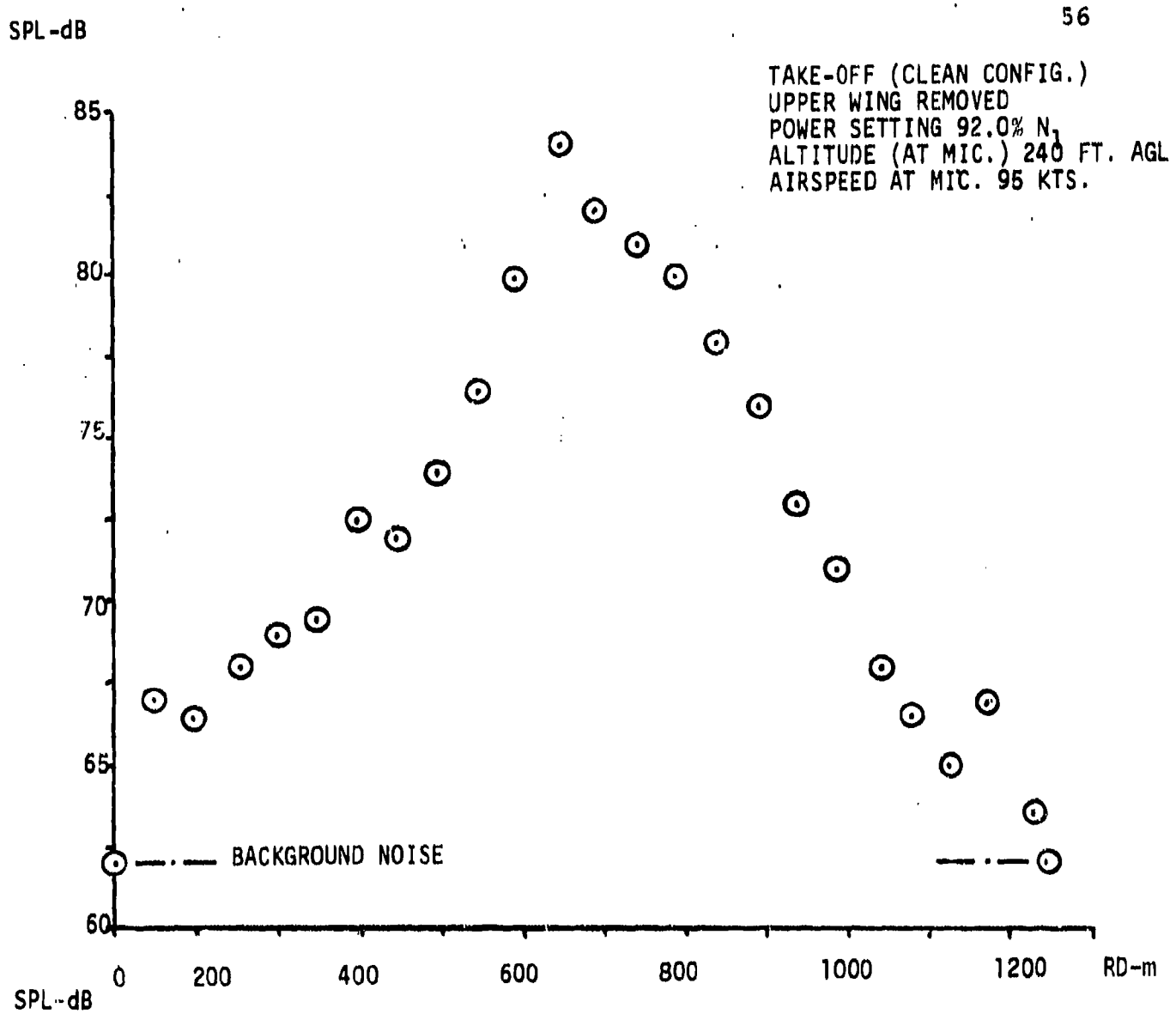

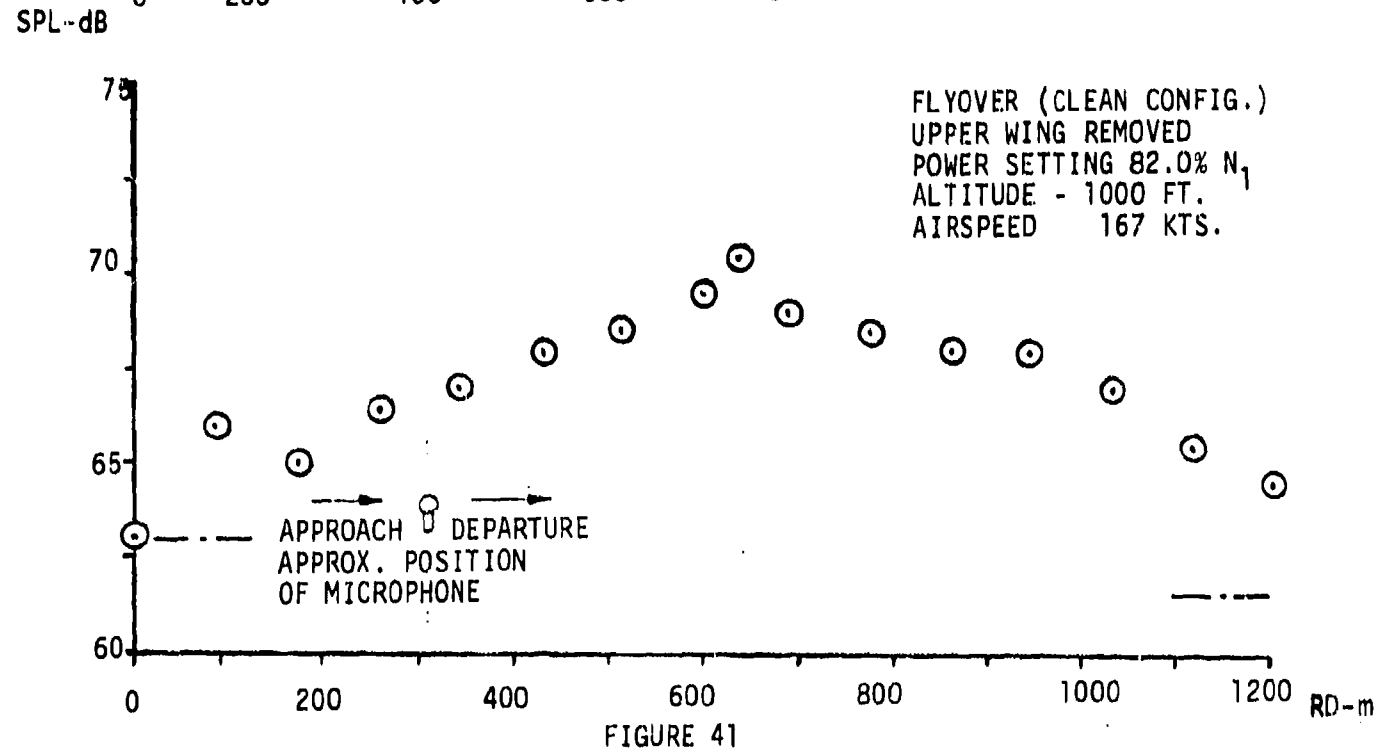

FIGURE 41
1000 FT. FLYOVER SOUND PRESSURE LEVEL SPL VS. RELATIVE DISTANCE RD

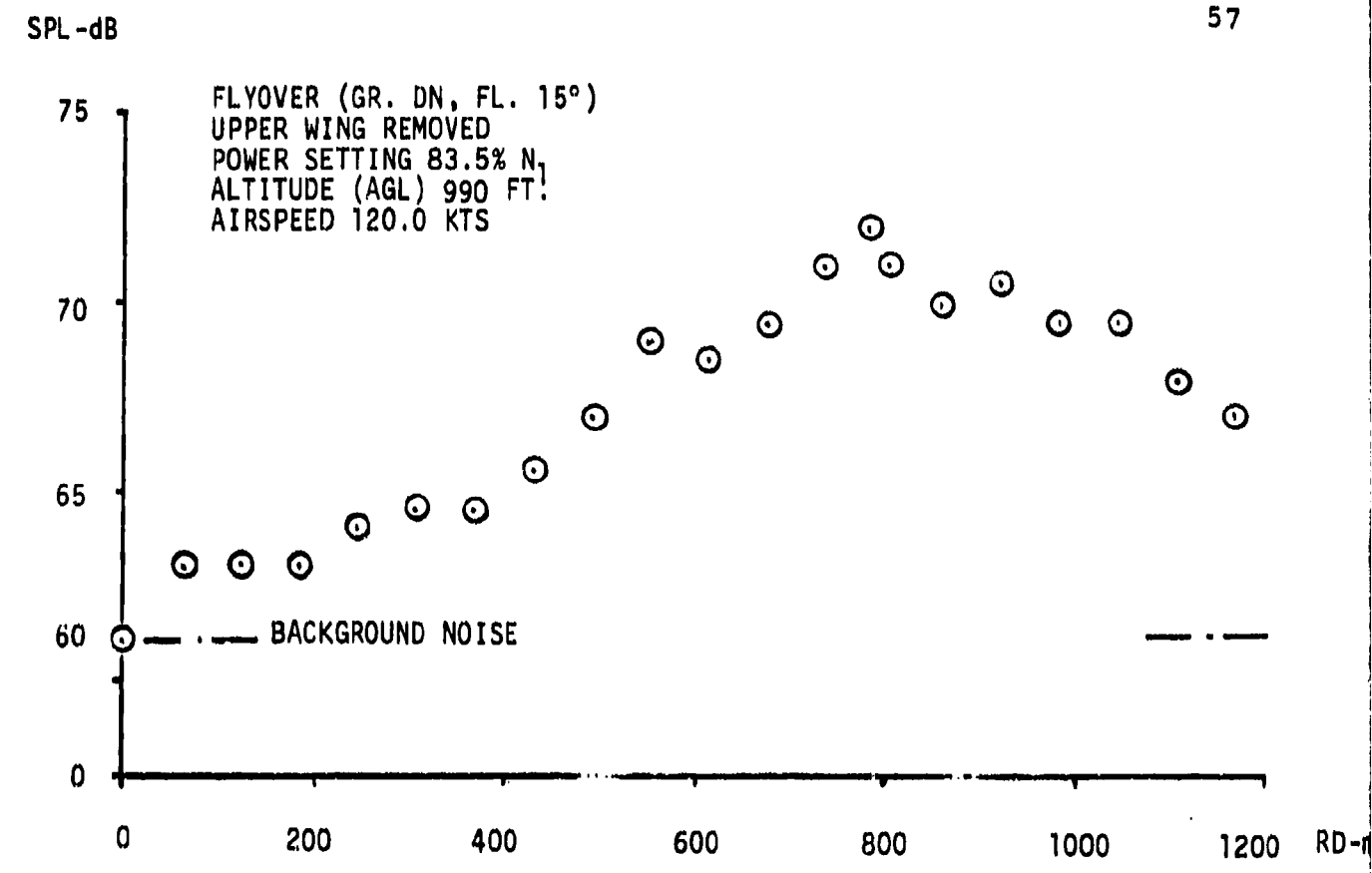

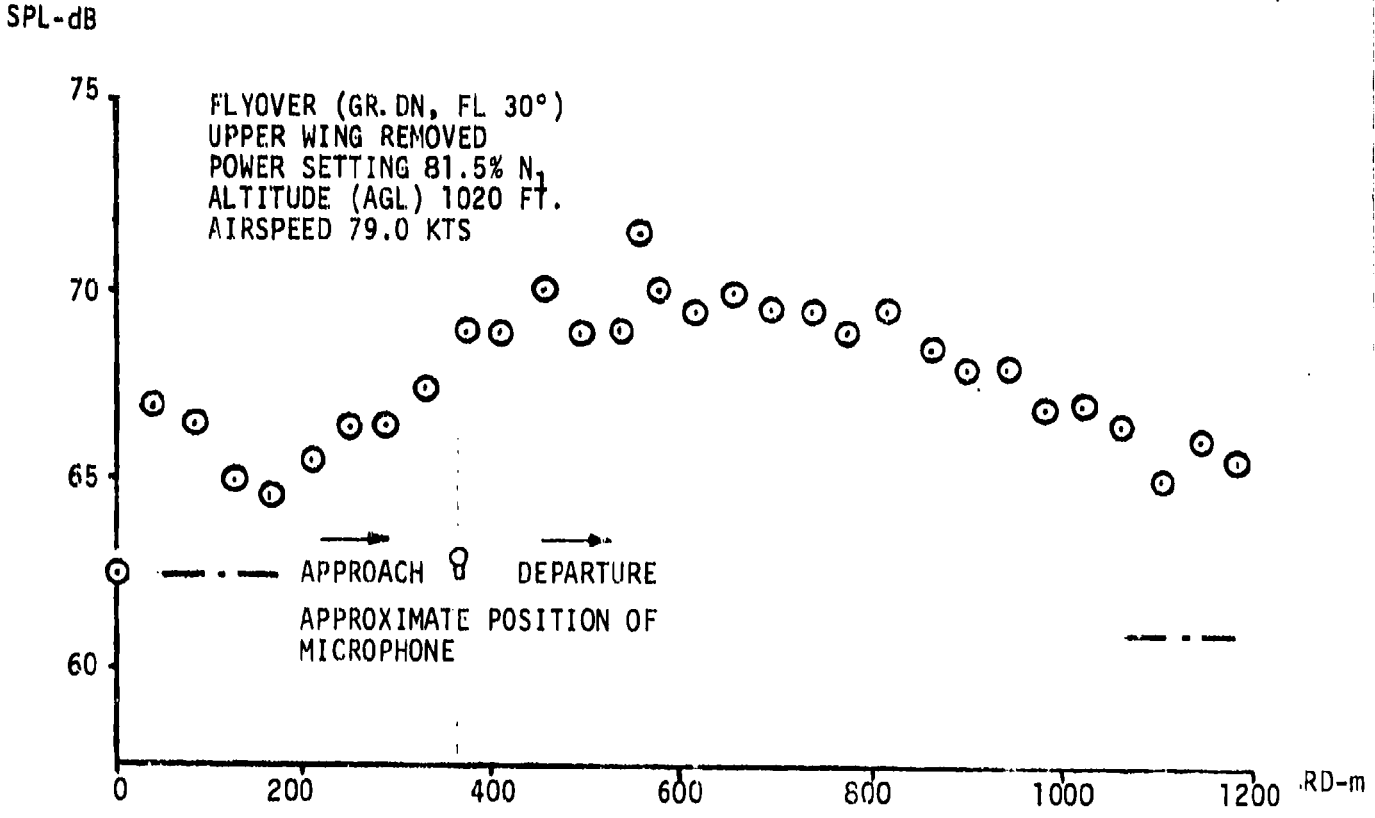

FIGURE 42
1000 FT. FLYOVER SOUND PRESSURE LEVEL SPL VS. RELATIVE DISTANCE RD

The data and results of the flyover noise measurements are listed in Table 2. From these data, the following average values for the peak noise pressure levels can be calculated:

a) Upper wing installed:

Clean configuration	71.5 dB
Gear down, flaps 30^0	71.5 dB

b) Upper wing removed:

Clean configuration	71.2 dB
Gear down, flaps 15^0	71.2 dB
Gear down, flaps 30^0	71.7 dB

These values show, that neither the upper wing, nor flap or gear position, have any significant effect on the flyover noise level. The overall peak noise of 71.7 dB proves the JETWING to be a very quiet jet aircraft.

Figure 43 shows the frequency spectrum of the JETWING while stationary on the ground, at idle power. The spectra were taken from three different positions relative to the aircraft (front, side, and rear), each from a distance of 60 feet.

As expected, in the rear spectrum the low frequency noise ($100 - 500 Hz$) dominates, coming from the exhaust nozzles and the turbulent interaction of the jet sheet with ambient air and aircraft structure.

The front sectrum is clearly dominated by the higher frequency noise ($2,000 - 10,000 Hz$) of the JT-15 engine compressor, while in the side spectrum both noise sources have similar amplitudes.

The upper wing panels show some effect in reducing the noise level, particularly in the side and rear spectra. For the lower frequencies, this can be explained by the fact that the upper wing panels act as ejectors, thereby thickening and slowing down the jet sheet. The turbulent break-up of this slower and thicker jet sheet is less noisy than the break up of the thinner jet sheet with higher velocity of the plain wing without winglet.

The reduction of high frequency noise may be due to shielding effects.

Table 2: JETWING FLYOVER NOISE DATA

A) UPPER WING REMOVED

Run	Description	Power Setting (% N_1)	Altitude (ft)	Airspeed (kts)	Elapsed Time (sec)	Max. Noise (dB)	Background Noise (dB)
1-1	Take-off	91.5	200	90.0	20.83	85.0	63.0/63.0
1-2	Gear down, flaps 15^0	82.5	1020	122.0	25.40	71.0	63.0/63.0
1-3	Gear down, flaps 15^0	82.5	1020	122.0	23.62	70.5	61.5/61.5
1-4	Gear down, flaps 15^{0*}	83.5	990	120.0	24.90	72.0	61.0/61.0
1-8	Clean configuration	81.9	1000	168.0	13.90	71.5	63.0/63.0
1-9	Clean configuration*	82.0	1000	167.0	17.75	70.5	63.0/61.0
1-10	Clean configuration	82.0	1000	168.0	14.50	74.0	61.5/63.5
2-1	Take-off*	92.0	240	95.0	23.30	84.0	62.0/62.0
2-2	Clean configuration	82.0	1000	167.0	14.60	69.5	61.0/61.0
2-4	Clean configuration	-	1000	165.0	13.00	70.5	63.0/61.5
2-7	Gear down, flaps 30^0	82.5	1000	76.0	32.00	71.5	64.5/64.5
2-8	Gear down, flaps 30^0	-	1010	77.0	29.35	72.0	62.5/62.5
2-10	Gear down, flaps 30^{0*}	81.5	1020	79.0	31.00	71.5	62.5/62.5

B) UPPER WING INSTALLED

Run	Description	Power Setting (% N_1)	Altitude (ft)	Airspeed (kts)	Elapsed Time (sec)	Max. Noise (dB)	Background Noise (dB)
3-0	Take-off	91.5	200	92.0	29.80	86.0	60.0/62.5
3-1	Clean configuration	82.0	1020	165.0	18.30	71.0	60.0/60.0
3-2	Clean configuration	83.0	990	164.5	19.00	72.0	60.0/60.0
3-3	Clean configuration	83.0	1010	166.5	22.50	71.0	60.0/60.5
3-4	Clean configuration	83.0	1000	167.5	21.10	72.0	60.0/60.5
3-7	Gear down, flaps 30^0	82.2	1030	82.0	37.30	73.0	60.0/60.0
3-8	Gear down, flaps 30^0	83.5	1000	75.0	37.80	70.0	61.0/60.0
3-10	Gear down, flaps 30^0	82.7	1020	77.0	35.90	71.5	61.5/60.5

* These runs are shown in figures 41 and 42.

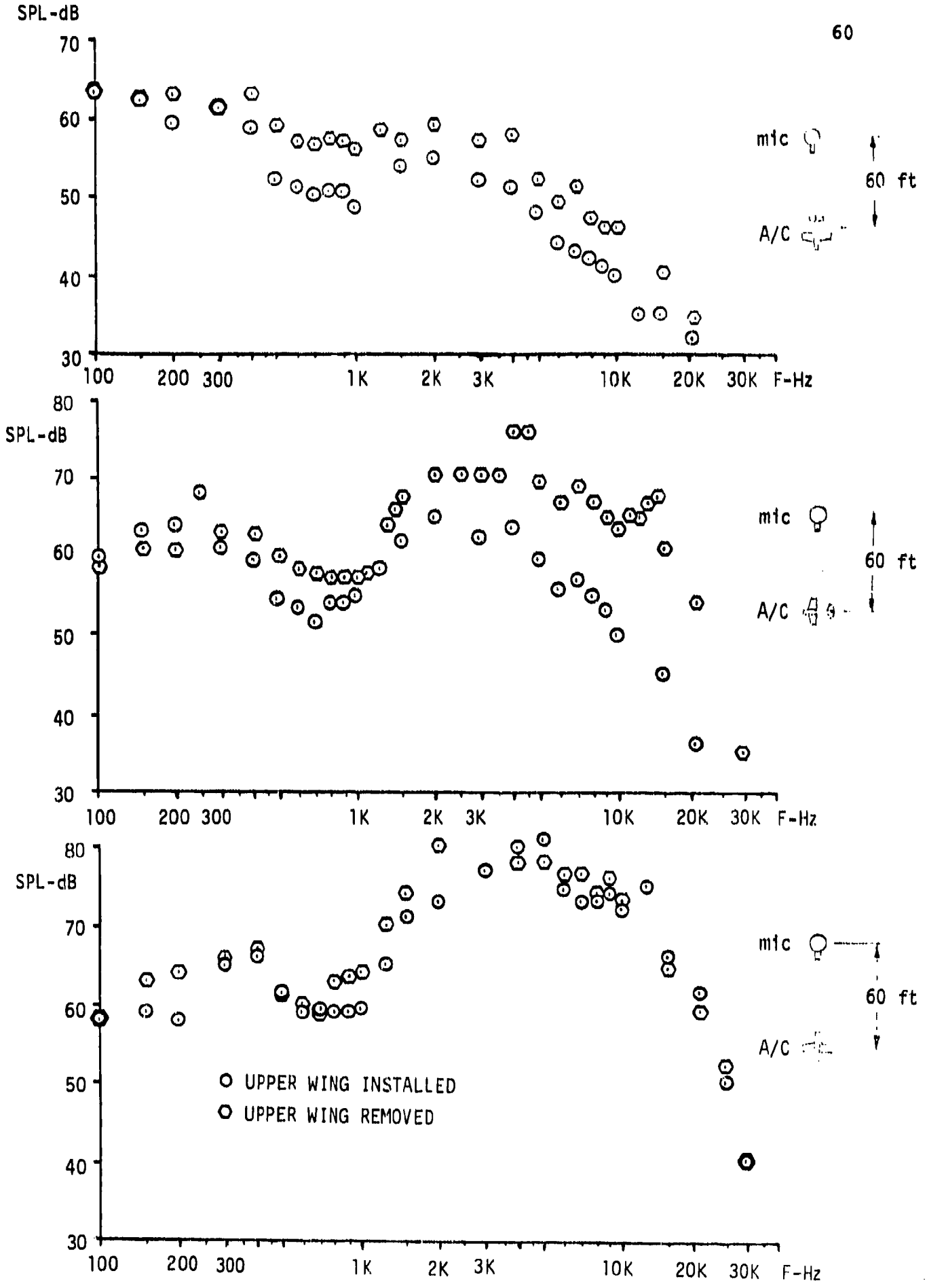

FIGURE 43
SOUND PRESSURE LEVEL (SPL) VS. FREQUENCY (F) FOR DIFFERENT JETWING POSITIONS

PART II

ANALYTICAL STUDY

SECTION I

INTRODUCTION

Analytical methods to predict forces of lift and drag as well as pitch, yaw and rolling moments on wings are essential for design purposes and have been developed for unblown wings to a high degree of accuracy and sophistication (e.g. finite element or panel methods). Some of these have been modified to include the effects of " powered lift", considering specific concepts like externally blown flaps, jet flaps, upper surface blowing etc. [6,7]. At this time, the consideration of such methods would be beyond the scope of this report and must be left to later investigations. Instead, the focus was on some less sophisticated methods that include simplifying assumptions and are likely to lead to results of lesser accuracy. However, these are valuable tools for the engineer who is concerned with preliminary design.

The basic theoretical properties of a thin two-dimensional jet in inviscid flow were formulated by Maskell and Gates [8], together with the overall momentum relations satisfied by the two-dimensional jet flapped aerofoil. Subsequently, jet flap theories were developed for the case of the thin wing and jet in inviscid incompressible flow, excluding mixing between the mainstream and the jet. The two-dimensional problem was solved by Spence using a treatment akin to classical "mean line " theory, both for ejection from the trailing edge [9] and over a plain hinged flap [10]. This treatment was extended to the case of a finite aspect ratio wing with a full span jet flap by Maskell and Spence [11], following the classical Prandtl lifting line theory; the equations being made tractable by prescribing an elliptic spanwise distribution of both wing chord and jet momentum with constant jet angle over the span. Yet in another approach, it was suggested to replace the jet by an equivalent mechanical flap extension in the plane of the flap [12] and treating the resulting wing just as any other wing .

The methods used by Williams [13], Wertz [14], and Jacobs [15] are based on this background, empirical methods [16], and experimental results. These three methods have been investigated and slightly modified for JETWING specifics and are presented in the following pages.

SECTION II

PREDICTION METHOD 1 (WILLIAMS)

This method closely follows a paper that was published by Williams, Butler and Wood [13] in 1963, which allows computation of not only the lift coefficient C_L as function of α, δ_F and C_J, but also the drag coefficient C_D vs. C_L.

LIFT COEFFICIENT

In their paper,"The Aerodynamics of Jet Flaps", they discussed historical, theoretical and experimental aspects of jet flaps in general and honored Spence's, Gate's and Maskell's work. Without further derivation the following formulas are then presented. The lift coefficient for a two-dimensional thin flat plate at angle of attack α, with blowing over a hinged flap to provide a jet deflection δ, is given by

$$C_\ell = C_{\ell\delta}\delta + C_{\ell\alpha}\alpha \qquad (II-1)$$

with

$$C_{\ell\delta} = \frac{\partial C_\ell}{\partial \delta} = [4\pi C_j(1 + 0.151C_j^{1/2} + 0.139C_j)]^{1/2} \qquad (II-2)$$

and

$$C_{\ell\alpha} = \frac{\partial C_\ell}{\partial \alpha} = 2\pi(1 + 0.151C_j^{1/2} + 0.219C_j) \qquad (II-3)$$

where

$$C_j = C_J\frac{S}{S'} \qquad (II-4)$$

is the mean sectional (2-D) blowing coefficient and S' is the wing reference area of the blown portion; C_J being the overall (3-D) blowing coefficient (see also Appendix I).

To obtain the three-dimensional lift coefficents for a finite aspect ratio wing, the two-dimensional values can be multiplied by the correction factor

$$G(A, C_j) = \frac{A + (2C_j/\pi)}{A + (2/\pi)C_{\ell\alpha} - 2(1+\sigma)} \qquad (II-5)$$

with

$$\sigma = \frac{(1-\varsigma)(C_j/\pi A)}{\varsigma - (1-\varsigma)(C_j/\pi A)} \qquad (II-6)$$

where

$$\varsigma = \frac{2C_\ell/(\delta+\alpha)}{\pi A + 2C_{\ell\alpha} - 2\pi(1+\sigma)} \qquad (II-7)$$

For small C_j or large A

$$G(A, C_j) \approx \frac{A + (2C_j/\pi)}{A + 2 + 0.604C_j{}^{1/2} + 0.876C_j} \qquad (II-8)$$

The simultaneous equations $(II-6)$ and $(II-7)$ in the two unknowns σ and ς are transformed into a transcendental equation in ς alone as

$$\varsigma\left(\pi A + 2C_{\ell\alpha} - 2\pi\left[1 + \frac{(1-\varsigma)(C_j/\pi A)}{\varsigma - (1-\varsigma)(C_j/\pi A)}\right]\right) = \frac{2C_\ell}{\delta+\alpha} \qquad (II-9)$$

Allowance for part-span flaps and fuselage cut-out is included by introducing spanwise extent factors λ and ν, where

$$\lambda = \frac{S'}{S} \qquad (II-10)$$

and

$$\nu = \frac{S'C_{\ell\alpha} + (S-S')\overline{C}_{\ell\alpha}}{SC_{\ell\alpha}}; \qquad \overline{C}_{\ell\alpha} = C_{\ell\alpha}\,|_{C_j=0} \qquad (II-11)$$

The effect of thickness to chord ratio t/c is taken into account by increasing the sectional pressure lift in the proportion $(1+t/c)$, roughly corresponding to the ratio of the sectional C_ℓ vs. α curve slope without blowing to the value 2π for a thin flat plate.

With these semi-empirical arguments, the lift on a jet-flap wing finally may be written as

$$C_L = G[(1+t/c)(\lambda C_{\ell\delta}\delta + \nu C_{\ell\alpha}\alpha)] - (t/c)C_J(\delta+\alpha) \qquad (II-12)$$

THRUST AND DRAG COEFFICIENTS

The excess thrust coefficient given by linearized inviscid flow theory for full-span jet flap wings becomes

$$C_{F_{ex}} = C_J - \frac{C_L^2}{\pi A + 2C_J} \qquad (II - 13)$$

where the last term on the right represents the "trailing vortex" drag associated with an elliptic spanwise distribution of loading. To examine the actual thrust deficiency in viscous flow, a more general form of equation $(II - 13)$ can usefully be considered:

$$C_{F_{ex}} = rC_J - C_{D0} - k\frac{C_L^2}{\pi A + 2C_J} \qquad (II - 14)$$

Here the "sectional thrust" is for convenience expressed as a proportion r of the theoretical value C_J, while the drag associated with finite aspect ratio effect is expressed as a proportion k of the theoretical value $C_L^2/(\pi A + 2C_J)$. The term C_{D0} represents the drag at zero lift, without flap deflection and blowing, as usual.

With a part-span jet flap, additional lift-dependent drag ΔC_{DP} can arise because of the departure from the normal spanwise distribution of lift, so equation $(II - 14)$ may be rewritten as

$$C_{F_{ex}} = rC_J - C_{D0} - k\frac{C_L^2}{\pi A + 2C_J} - \Delta C_{DP} \qquad (II - 15)$$

As a crude estimate the loss can be written

$$\Delta C_{DP} = \frac{\kappa \Delta C_L^2}{\pi A} \qquad (II - 16)$$

However, there is yet no sound theoretical basis for its prediction. Hence for estimation of excess thrust coefficient $C_{F_{ex}}$, ΔC_{DP} has been neglected and the factors r and k have been assumed to be unity in equation $(II - 15)$.

RESULTS

A FORTRAN program was developed using equation $(II - 12)$ for computation of C_L vs. α employing JETWING parameters. For our calculation of correction factor $G(A, C_j)$ equation $(II - 8)$ was used for values of $C_j < 1$. For values of $C_j > 1$, equation $(II - 5)$ was used with σ obtained from equation $(II - 6)$ after solving equation $(II - 9)$ for ς by a multivariate search program [17] for error minimization. For the computation of excess thrust coefficient $C_{F_{ex}}$ equation $(II - 15)$ was used. The zero lift drag coefficient C_{D0} was taken from wind tunnel data. The resulting C_L vs. α and C_L vs. $C_{F_{ex}}$ curves were plotted and are shown in figure 44 thru figure 51. For comparison, the NASA full scale wind tunnel data for the JETWING with upper wing removed were also plotted on these figures.

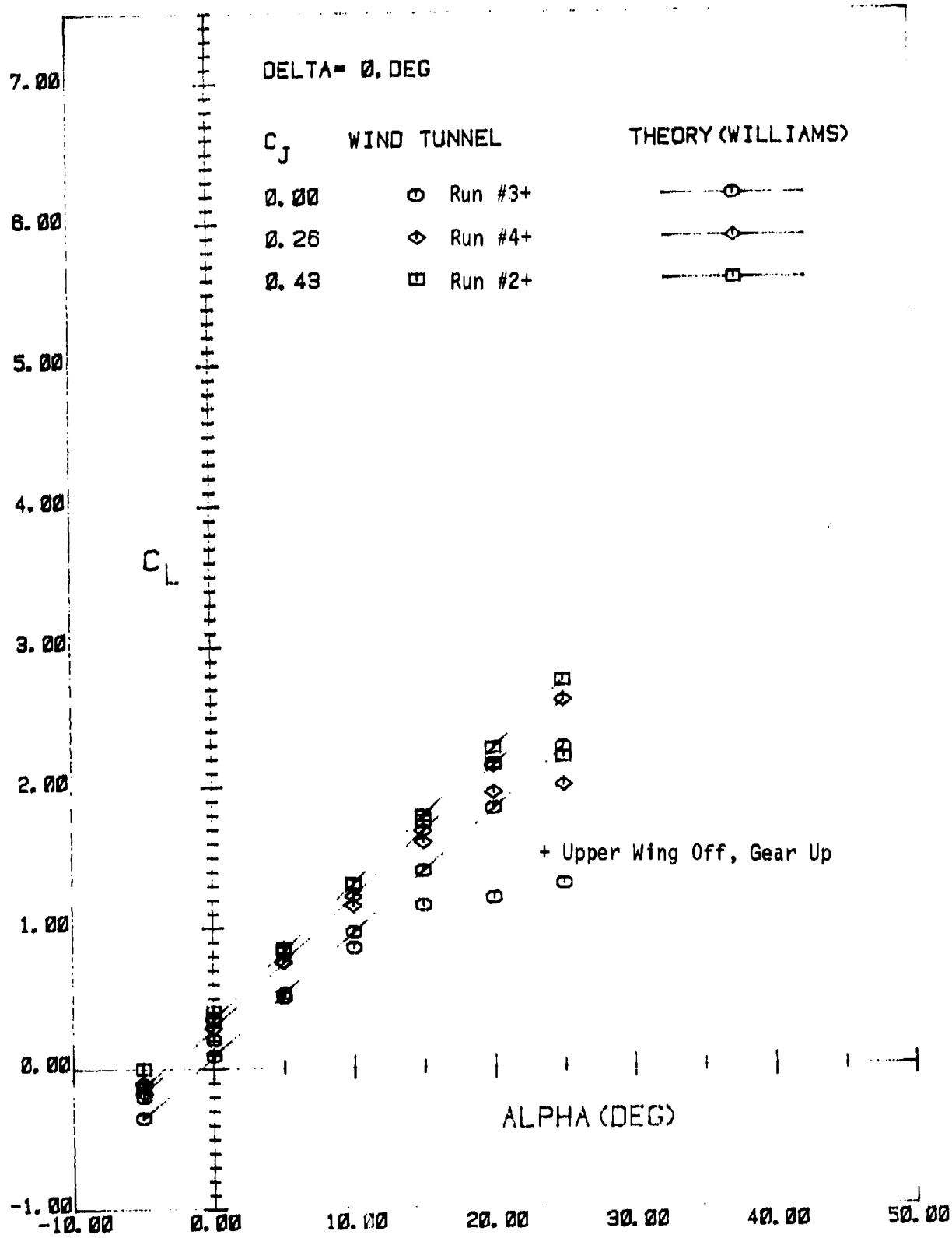

FIGURE 44

COMPARISON OF WILLIAMS METHOD THEORETICAL C_L vs α RESULTS AND NASA FULL SCALE WIND TUNNEL DATA ON JETWING JW-1 FOR $\delta_F = 0°$, UPPER WING REMOVED

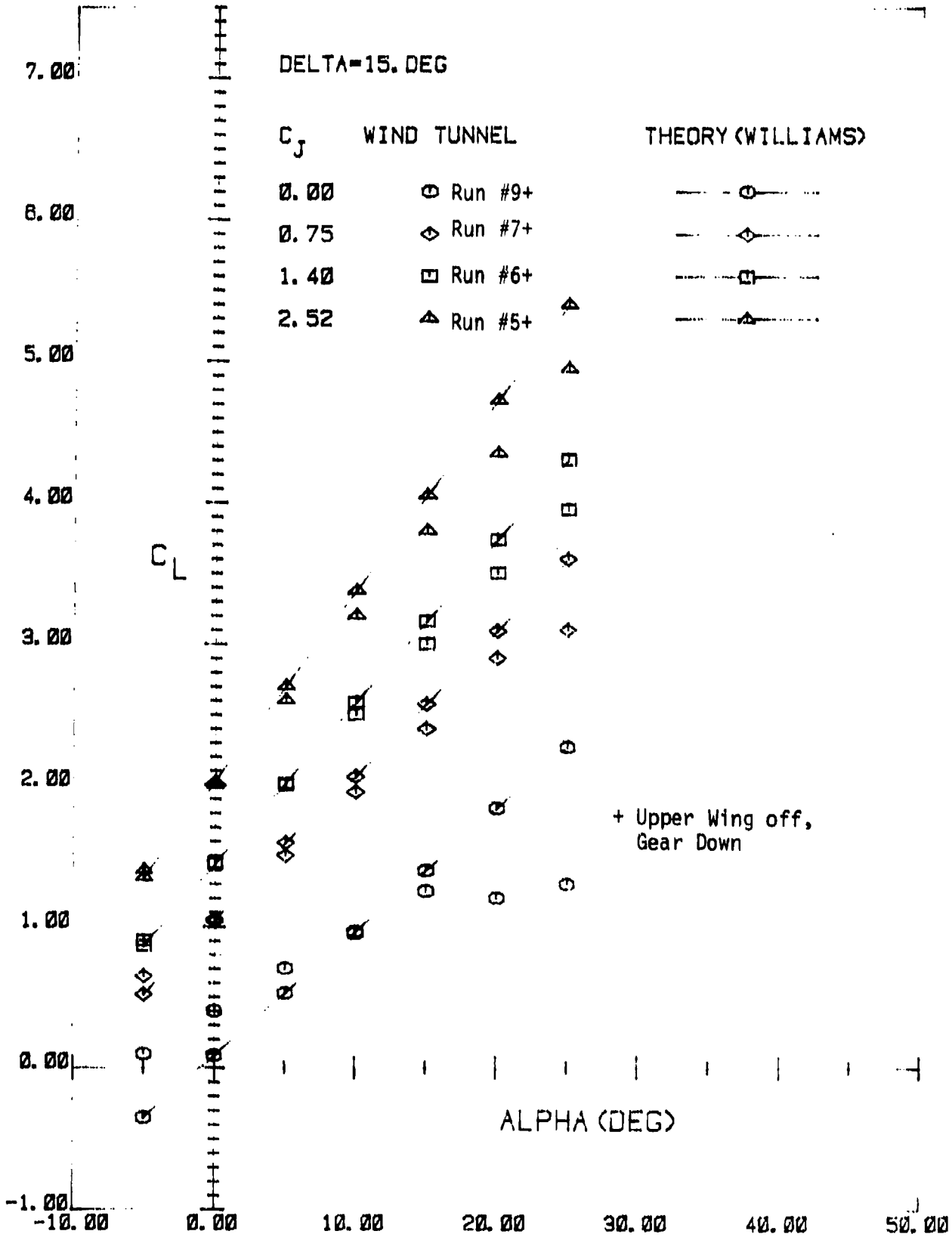

FIGURE 45

COMPARISON OF WILLIAMS METHOD THEORETICAL C_L vs α RESULTS AND NASA FULL SCALE WIND TUNNEL DATA ON JETWING JW-1 FOR δ_F = 15°, UPPER WING REMOVED

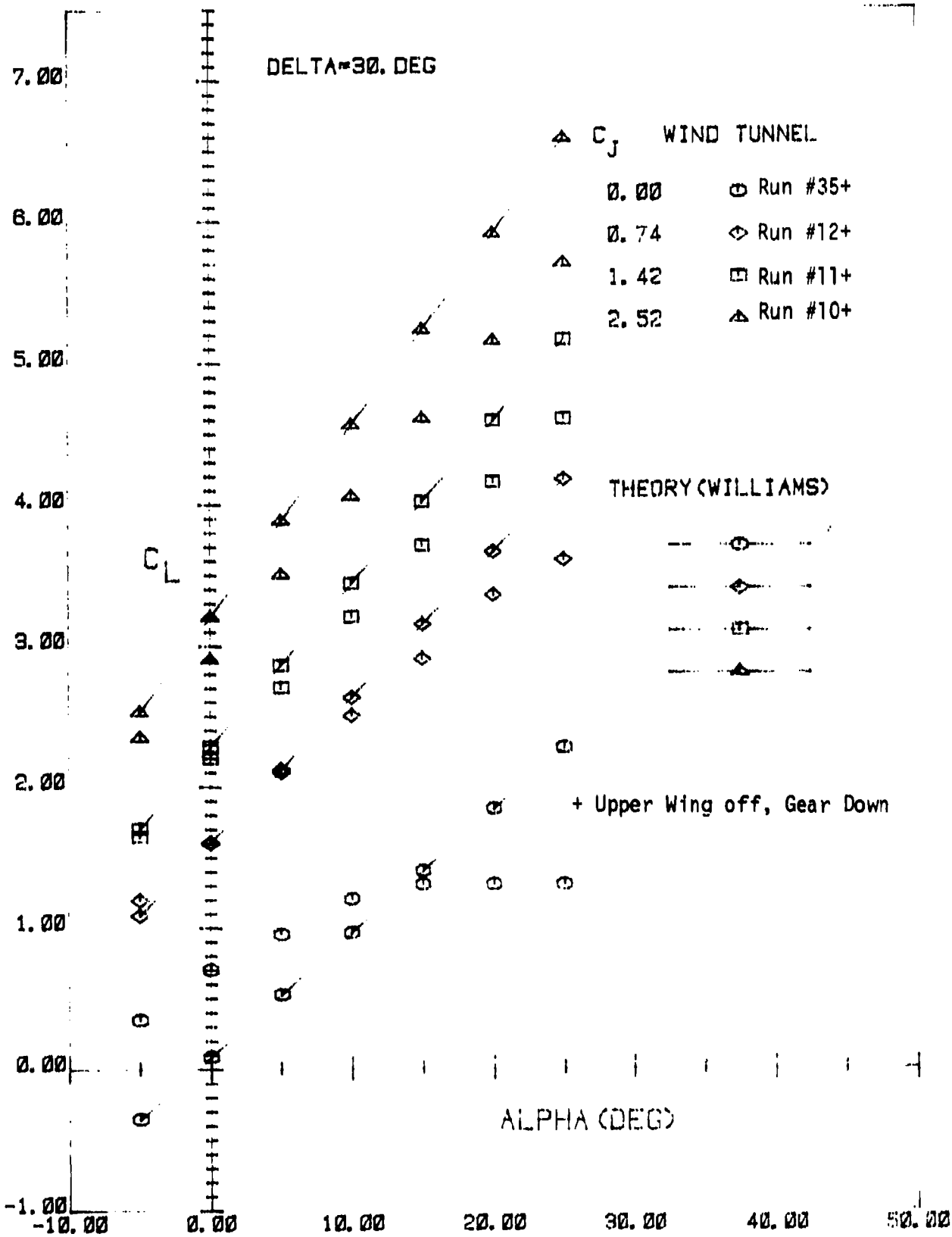

FIGURE 46

COMPARISON OF WILLIAMS METHOD THEORETICAL C_L vs α RESULTS AND NASA FULL SCALE WIND TUNNEL DATA ON JETWING JW-1 FOR δ_F = 30°, UPPER WING REMOVED

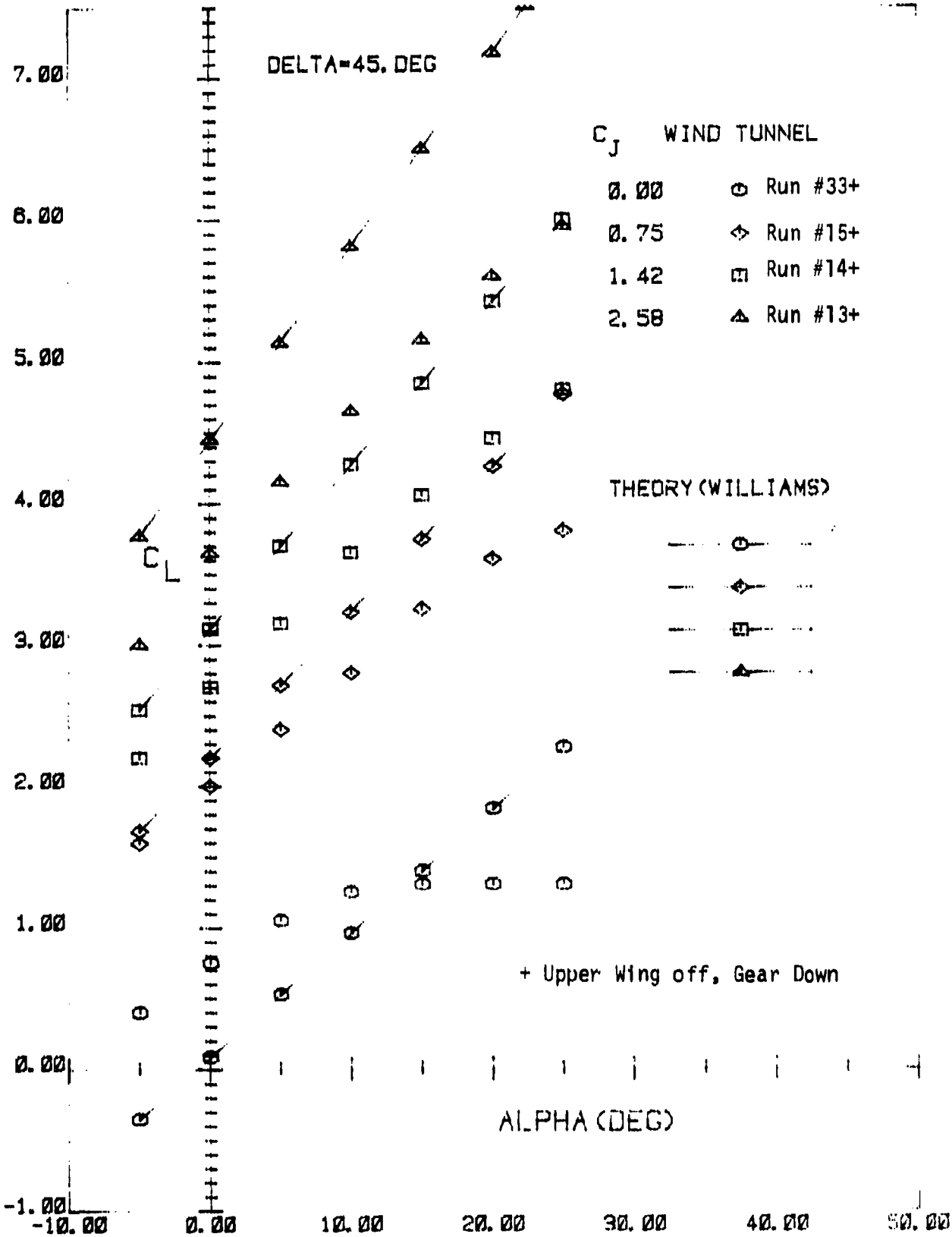

FIGURE 47

COMPARISON OF WILLIAMS METHOD THEORETICAL C_L vs α RESULTS AND NASA FULL SCALE WIND TUNNEL DATA ON JETWING JW-1 FOR δ_F = 45°, UPPER WING REMOVED

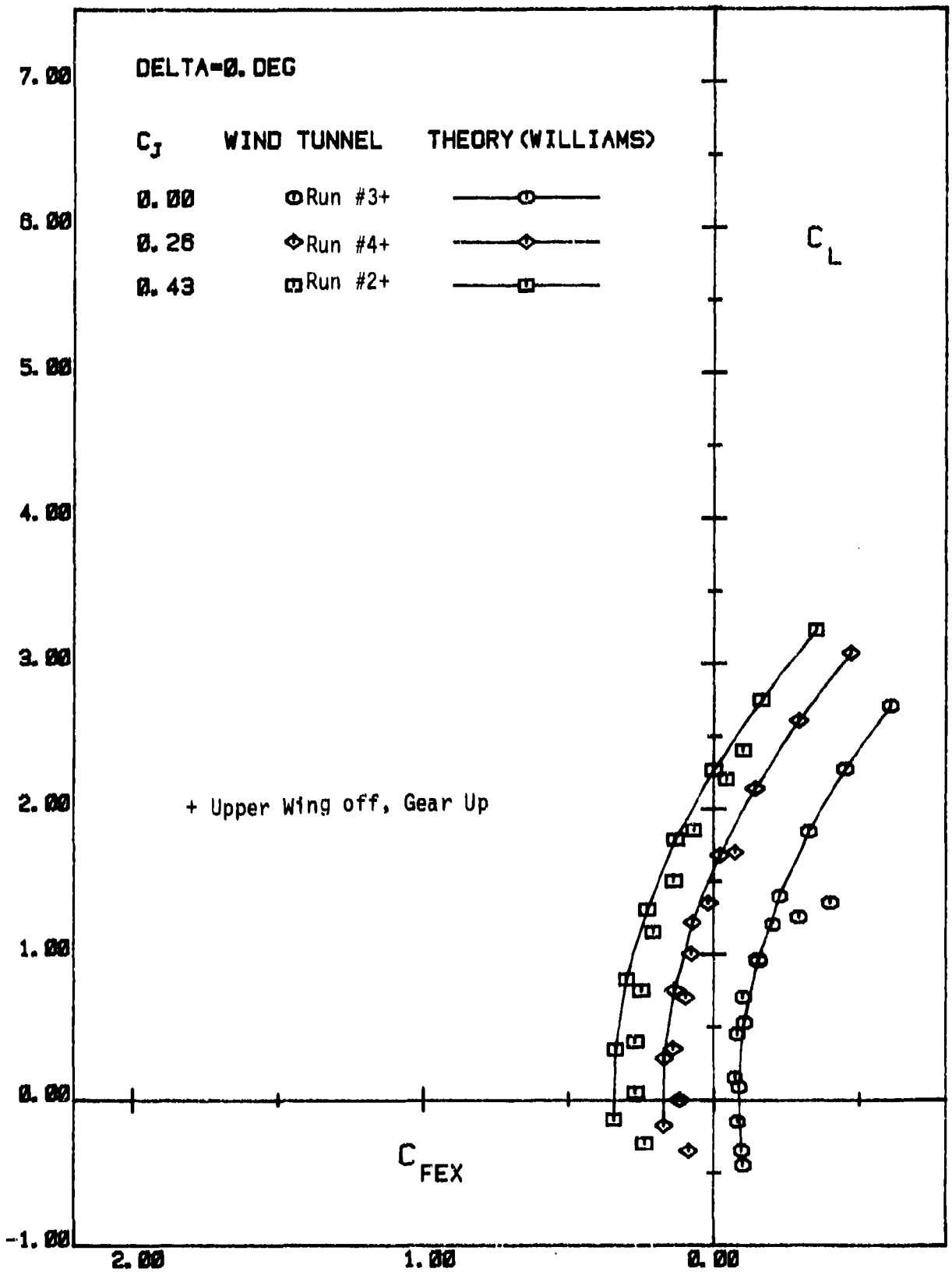

FIGURE 48

COMPARISON OF WILLIAMS METHOD THEORETICAL C_L vs C_{FEX} RESULTS AND NASA FULL SCALE WIND TUNNEL DATA ON JETWING JW-1 FOR $\delta_F = 0°$, UPPER WING REMOVED

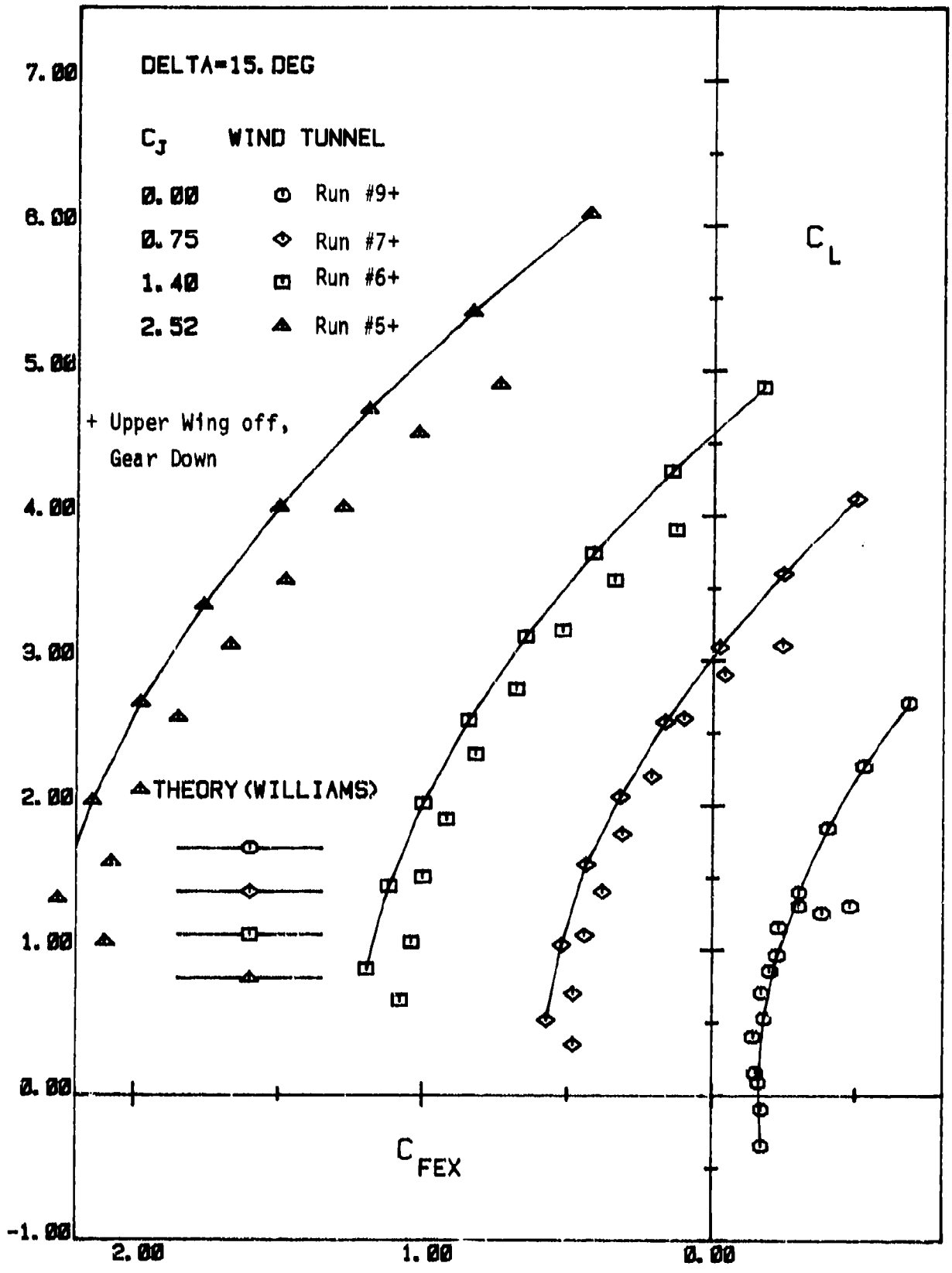

FIGURE 49

COMPARISON OF WILLIAMS METHOD THEORETICAL C_L vs C_{FEX} RESULTS AND NASA FULL SCALE WIND TUNNEL DATA ON JETWING JW-1 FOR $\delta_F = 15°$, UPPER WING REMOVED

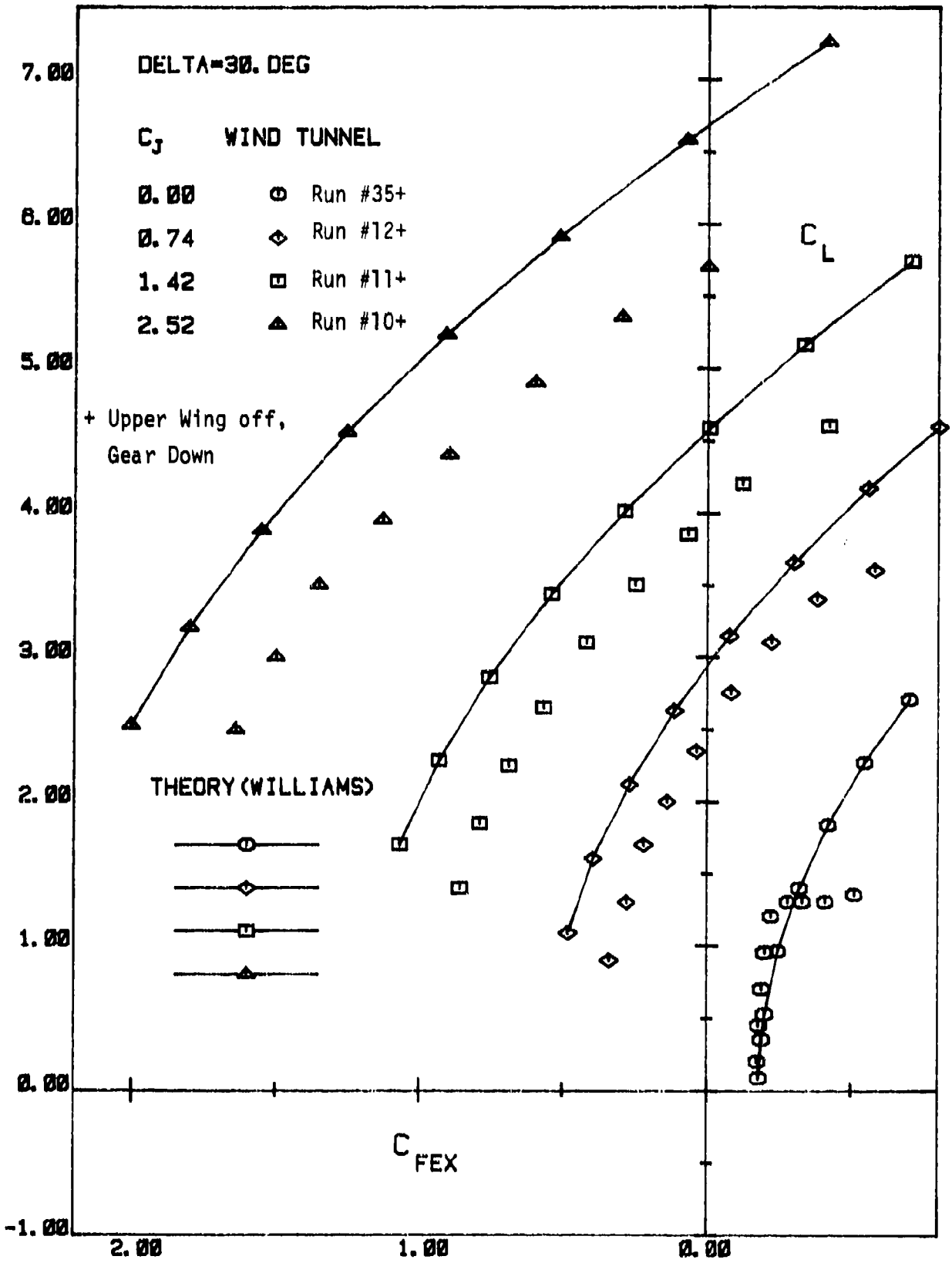

FIGURE 50

COMPARISON OF WILLIAMS METHOD THEORETICAL C_L vs C_{FEX} RESULTS AND NASA FULL SCALE WIND TUNNEL DATA ON JETWING JW-1 FOR $\delta_F = 30°$, UPPER WING REMOVED

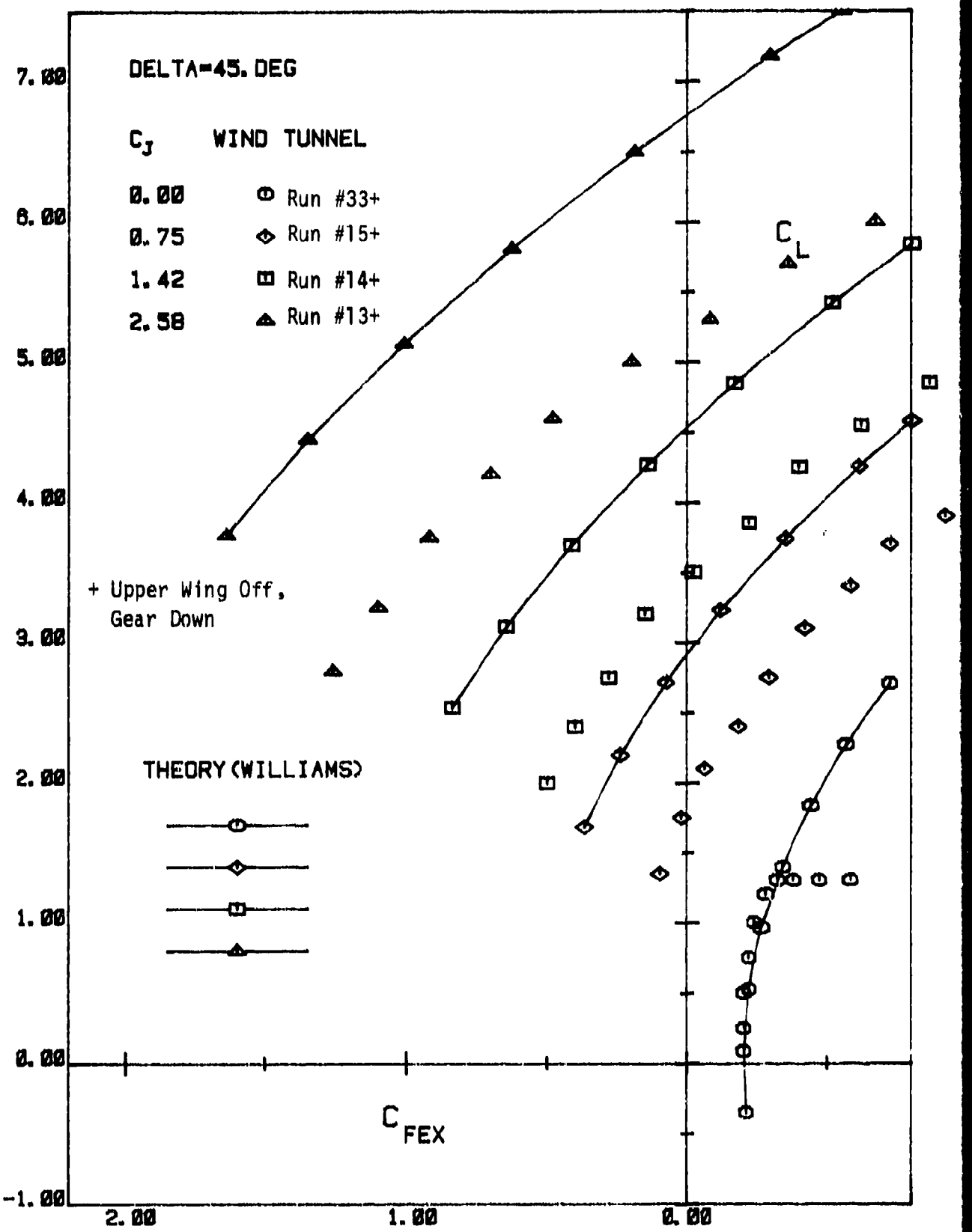

FIGURE 51

COMPARISON OF WILLIAMS METHOD THEORETICAL C_L vs C_{FEX} RESULTS AND NASA FULL SCALE WIND TUNNEL DATA ON JETWING JW-1 FOR δ_F = 45°, UPPER WING REMOVED

SECTION III

PREDICTION METHOD 2 (WERTZ)

This method follows an approach done by R. D. Wertz [14] in 1976, where he used the then known design parameters of the JETWING to predict the lift coefficient as functions of blowing coefficient, flap deflection and angle of attack. Since this work was done, some of the design features have changed. These were incorporated into Wertz's method and equations were modified accordingly to account for actual JETWING data.

SUMMARY

In his paper "Application of Spence's Methods and Data to Prediction of Lift Coefficients of the JETWING," Wertz started out with Spence's formula for two dimensional blown jet flap lift [10] and separated the total lift into three contributions:

- aerodynamic lift of airfoil due to angle of attack and flap deflection
- supercirculation lift due to blowing
- direct jet lift due to the vertical component of jet momentum

In going to three dimensions, Wertz used Maskell and Spence's techniques [11] and the Rockwell method described in Woodward's paper [16]. At several points Wertz departed from these procedures and used empirical curves [18] or JETWING specific data [19]. His final equation then is of the following form:

$$C_L = [C_{LA\alpha} + C_{L\Gamma\alpha}]\sin(\alpha - \alpha_0) + [C_{LA\delta} + C_{L\Gamma\delta}]\sin\delta + C_J \sin(\alpha + \delta)$$

To account for the actual difference between flap and jet deflection angles, Wertz's approach was modified and the following equation derived:

$$C_L = [C_{LA\alpha} + C_{L\Gamma\alpha}]\sin(\alpha - \alpha_0) + C_{LA\delta}\sin\delta_F + C_{L\Gamma\delta}\sin\delta_J + C_J \sin(\alpha + \delta_J)$$

DERIVATION

1. Breaking up Two-Dimensional Lift into Components.

The starting point is equation (35) in Spence's paper [10].

$$C_\ell = 2\pi(1 + 2B_0)\alpha + 2(\chi + \sin\chi + 2\pi D_0)\delta \qquad (III - 1)$$

This assumes potential flow over a flat plate with flap, therefore the geometric and aerodynamic angle of attack coincide as well as the jet and flap deflection angle.

In this equation the conventional aerodynamic lift coefficients for the basic airfoil are contained in

$$C_{\ell_a} = 2\pi\alpha + 2(\chi + \sin\chi)\delta \qquad (III-2)$$

where the χ terms are defined in Spence [10] as:

$$\chi = 2\sin^{-1}\sqrt{c_f/c}$$

The jet terms including the direct jet lift are contained in

$$C_{\ell_j} = 4\pi(B_0\alpha + D_0\delta) \qquad (III-3)$$

where the B_0 and D_0 terms are leading Fourier coefficients developed in Spence [9,10].
In order to separate direct jet lift from supercirculation lift, equation $(III-3)$ is rewritten

$$C_{\ell_j} = C_{\ell_r} + C_j\sin(\alpha+\delta) \qquad (III-4)$$

where C_{ℓ_r} is the section supercirculation lift coefficient. For small angles we can write

$$C_{\ell_j} = C_{\ell_r} + C_j(\alpha+\delta) \qquad (III-5)$$

Now from equation $(III-3)$

$$C_{\ell_r} = 4\pi(B_0\alpha + D_0\delta) - C_j(\alpha+\delta)$$

or

$$C_{\ell_r} = (4\pi B_0 - C_j)\alpha + (4\pi D_0 - C_j)\delta \qquad (III-6)$$

and the total lift coefficient is then

$$C_\ell = C_{\ell_a} + C_{\ell_r} + C_j(\alpha+\delta) \qquad (III-7)$$

2. Airfoil Pressure Lift Correction for Three Dimensions

Equation $(III-2)$ gives:

$$C_{\ell a} = 2\pi\alpha + 2(\chi + \sin\chi)\delta$$

or in general:

$$C_{\ell a} = C_{\ell a\alpha}(\alpha - \alpha_0) + C_{\ell a\delta}\delta \qquad (III-8)$$

and for three dimensions:

$$C_{LA} = C_{LA\alpha}(\alpha - \alpha_0) + C_{LA\delta}\delta \qquad (III-9)$$

From Perkins and Hage [18], pp. 84 we get:

$$C_{LA\alpha} = f\frac{a_0}{1 + 57.3a_0/\pi A} \qquad (III-10)$$

where a_0 is a representative section lift curve slope per degree. For a NACA 23015 airfoil $a_0 = 0.104$ per degree or $C_{\ell a\alpha} = 5.958$ rather than $C_{\ell a\alpha} = 2\pi$ as given in equation $(III-2)$. The factor f is a function of the taper ratio c_t/c_r which is 0.46 for the JETWING. Figure 2-55 in Perkins and Hage [18] gives an f of approximately 1. With the JETWING aspect ratio $A = 4.48$ we get

$$a_W = C_{LA\alpha} = 0.0731 \qquad (III-11)$$

The flap term can be written as:

$$C_{LA\delta} = \frac{S'}{S}\frac{a_W}{a_0}C_{\ell a\delta} = \frac{S'}{S}\frac{a_W}{a_0}2(\chi + \sin\chi) \qquad (III-12)$$

With the JETWING data, flapped wing area $S' = 77ft^2$, wing area $S = 105.6ft.^2$, $\chi = 1.22/rad$,

$$C_{LA\delta} = 2.23/rad = .0388/deg \qquad (III-13)$$

This yields

$$C_{LA} = 0.0731(\alpha - \alpha_0) + 0.0388(\delta_F) \qquad (III-14)$$

Wertz mentioned that because the airfoil was altered from the NACA 23015 to accomodate the jet slot, Bartoe had used for a_W an estimate of 0.065. Adjusting equation (III – 14) by that factor results in

$$C_{LA} = 0.065(\alpha - \alpha_0) + 0.0345(\delta_F) \qquad (III - 15)$$

with angles in degrees and

$$C_{LA} = 3.7(\alpha - \alpha_0) + 2.0(\delta_F) \qquad (III - 16)$$

with angles in radians.

Wertz thought that the flap term still appeared too large, so using the elevator effectiveness curve of Perkins and Hage [18] p. 250, he determined that the $C_{LA\delta}$ should not be more than $0.5C_{LA\alpha}$. Therefore using this assumption:

$$C_{LA} = 3.7(\alpha - \alpha_0) + 1.4(\delta_F) \qquad (III - 17)$$

3. Supercirculation Lift Correction for Three Dimensions

Equation (III – 6) gives:

$$C_{\ell\Gamma} = (4\pi B_0 - C_j)\alpha + (4\pi D_0 - C_j)\delta$$

or in general

$$C_{\ell\Gamma} = C_{\ell\Gamma\alpha}(\alpha - \alpha_0) + C_{\ell\Gamma\delta}(\delta) \qquad (III - 18)$$

and for three dimensions:

$$C_{L\Gamma} = C_{L\Gamma\alpha}(\alpha - \alpha_0) + C_{L\Gamma\delta}(\delta) \qquad (III - 19)$$

Equation (14) of Woodlard's paper (Rockwell's method) [16] writes:

$$C_{L\Gamma} = (1 + t/c)F[\nu C_{\ell\Gamma\alpha}\alpha + \lambda C_{\ell\Gamma\delta}\sin\delta] \qquad (III - 20)$$

Instead of using the thickness correction $(1 + t/c)$, Wertz used $(a_0/2\pi)$, with a_0 being the specific wing section characteristic.

For calculation of the derivatives and 3-D correction factors, the overall three-dimensional blowing coefficient C_J is modified, using Rockwell's method [16] (see also Appendix I):

$$C_j = C_J \frac{S}{S''} \qquad (III-21)$$

where

$$S'' = S' + \frac{1}{2}(S - S') \qquad (III-22)$$

For the JETWING this yields

$$C_j = 1.19 C_J \qquad (III-23)$$

Rockwell also modifies the section lift coefficients by coefficients λ and ν, to correct for partial span flaps and blowing.

$$\lambda = \frac{S''}{S} \qquad (III-24)$$

For the JETWING

$$\lambda = 0.84 \qquad (III-25)$$

The coefficient ν is a function of $\lambda, C_J, C_{l\alpha}$ and Wertz assumed it to be

$$\nu = 1 \qquad (III-26)$$

From Woolard's paper [16] we have

$$F(A, \eta C_j) = G + \frac{2G^2\sigma}{A + (2/\pi)C_j} \qquad (III-27)$$

where η is the jet turning efficiency. It is assumed to be 1. Spence has used in [11]

$$G = \frac{A + 0.637 C_j}{A + 2 + 0.604 C_j{}^{1/2} + 0.870 C_j} \qquad (III-28)$$

Also

$$\sigma = \frac{(1-\varsigma)(C_j/\pi A)}{\varsigma - (1-\varsigma)(C_j/\pi A)} \qquad (III-29)$$

where

$$\varsigma = \frac{(2/\pi)C_\ell/(\alpha+\delta)}{A+(2/\pi)C_{\ell\alpha}-2} \qquad (III-30)$$

To get an estimate for ς, Wertz assumed the following:

a) Let

$$\frac{C_\ell}{(\alpha+\delta)} = \frac{C_\ell}{\alpha} = \frac{\partial C_\ell}{\partial \alpha} = C_{\ell\alpha} = 2\pi,$$

then

$$\varsigma = \frac{(2/\pi)2\pi}{A+(2/\pi)2\pi-2} = 0.62 \qquad (III-31)$$

b) Let

$$\frac{C_\ell}{(\alpha+\delta)} = \frac{C_{\ell\alpha}+C_{\ell\delta}}{2} = \frac{2\pi(1+0.5)}{2} = 1.5\pi,$$

then

$$\varsigma = \frac{(2/\pi)1.5\pi}{A+(2/\pi)1.5\pi-2} = 0.55 \qquad (III-32)$$

Arguing that the σ term is small compared to the other terms for the 3-D correction, Wertz felt justified to use an average value of

$$\lambda = 0.6 \qquad (III-33)$$

This yields

$$\sigma = \frac{0.1C_j}{0.6\pi - 0.1C_j} \qquad (III-34)$$

Now the function F can be computed for parametric blowing coefficients. The derivatives in equation $(III-20)$ can be expressed through equation $(III-6)$:

$$C_{\ell\Gamma\alpha} = 4\pi B_0 - C_j \qquad (III-35)$$

and

$$C_{\ell\Gamma\delta} = 4\pi D_0 - C_j \qquad (III-36)$$

The Fourier coefficient terms B_0 are evaluated for a number of blowing coefficients in Spence [9], Table 1 ,p.58 From equation $(III-1)$ we know that

$$C_{\ell\delta} = 2(\chi + \sin\chi + 2\pi D_0)$$

and the terms D_0 can be determined by

$$D_0 = \frac{C_{\ell\delta} - 2(\chi + \sin\chi)}{4\pi} \qquad (III-37)$$

where values of $C_{\ell\delta}$ are contained in Spence [10], Table 1 ,p.294. It is a function of the flap chord to wing chord ratio c_f/c and the blowing coefficient C_j, and has to be interpolated for JETWING values ($c_f/c = 0.33$). Knowing the coefficients B_0 and D_0 for a number of C_J, the derivatives $C_{\ell\Gamma\alpha}$ and $C_{\ell\Gamma\delta}$ can be computed also.

The three-dimensional derivatives $C_{L\Gamma\alpha}$ and $C_{L\Gamma\delta}$ can then be calculated as

$$C_{L\Gamma\alpha} = \frac{a_0}{2\pi} F C_{\ell\Gamma\alpha} \qquad (III-38)$$

and

$$C_{L\Gamma\delta} = \frac{a_0}{2\pi}\frac{S''}{S} F C_{\ell\Gamma\delta} \qquad (III-39)$$

These can be substituted into equation $(III-19)$

$$C_{L\Gamma} = C_{L\Gamma\alpha}(\alpha - \alpha_0) + C_{L\Gamma\delta}(\delta).$$

4. Final Equation

Starting out from two-dimensional lift components, equation $(III-7)$, Wertz arrived at the equation for the three-dimensional lift coefficient:

$$C_L = C_{LA} + C_{L\Gamma} + C_J \sin(\alpha + \delta) \qquad (III-40)$$

For the total lift, he then let the basic aerodynamic and supercirculation lift terms also vary with the sine of the angle. He gave no explanation, but for justification it may be argued, that for higher angles of attack and higher flap angles the lift generation becomes nonlinear due to partial separation and non perfect turning of the jet. Therefore, the idea of linear terms variation with the sine of the angles, may be a reasonable approximation that accounts for these effects.

We have then

$$C_L = [C_{LA\alpha} + C_{LT\alpha}]\sin(\alpha - \alpha_0) + [C_{LA\delta} + C_{LT\delta}]\sin\delta + C_J \sin(\alpha + \delta) \qquad (III - 41)$$

This assumes, that the thrust line is parallel to the flap chord. Actually, the upper surface of the flap is inclined 9^0 to the flap chord ($\delta_j = 9^0$). This can be corrected in the jet lift terms by setting

$$\delta_J = \delta_F + \delta_j \qquad (III - 42)$$

This, together with the zero lift angle of attack $\alpha_0 = -1^0$ from NACA 23015 airfoil data makes the final equation write:

$$C_L = [3.7 + C_{LT\alpha}]\sin(\alpha + 1) + 1.4\sin\delta_F + C_{LT\delta}\sin\delta_J + C_J \sin(\alpha + \delta_J). \qquad (III - 43)$$

RESULTS

A Fortran program was written, using Table 1 from [9] and Table 1 from [10] for interpolation, and equation $(III - 43)$ for calculating the lift coefficient C_L vs. α and parametric values of flap deflection δ_F and blowing coefficient C_J. Wertz method also permit the total lift coefficient to be broken up into contributions from basic aerodynamic lift, supercirculation lift and lift from jet reaction. The corresponding components of the wind tunnel data were determined as follows:

- $C_L(AE)$, the basic aerodynamic lift of the wing was taken from a no blowing data run.

- $C_L(J)$, the lift from jet reaction was determined from

$$C_L(J) = C_J \sin(\alpha + \delta_J)$$

- $C_L(TOT)$, the total lift was taken derectly from wind tunnel data.

- $C_L(S)$, the supercirculation lift was determined from

$$C_L(S) = C_L(TOT) - C_L(AE) - C_L(J)$$

Data from the NASA full scale wind tunnel tests with upper wing removed are plotted together with the theoretical results in figures 52 thru 55. Some of these wind tunnel data are broken up into components and compared to similar components derived by Wertz method. These comparisons are shown in figures 56 thru 59.

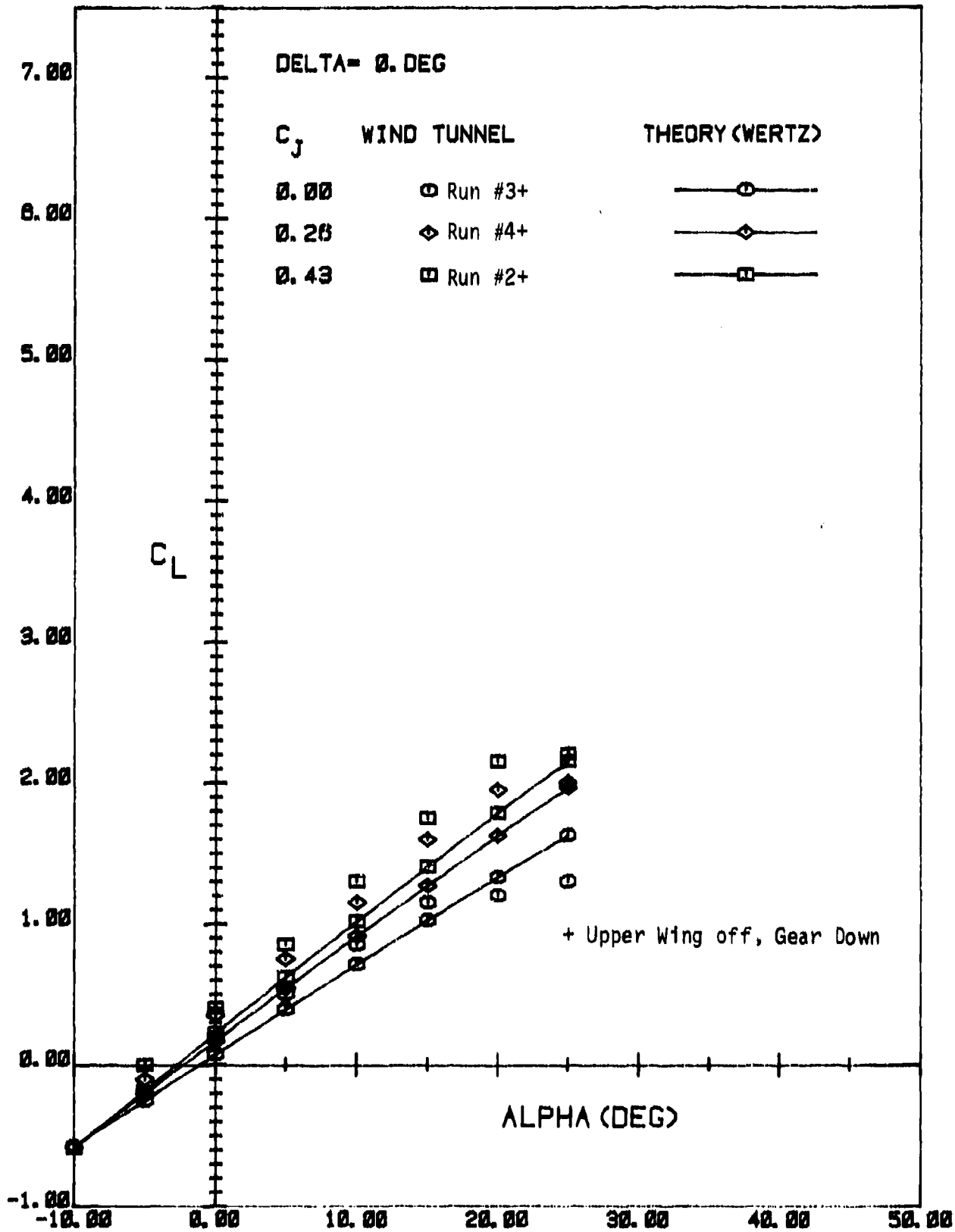

FIGURE 52

COMPARISON OF WERTZ METHOD THEORETICAL C_L vs α RESULTS AND NASA FULL SCALE WIND TUNNEL DATA ON JETWING JW-1 FOR δ_F = 0°, UPPER WING REMOVED

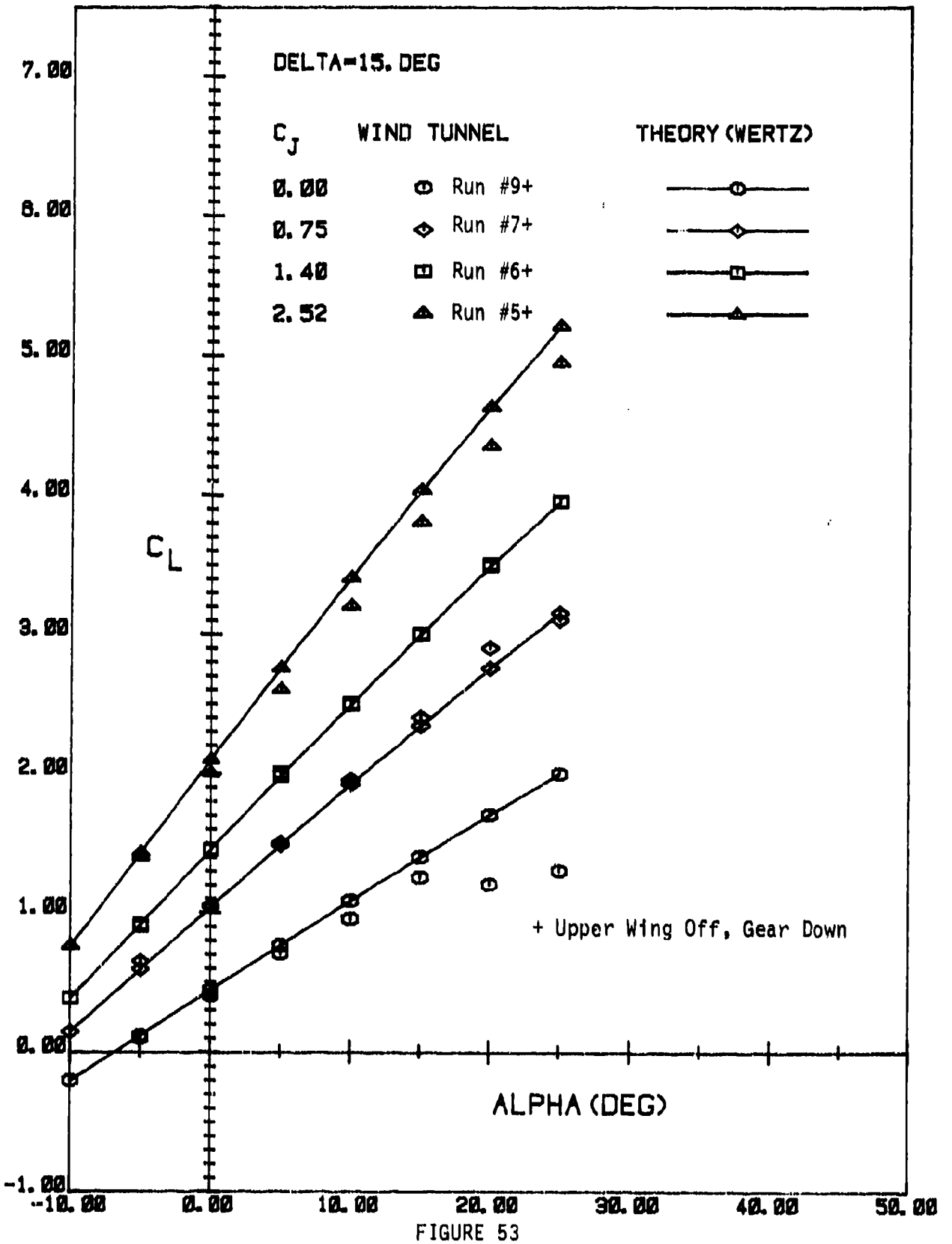

FIGURE 53

COMPARISON OF WERTZ METHOD THEORETICAL C_L vs α RESULTS AND NASA FULL SCALE WIND TUNNEL DATA ON JETWING JW-1 FOR δ_F = 15°, UPPER WING REMOVED

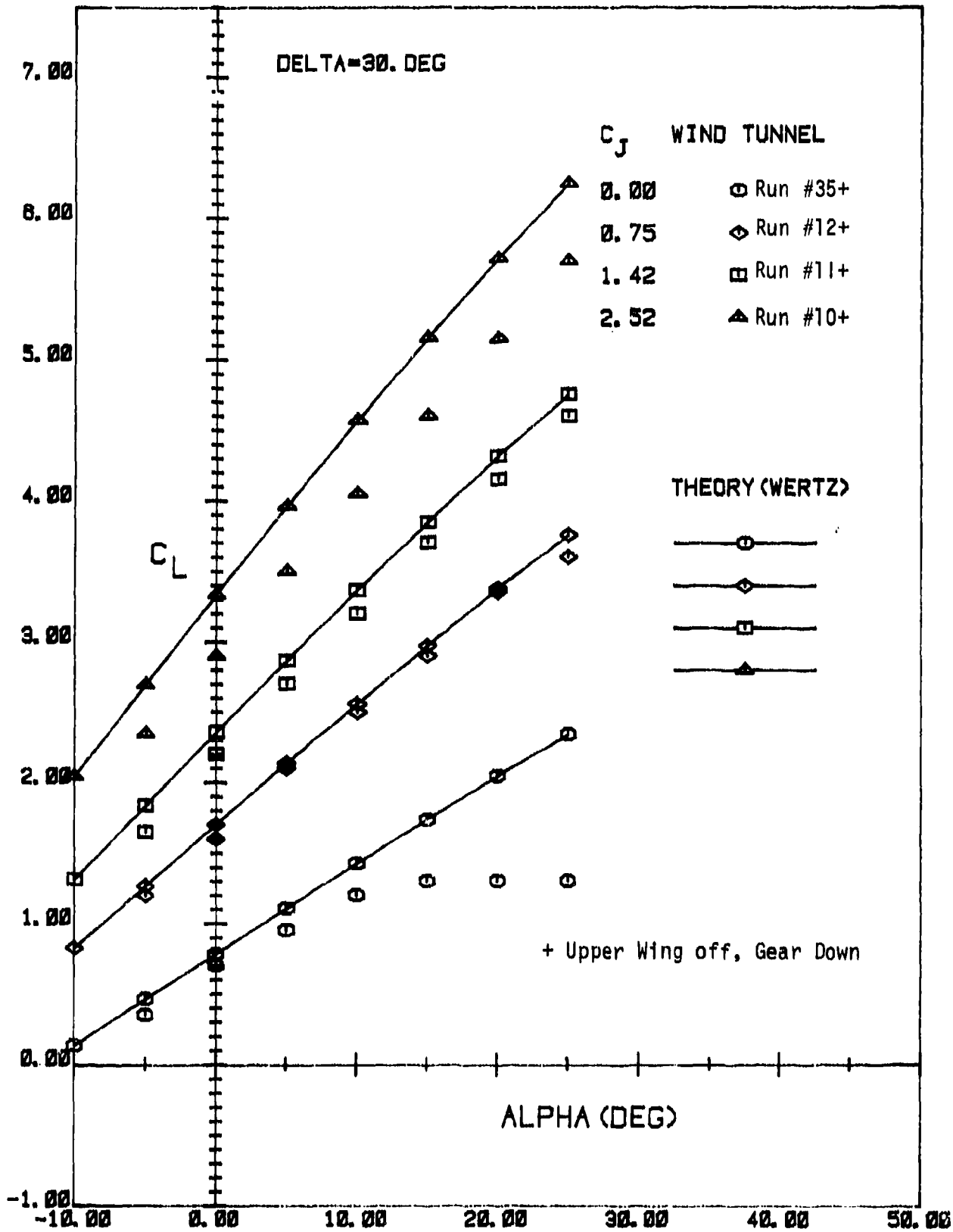

FIGURE 54

COMPARISON OF WERTZ METHOD THEORETICAL C_L vs α RESULTS AND NASA FULL SCALE WIND TUNNEL DATA ON JETWING JW-1 FOR δ_F = 30°, UPPER WING REMOVED

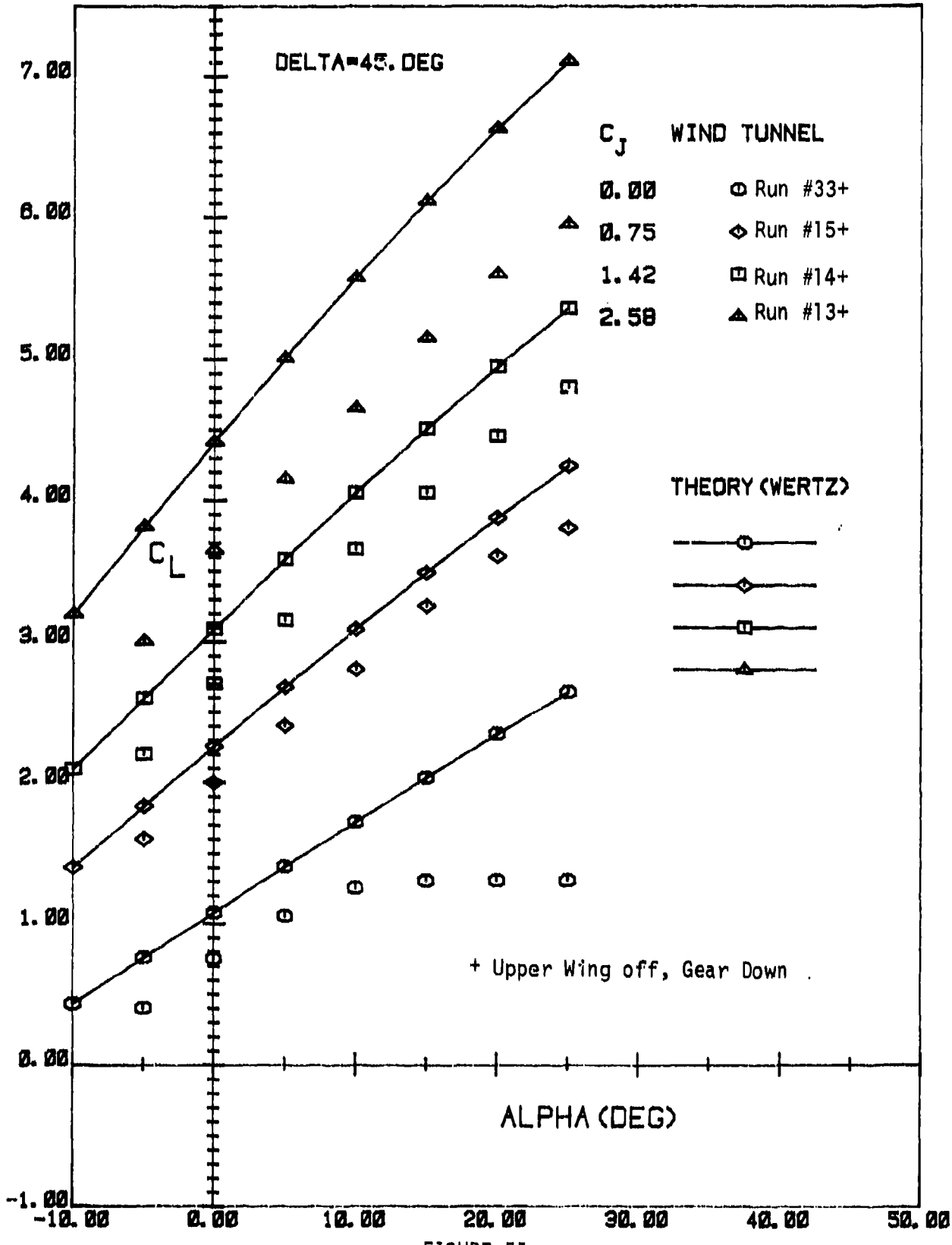

FIGURE 55

COMPARISON OF WERTZ METHOD THEORETICAL C_L vs α RESULTS AND NASA FULL SCALE WIND TUNNEL DATA ON JETWING JW-1 FOR δ_F = 45°, UPPER WING REMOVED

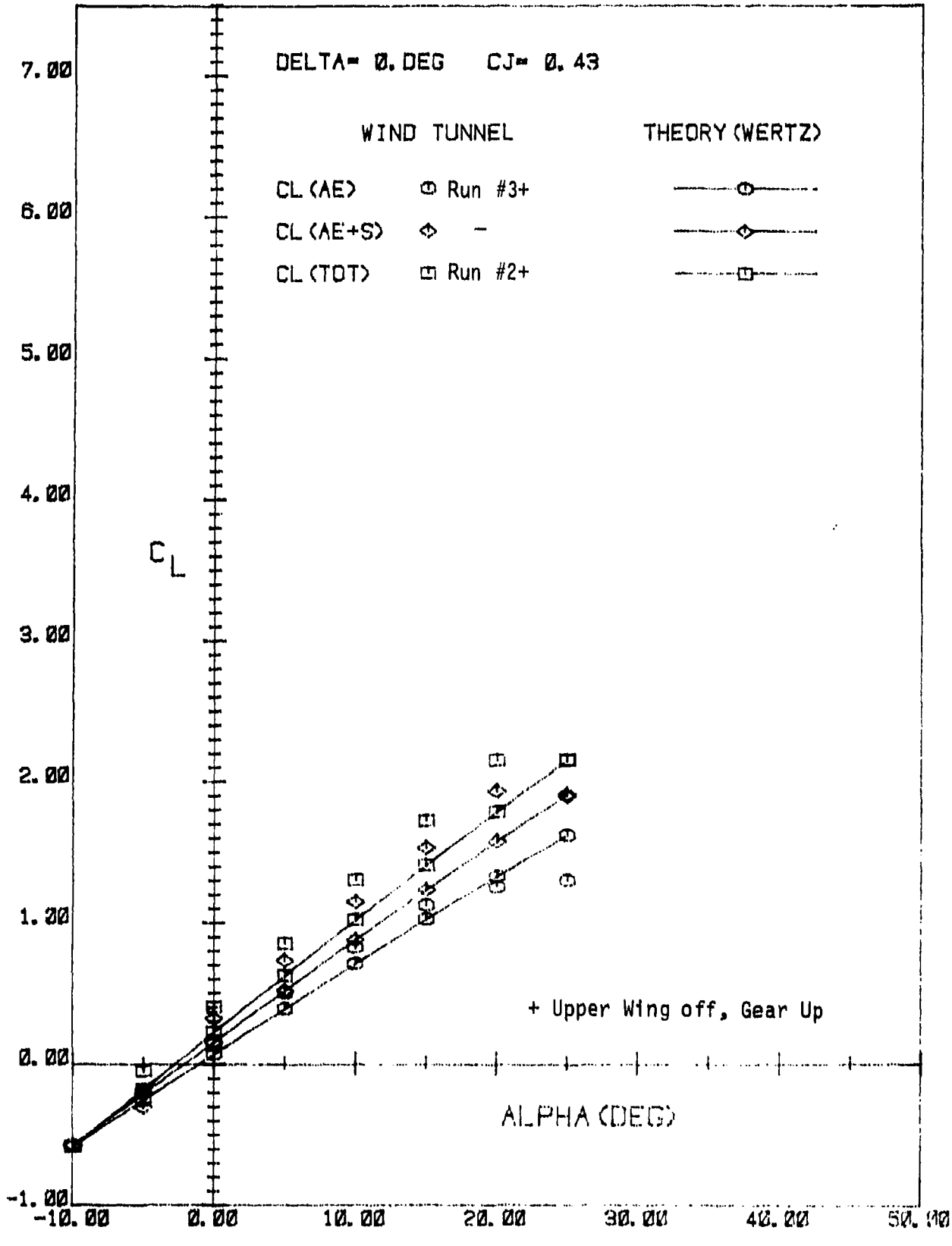

FIGURE 56

COMPARISON OF WERTZ METHOD THEORETICAL C_L vs α RESULTS AND NASA FULL SCALE WIND TUNNEL DATA ON JETWING JW-1 FOR BREAKDOWN OF LIFT COEFFICIENT INTO COMPONENTS OF BASIC AERODYNAMIC LIFT (AE), SUPERCIRCULATION LIFT (S), AND JET MOMENTUM LIFT INCLUDED IN TOTAL LIFT (TOT) FOR $\delta_F = 0°$

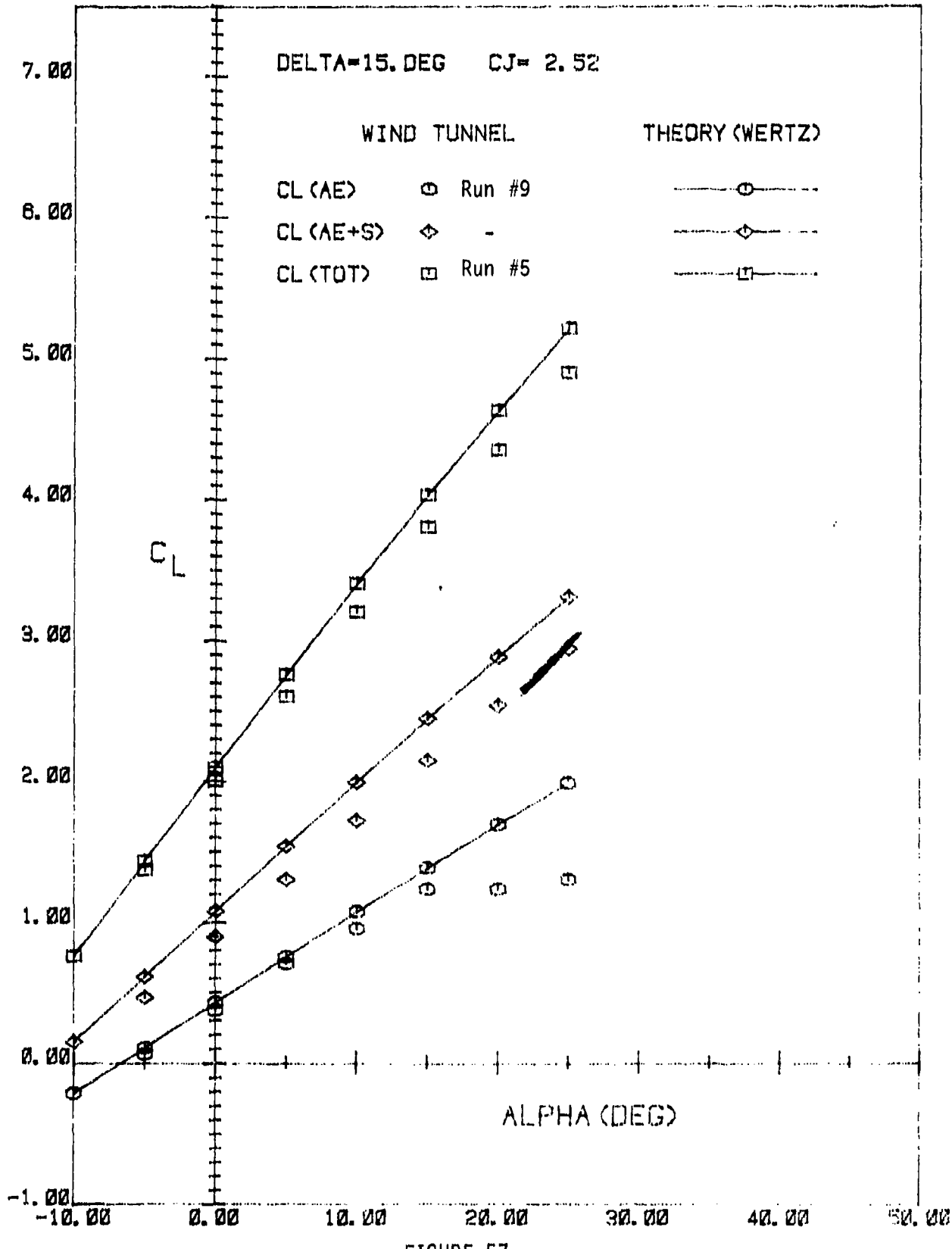

FIGURE 57

COMPARISON OF WERTZ METHOD THEORETICAL C_L vs α RESULTS AND NASA FULL SCALE WIND TUNNEL DATA ON JETWING JW-1 FOR BREAKDOWN OF LIFT COEFFICIENT INTO COMPONENTS OF BASIC AERODYNAMIC LIFT (AE), SUPERCIRCULATION LIFT (S), AND JET MOMENTUM LIFT INCLUDED IN TOTAL LIFT (TOT) FOR $\delta_F = 15°$

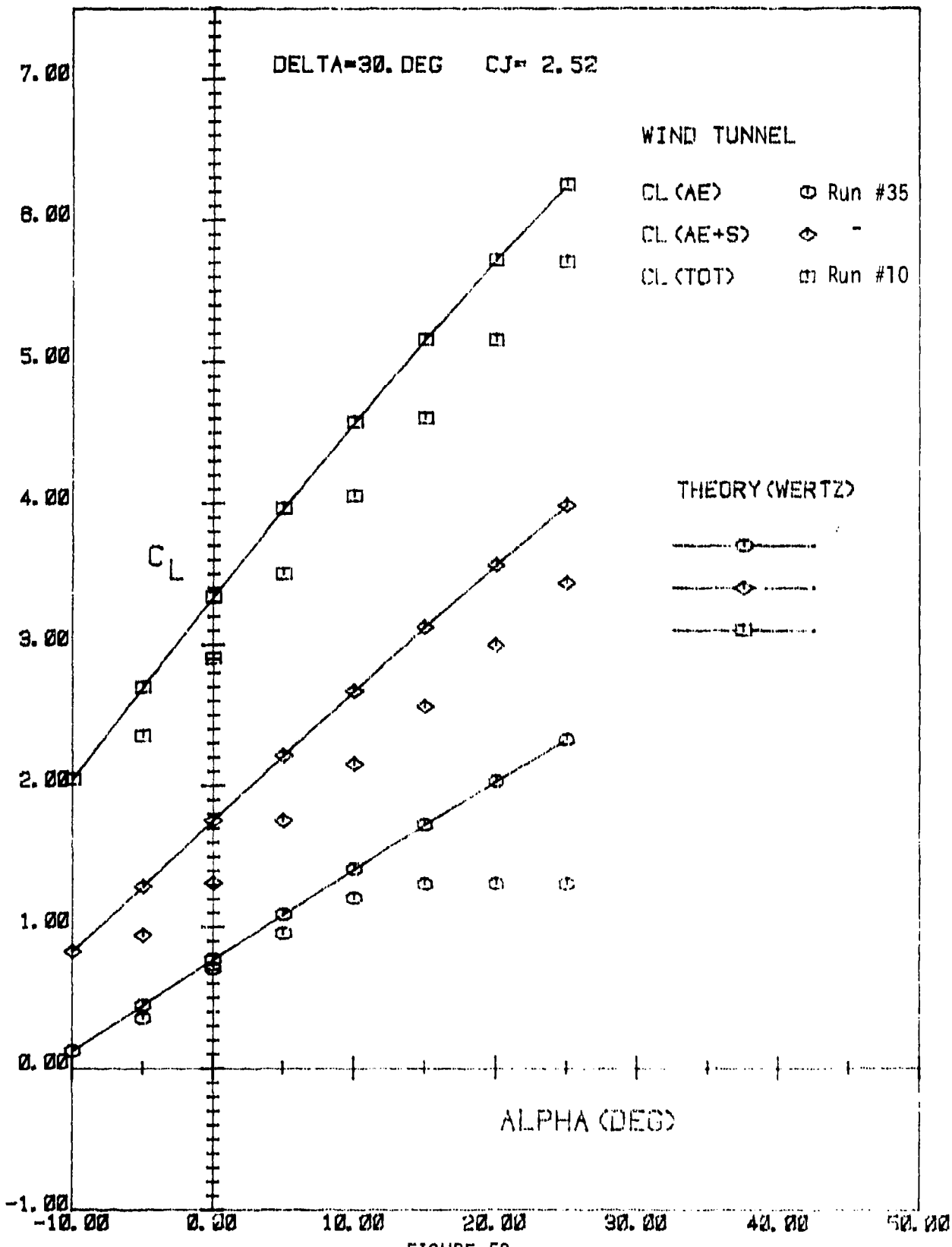

FIGURE 58

COMPARISON OF WERTZ METHOD THEORETICAL C_L vs α RESULTS AND NASA FULL SCALE WIND TUNNEL DATA ON JETWING JW-1 FOR BREAKDOWN OF LIFT COEFFICIENT INTO COMPONENTS OF BASIC AERODYNAMIC LIFT (AE), SUPERCIRCULATION LIFT (S), AND JET MOMENTUM LIFT INCLUDED IN TOTAL LIFT (TOT) FOR $\delta_F = 30°$

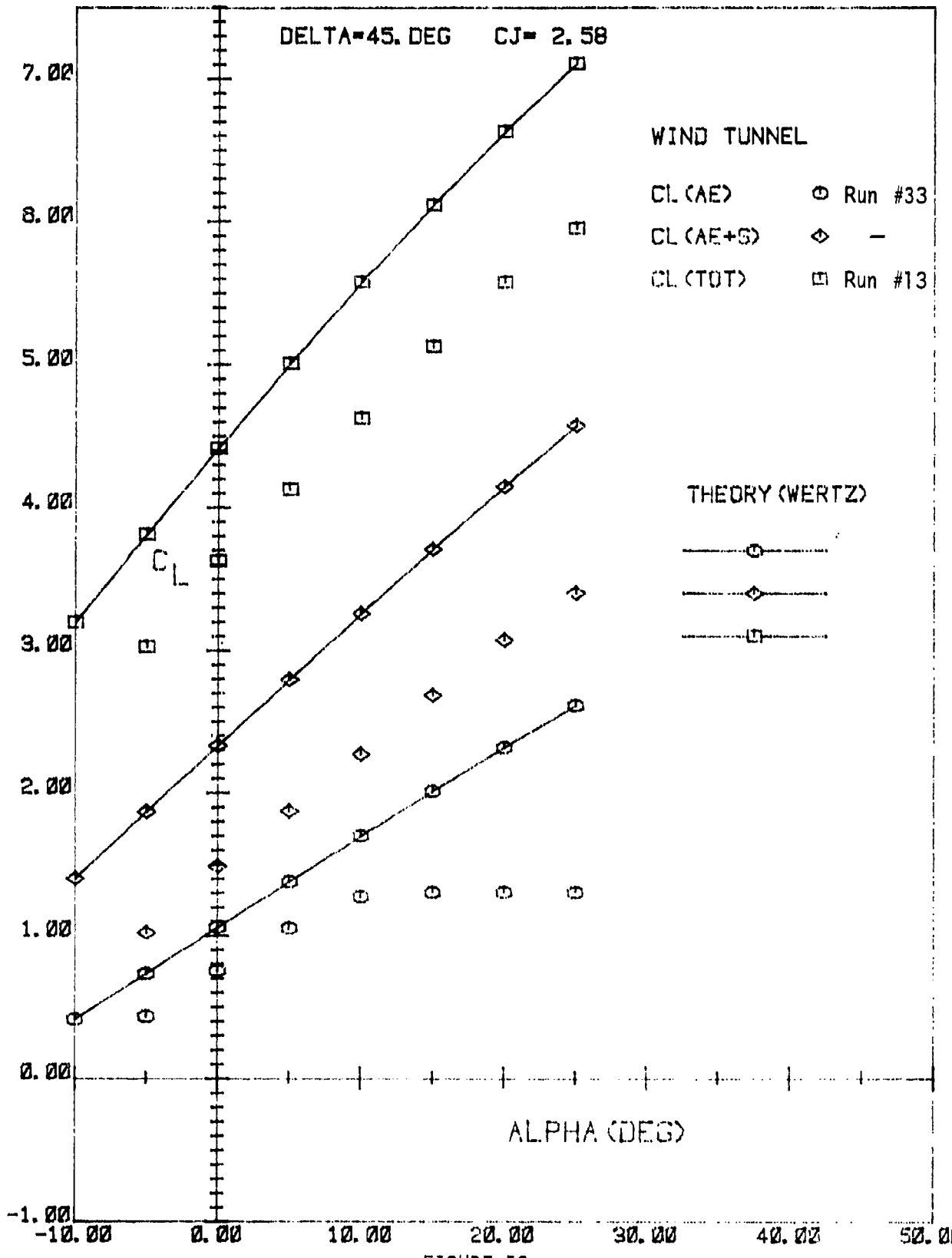

FIGURE 59

COMPARISON OF WERTZ METHOD THEORETICAL C_L vs α RESULTS AND NASA FULL SCALE WIND TUNNEL DATA ON JETWING JW-1 FOR BREAKDOWN OF LIFT COEFFICIENT INTO COMPONENTS OF BASIC AERODYNAMIC LIFT (AE), SUPERCIRCULATION LIFT (S), AND JET MOMENTUM LIFT INCLUDED IN TOTAL LIFT (TOT) FOR $\delta_F = 45°$

SECTION IV

PREDICTION METHOD 3 (JACOBS)

EQUIVALENT FLAP THEORY

SUMMARY

An approximate method was presented by Jacobs [12,15] for calculating the lift and pitching moment of an airfoil with a mechanical flap and a jet issuing at the trailing edge of the flap into the main stream. The jet may form any angle with respect to the flap or the free stream. In the case of a two dimensional airfoil the effect of the jet on the lift forces was related to that of an equivalent mechanical flap extension in the plane of the existing flap with the lift on the equivalent flap being equal to the vertical component of jet reaction. In the case of a three-dimensional wing, the effect of induced downwash field was considered in the form of a decrease in effective angle of attack distribution. Hence, jet reaction lift would decrease, which in turn would reduce the length of the equivalent mechanical flap, as both the jet reaction lift and the lift on the equivalent flap have to be the same. The method described here employs the equivalent flap theory of Jacobs to calculate the equivalent mechanical flap extension of every spanwise section knowing the corresponding jet blowing velocity and then uses the well known Multhopp's lifting line theory to predict the spanwise load and induced angle of attack distribution. The approach adopted here calls for an iteration on induced angle of attack distribution, starting with zero throughout the span. The equivalent wing shape is determined by going through lifting line theory to predict the load and new induced angle of attack distribution. The equivalent wing shape is then recalculated along with corresponding load, and induced angle of attack distribution, until the process converges. Once the circulation distribution is known, pitching moment is easily obtained as the integrated (spanwise and chordwise) result of the product of density, velocity, circulation and distance from the moment center. Pitching moment of the fuselage is also calculated from an empirical formula. The method has the capability of handling leading edge flap along with the more conventional trailing edge flap.

CALCULATION OF LIFT

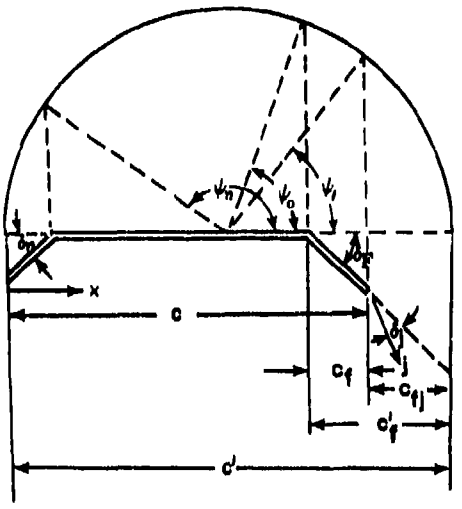

FIGURE 60. GEOMETRY OF AIRFOIL WITH JET AUGUMENTED FLAP

From geometric consideration, the following relations can be derived.

$$x = \frac{c'}{2}(1 + \cos\psi)$$

$$c_{fj} = c' - c = c' - \frac{c'}{2}(1 + \cos\psi_1) = \frac{c'}{2}(1 - \cos\psi_1)$$

$$c = c' - c_{fj} = c' - \frac{c'}{2}(1 - cos\psi_1) = \frac{c'}{2}(1 + \cos\psi_1)$$

$$\frac{c_{fj}}{c} = \frac{1 - \cos\psi_1}{1 + \cos\psi_1}$$

Again ,

$$c'_f = c' - \frac{c'}{2}(1 + \cos\psi_o) = \frac{c'}{2}(1 - \cos\psi_o)$$

$$c_f = c'_f - c_{fj} = \frac{c'}{2}(1-\cos\psi_o) - \frac{c'}{2}(1-\cos\psi_1) = \frac{c'}{2}(\cos\psi_1 - \cos\psi_o)$$

$$\frac{c_f}{c} = \frac{\cos\psi_1 - \cos\psi_o}{1+\cos\psi_1}$$

$$\frac{c_f}{c}(1+\cos\psi_1) = \cos\psi_1 - \cos\psi_o$$

$$\cos\psi_o = \cos\psi_1 - \frac{c_f}{c}(1+\cos\psi_1) \qquad (IV-1)$$

The circulation distribution $\gamma(\psi)$ over a thin airfoil with leading edge flap deflection δ_n, trailing edge flap deflection δ_F and overall angle of attack α, is given by Glauert as,

$$\gamma(\psi) = \frac{2V_T}{\pi}\Bigg[-\delta_n\left\{(\pi-\psi_n)\tan\frac{\psi}{2} - \ln\left|\frac{\sin\frac{\psi+\psi_n}{2}}{\sin\frac{\psi-\psi_n}{2}}\right|\right\}$$
$$+\delta_F\left\{\psi_o\tan\frac{\psi}{2} + \ln\left|\frac{\sin\frac{\psi+\psi_n}{2}}{\sin\frac{\psi-\psi_n}{2}}\right|\right\}$$
$$+\alpha\left\{\pi\tan\frac{\psi}{2} + \ln\left|\frac{\sin\frac{\psi+\pi}{2}}{\sin\frac{\psi-\pi}{2}}\right|\right\}\Bigg] \qquad (IV-2)$$

As per Jacobs equivalent flap theory, the length of the equivalent flap extension can be calculated by equating the integrated lift over its length with the vertical component of jet reaction lift.

$$L_{fj} = \rho V_T \int_o^{c'} \gamma(x)dx = \dot{M}_j V_j \sin(\delta_F + \delta_j + \alpha) \qquad (IV-3)$$

Substituting $\gamma(x)$ from equation $(IV-2)$ into equation $(IV-3)$ and setting leading edge flap deflection δ_n to be zero, we get,

$$\frac{\dot{M}_j V_j}{\frac{1}{2}\rho V_T{}^2 c'}\sin(\delta_F + \delta_j + \alpha) = \frac{2}{\pi}\int_0^{\psi_1}\Bigg[\delta_F\left\{\psi_o\tan\frac{\psi}{2} + \ln\left|\frac{\sin\frac{\psi+\psi_n}{2}}{\sin\frac{\psi-\psi_n}{2}}\right|\right\}$$
$$+\alpha\left\{\pi\tan\frac{\psi}{2} + \ln\left|\frac{\sin\frac{\psi+\pi}{2}}{\sin\frac{\psi-\pi}{2}}\right|\right\}\Bigg]\sin\psi d\psi \qquad (IV-4)$$

The integral on the right hand side of equation $(IV-4)$ has been evaluated separately.

Defining the blowing coefficient with respect to the equivalent chord c' as,

$$C'_j = \frac{\dot{M}_j V_j}{\frac{1}{2}\rho V_T{}^2 c'}$$

we can rewrite equation $(IV-4)$ as:

$$C'_j \sin(\delta_F + \delta_j + \alpha) = \frac{2}{\pi}\left[(\delta_F\psi_o + \alpha\pi)(\psi_1 - \sin\psi_1) + \delta_F\left\{\psi_1 \sin\psi_o + (\cos\psi_1 - \cos\psi_o)\cdot \ln\frac{\sin\frac{\psi_o-\psi_1}{2}}{\sin\frac{\psi_o+\psi_1}{2}}\right\}\right] \qquad (IV-5)$$

Knowing the relation between c and c', we can write

$$C'_j = C_j\frac{1+\cos\psi_1}{2} \qquad (IV-6)$$

where C_j is obtained by the procedure given in Appendix II.
Hence, equation $(IV-5)$ transforms to:

$$C_j\frac{1+\cos\psi_1}{2}\sin(\delta_F + \delta_j + \alpha) = \frac{2}{\pi}\left[(\delta_F\psi_o + \alpha\pi)(\psi_1 - \sin\psi_1) + \delta_F\left\{\psi_1 \sin\psi_o + (\cos\psi_1 - \cos\psi_o)\ln\frac{\sin\frac{\psi_o-\psi_1}{2}}{\sin\frac{\psi_o+\psi_1}{2}}\right\}\right] \qquad (IV-7)$$

Equation $(IV-7)$ is valid for a 2-D airfoil. The three-dimensional effects express themselves only in changes of angle of attack. For a 3-D wing, Equation $(IV-7)$ should be modified as:

$$C_j\frac{1+\cos\psi_1}{2}\cdot\left\{\sin(\delta_F + \alpha + \delta_j - \alpha_i) - \sin\alpha_i\right\} = \frac{2}{\pi}\left[(\delta_F\psi_o + \alpha\pi)(\psi_1 - \sin\psi_1) + \delta_F\left\{\psi_1 \sin\psi_o + (\cos\psi_1 - \cos\psi_o)\ln\frac{\sin\frac{\psi_o-\psi_1}{2}}{\sin\frac{\psi_o+\psi_1}{2}}\right\}\right] \qquad (IV-8)$$

Equations $(IV-1)$ and $(IV-8)$ must be solved simultaneously for the two unknowns ψ_o and ψ_1. This problem is transformed into finding one unknown in one equation as described below.

Let

$$\cos\psi_1 = y$$

$$\sin\psi_1 = \sqrt{1-y^2}$$

From equations $(IV-1)$,

$$\cos\psi_o = y - \frac{c_f}{c}(1+y)$$

and

$$\sin\psi_o = \sqrt{1-\left(y-\frac{c_f}{c}(1+y)\right)^2}$$

Also ,

$$\sin\left(\frac{\psi_o}{2}-\frac{\psi_1}{2}\right) = \sin\frac{\psi_o}{2}\cdot\cos\frac{\psi_1}{2} - \cos\frac{\psi_o}{2}\cdot\sin\frac{\psi_1}{2}$$
$$= \sqrt{\frac{1-\cos\psi_o}{2}}\cdot\sqrt{\frac{1+\cos\psi_1}{2}} - \sqrt{\frac{1+\cos\psi_o}{2}}\cdot\sqrt{\frac{1-\cos\psi_1}{2}}$$

and

$$\sin\left(\frac{\psi_o}{2}+\frac{\psi_1}{2}\right) = \sqrt{\frac{1-\cos\psi_o}{2}}\cdot\sqrt{\frac{1+\cos\psi_1}{2}} + \sqrt{\frac{1+\cos\psi_o}{2}}\cdot\sqrt{\frac{1-\cos\psi_1}{2}}$$

Substituting these in Equation $(IV-8)$ we get,

$$C_f\left(\frac{1+y}{2}\right)\left\{\sin(\delta_F+\delta_f+\alpha-\alpha_i)-\sin\alpha_i\right\} = \frac{2}{\pi}\left[\left\{\delta_F\cdot\cos^{-1}\left(y-\frac{c_f}{c}(1+y)\right)+\alpha\pi\right\}\cdot(\cos^{-1}y-\sqrt{1-y^2})\right.$$

$$+\delta_F\cdot\left\{\cos^{-1}y\cdot\sqrt{1-\left(y-\frac{c_f}{c}(1+y)\right)^2}\right.$$

$$\left.\left.+\frac{c_f}{c}(1+y)\cdot\ln\frac{\sqrt{\frac{1-y+(c_f/c)(1+y)}{2}}\cdot\sqrt{\frac{1+y}{2}}-\sqrt{\frac{1+y-(c_f/c)(1+y)}{2}}\cdot\sqrt{\frac{1-y}{2}}}{\sqrt{\frac{1-y+(c_f/c)(1+y)}{2}}\cdot\sqrt{\frac{1+y}{2}}+\sqrt{\frac{1+y-(c_f/c)(1+y)}{2}}\cdot\sqrt{\frac{1-y}{2}}}\right\}\right] \qquad (IV-9)$$

This is a transcendental equation in one variable y. Initially we assume induced angle of attack α_i to be zero throughout the span. Then knowing $C_j, \delta_F, \delta_j, \alpha, c, c_f$ for each and every spanwise section, equation $(IV-9)$ is solved for y by a multivariate search program [17] for error minimization. Once y has been obtained, ψ_1, ψ_o, and c' can be determined from the relations developed earlier. That means , we can replace our jet flapped wing by the actual hard wing and a hypothetical extension of the mechanical flap in the same plane as the actual flap. Now, the spanwise lift distribution, lift curve slope and overall C_L can be calculated by the well known Multhopp's Lifting Line Theory.

The input for Lifting Line Theory will need the local chord and effective angle of attack (α_e) for each spanwise section. The last term, according to Glauert, can easily be obtained as

$$\alpha_e = \alpha + \frac{\partial \alpha}{\partial \delta_F} \delta_F$$

where

$$\frac{\partial \alpha}{\partial \delta_F} = \frac{2}{\pi}\left[\sqrt{\lambda_F(1-\lambda_F)} + \sin^{-1}\sqrt{\lambda_F}\right], \qquad \lambda_F = \frac{c'_f}{c'}$$

The output of Multhopp's program will contain spanwise variation of induced angles of attack which then can be fed in equation ($IV-9$) to obtain a new set of y, ie., a new equivalent wing, which will produce another set of induced angles of attack. This process is continued until the induced angles of attack in two successive iterations matches within the desired accuracy.

CALCULATION OF PITCHING MOMENT

Pitching moment of an airfoil with jet augumented flap can be written as:

$$M = -\rho V_T \int_0^{c'} \gamma(x)(x+z)dx + \rho V_T \int_0^{c'} \gamma(x)(x+z)dx - j\sin(\delta_F + \delta_j)(c+z) \qquad (IV-10)$$

$$M = -\rho V_T \int_0^{\pi} \gamma(\psi)\left\{\frac{c'}{2}(1+\cos\psi) + pc'\right\}\frac{c'}{2}\sin\psi d\psi$$

$$+\rho V_T \int_0^{\psi_1} \gamma(\psi)\left\{\frac{c'}{2}(1+\cos\psi) + pc'\right\}\frac{c'}{2}\sin\psi d\psi$$

$$-j\sin(\delta_F + \delta_j)\left\{\frac{c'}{2}(1+\cos\psi_1) + pc'\right\}$$

$$M = -\rho V_T \frac{c'^2}{4}\int_0^{\pi} \gamma(\psi)(1+\cos\psi+2p)\sin\psi d\psi$$

$$+\rho V_T \frac{c'^2}{4}\int_0^{\psi_1} \gamma(\psi)(1+\cos\psi+2p)\sin\psi d\psi$$

$$-j\sin(\delta_F + \delta_j)\frac{c'}{2}(1+\cos\psi_1+2p) \qquad (IV-11)$$

In non-dimensional form equation $(IV-11)$ can be written as:

$$C'_m = \frac{M}{\frac{1}{2}\rho V_T{}^2 c'^2} = -\frac{1}{2V_T}\int_0^{\pi} \gamma(\psi)(1+\cos\psi+2p)\sin\psi d\psi$$

$$+\frac{1}{2V_T}\int_0^{\psi_1} \gamma(\psi)(1+\cos\psi+2p)\sin\psi d\psi$$

$$-C'_j\sin(\delta_F + \delta_j)\left(\frac{1+\cos\psi_1+2p}{2}\right) \qquad (IV-12)$$

The integrals in equations $(IV-12)$ have been evaluated separately.

The pitching moment coefficient based on the actual airfoil chord is then

$$C_m = C'_m\left(\frac{2}{1+\cos\psi_1}\right)^2 \qquad (IV-13)$$

Rewriting equation $(IV-11)$ we obtain:

$$M = -\frac{\rho V_T{}^2 c'^2}{4}\left[(1+4p)(\delta_F\psi_o+\alpha\pi)+\delta_F\sin\psi_o\left\{2(1+2p)+\cos\psi_o\right\}\right]$$

$$+\frac{\rho V_T{}^2 c'^2}{4\pi}\left[(\delta_F\psi_o+\alpha\pi)\left\{(\psi_1-\sin\psi_1\cos\psi_1)+4p(\psi_1-\sin\psi_1)\right\}\right.$$

$$+\delta_F\,\frac{\sin\frac{\psi_o+\psi_1}{2}}{\sin\frac{\psi_o-\psi_1}{2}}\cdot\left\{2(1+2p)(\cos\psi_o-\cos\psi_1)+\frac{1}{2}(\cos 2\psi_o-\cos 2\psi_1)\right\}$$

$$+2(1+2p)\delta_F\psi_1\sin\psi_o$$

$$-\frac{\delta_F}{2}\left\{\cos 2\psi_o(2\sin\psi_o\sin\psi_1+\frac{1}{2}\sin 2\psi_1\sin 2\psi_o)\right.$$

$$\left.\left.-\sin 2\psi_o\left(\psi_1+2\sin\psi_1\cos\psi_o+(\cos 2\psi_o-\sin 2\psi_o)\cdot(\cos 2\psi_1+\sin 2\psi_1-1)\right)\right\}\right]$$

$$-\dot{M}_j V_j\sin(\delta_F+\delta_j)\frac{c'}{2}(1+\cos\psi_1+2p) \qquad (IV-14)$$

Equation $(IV-14)$ is the expression for pitching moment for unit spanwise length. First two terms of the right hand side have to be multiplied by unit length in order to get consistancy in units, whereas $\dot{M}_j$ in the last term denotes mass flow rate per unit span. All the terms in right hand side have to be divided by g_c(i.e.,32.174 lbm-ft/lbf-sec^2) if the final result is desired in English Engineering Unit,i.e., ft-lbf. The contribution of the fuselage to the pitching moment can be estimated as follows. As per Max Munk, for a very slender body of revolution, the variation of the pitching moment with angle of attack in degrees is a function of the fuselage volume and dynamic pressure.

$$\frac{dM}{d\alpha} = \frac{Volume}{28.7}\,q \qquad (IV-15)$$

This expression is corrected by a factor (K_2-K_1), which is a function of fuselage fineness ratio as given by Perkins and Hage [18], figure 5-13, p. 226.

$$\frac{dM}{d\alpha} = \frac{Volume}{28.7}\cdot q\cdot(K_2-K_1) \qquad (IV-16)$$

For the JETWING aircraft the fineness ratio is 10. Correspondingly, $K_2 - K_1 = 0.95$. Hence, equation $(IV - 16)$ can be written as:

$$\frac{dM}{d\alpha} = 0.033101 \cdot Volume \cdot q \qquad (IV - 17)$$

Therefore, the pitching moment contribution of the fuselage is

$$M_{FU} = 0.033101 \cdot Volume \cdot q \cdot \alpha \qquad (IV - 18)$$

The overall pitching moment coefficient can be calculated by summing up individual moments for all the spanwise sections of the wing along with the fuselage pitching moment, and then dividing by the product of the dynamic pressure, actual gross wing area and mean aerodynamic chord.

RESULTS

The method described here has been coded in FORTRAN. The code comprises of around 700 instructions and occupies a core memory of about 40 blocks (1 block=512 bytes). The computer time required in a VAX-11/780 system for each combination of C_J, δ_F, and α (with α varying between 0^0 and 30^0 in steps of 5^0) does not exceed 5 minutes for the cases for which results have been included. Figure 61 thru figure 66 show the comparison of predicted values of C_L vs. α and C_L vs. C_M with that of full scale wind tunnel experiments for the JETWING aircraft with the upper wing removed. Figure 67 thru figure 71 show the predicted spanwise distribution of local C_l and local C_m.

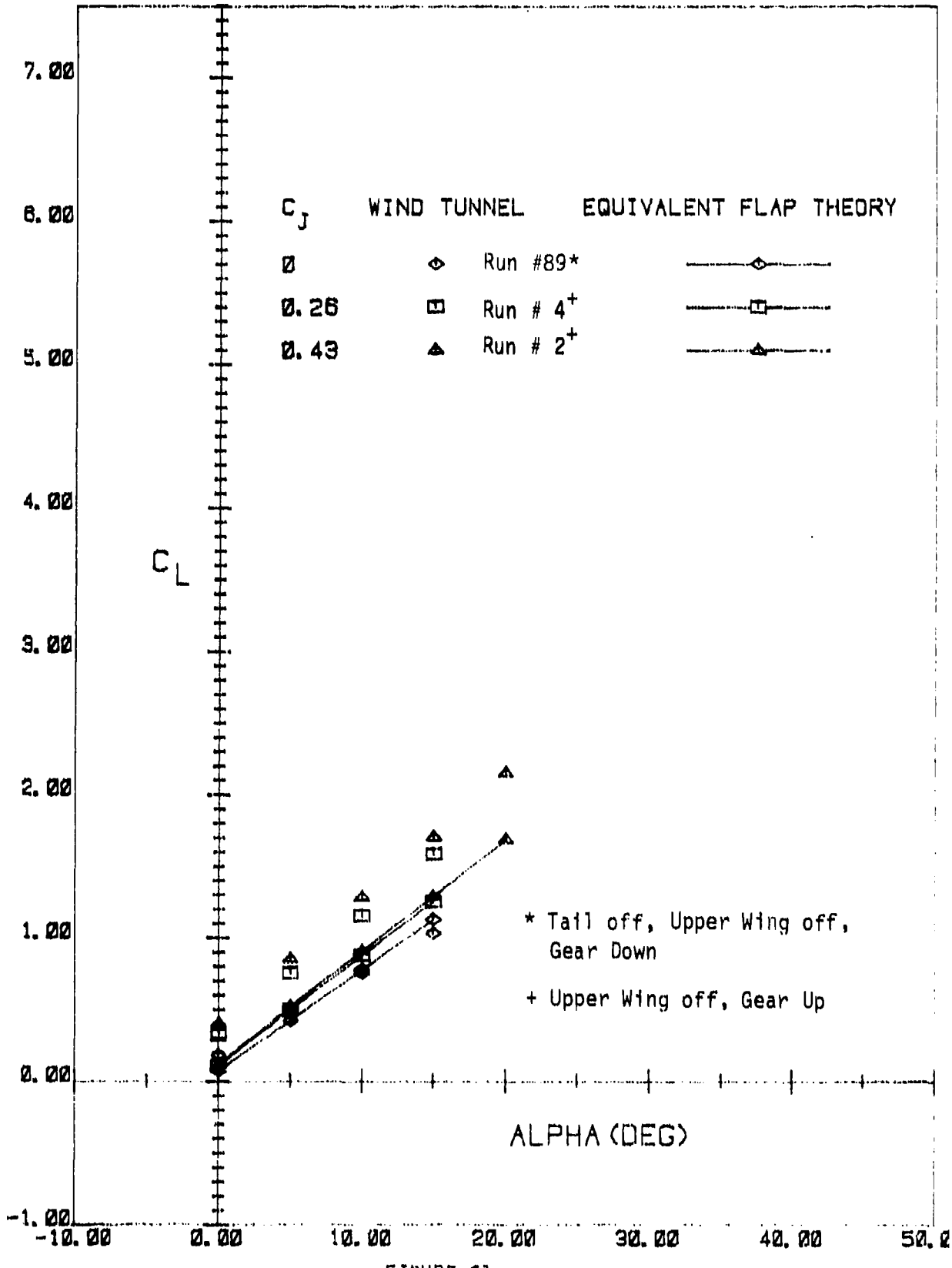

FIGURE 61

COMPARISON OF JACOBS METHOD THEORETICAL C_L vs α RESULTS AND NASA FULL SCALE WIND TUNNEL DATA ON JETWING JW-1 FOR $\delta_F = 0°$, UPPER WING REMOVED

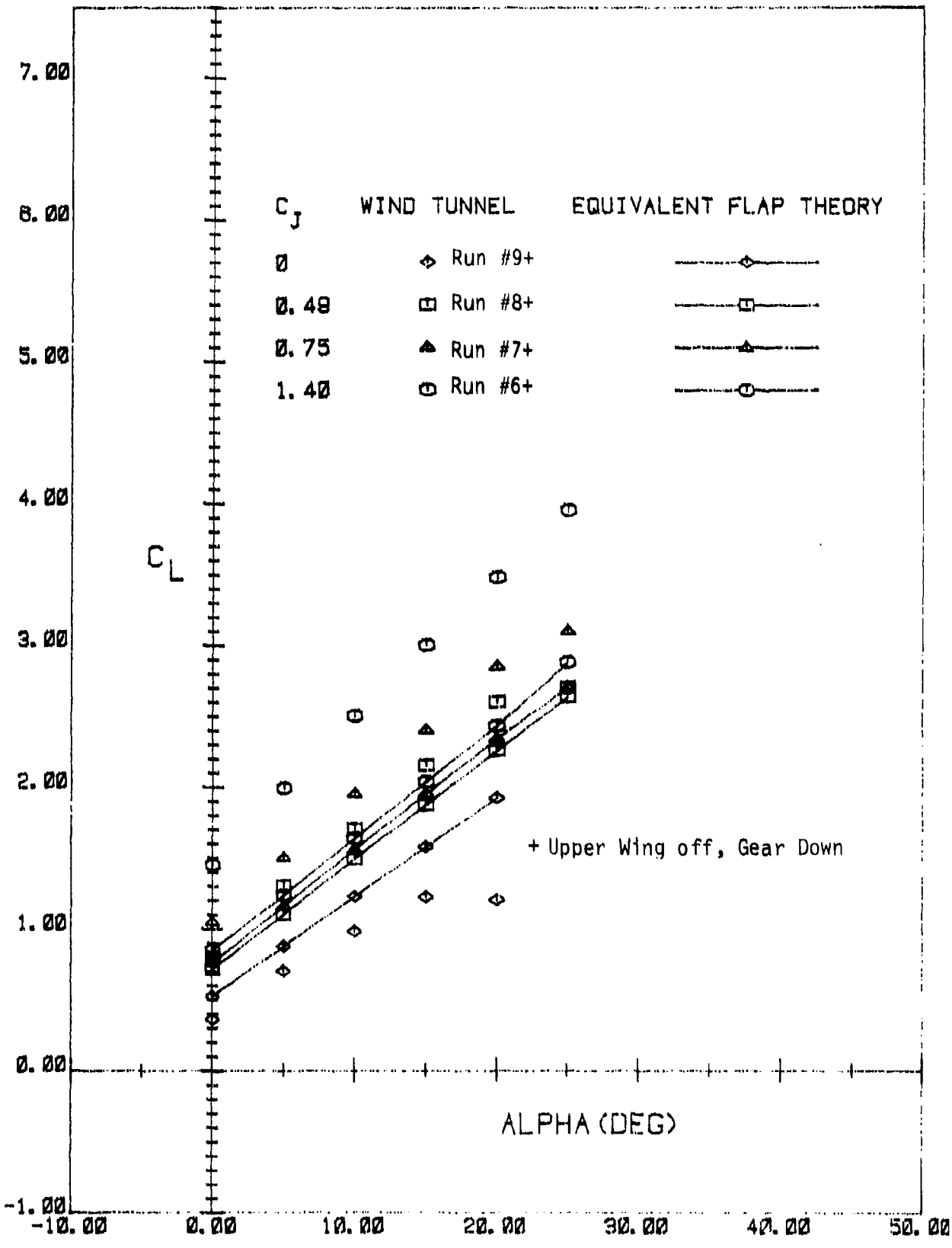

FIGURE 62

COMPARISON OF JACOBS METHOD THEORETICAL C_L vs α RESULTS AND NASA FULL SCALE WIND TUNNEL DATA ON JETWING JW-1 FOR δ_F = 15°, UPPER WING REMOVED

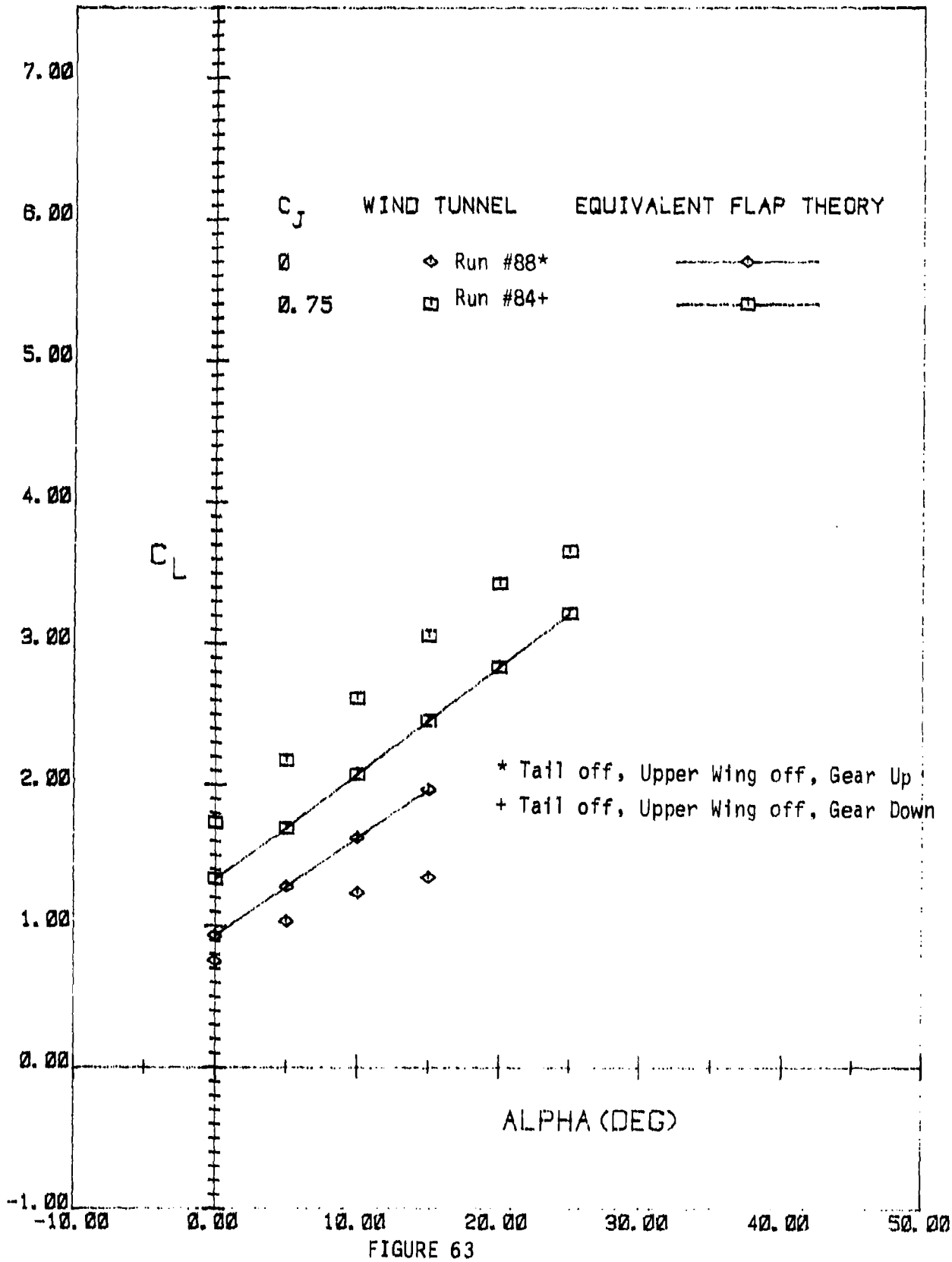

FIGURE 63

COMPARISON OF JACOBS METHOD THEORETICAL C_L vs α RESULTS AND NASA FULL SCALE WIND TUNNEL DATA ON JETWING JW-1 FOR $\delta_F = 30°$, UPPER WING REMOVED

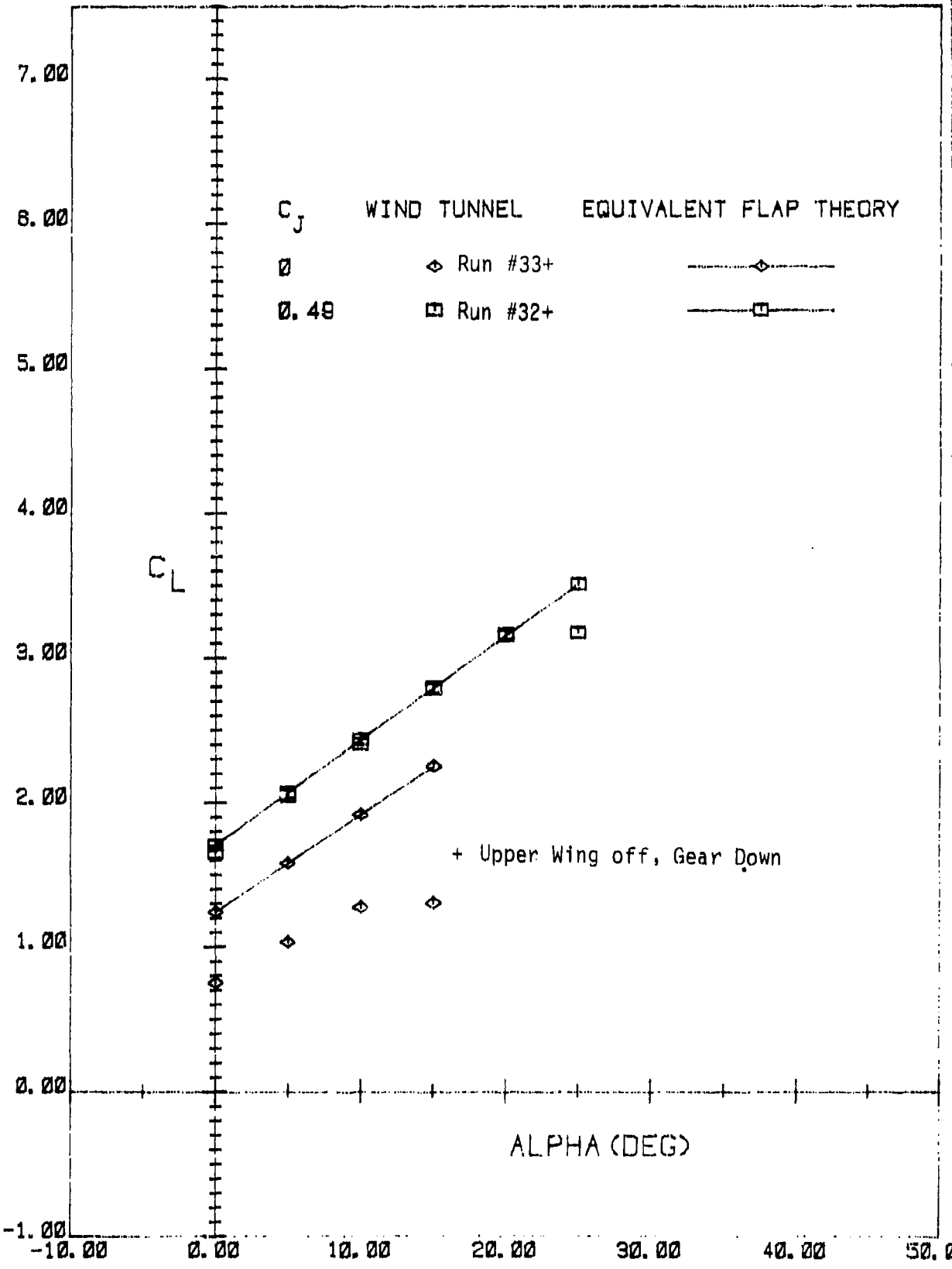

FIGURE 64

COMPARISON OF JACOBS METHOD THEORETICAL C_L vs α RESULTS AND NASA FULL SCALE WIND TUNNEL DATA ON JETWING JW-1 FOR $\delta_F = 45°$, UPPER WING REMOVED

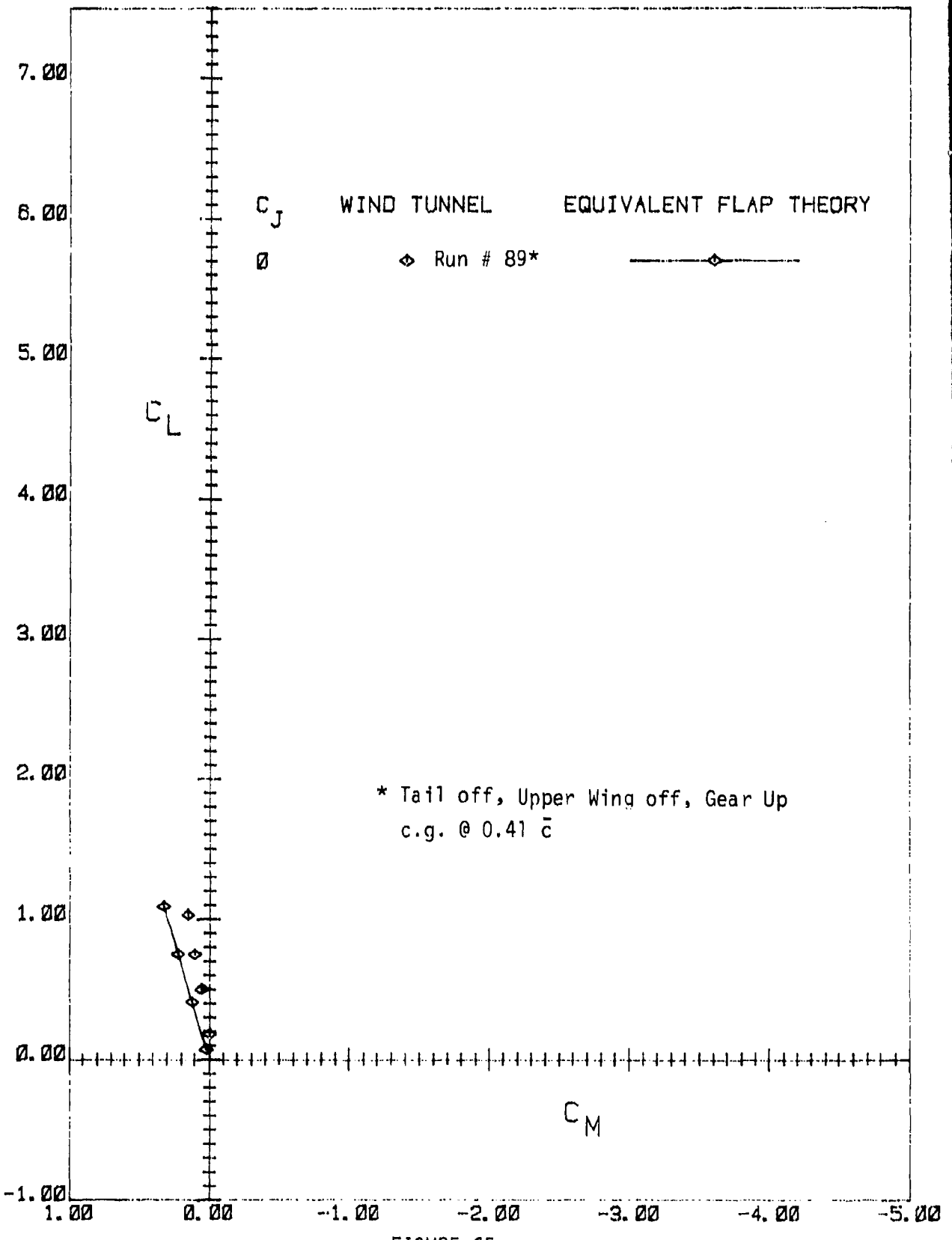

FIGURE 65

COMPARISON OF JACOBS METHOD THEORETICAL C_L vs α RESULTS AND NASA FULL SCALE WIND TUNNEL DATA ON JETWING JW-1 FOR $\delta_F = 0°$, UPPER WING REMOVED

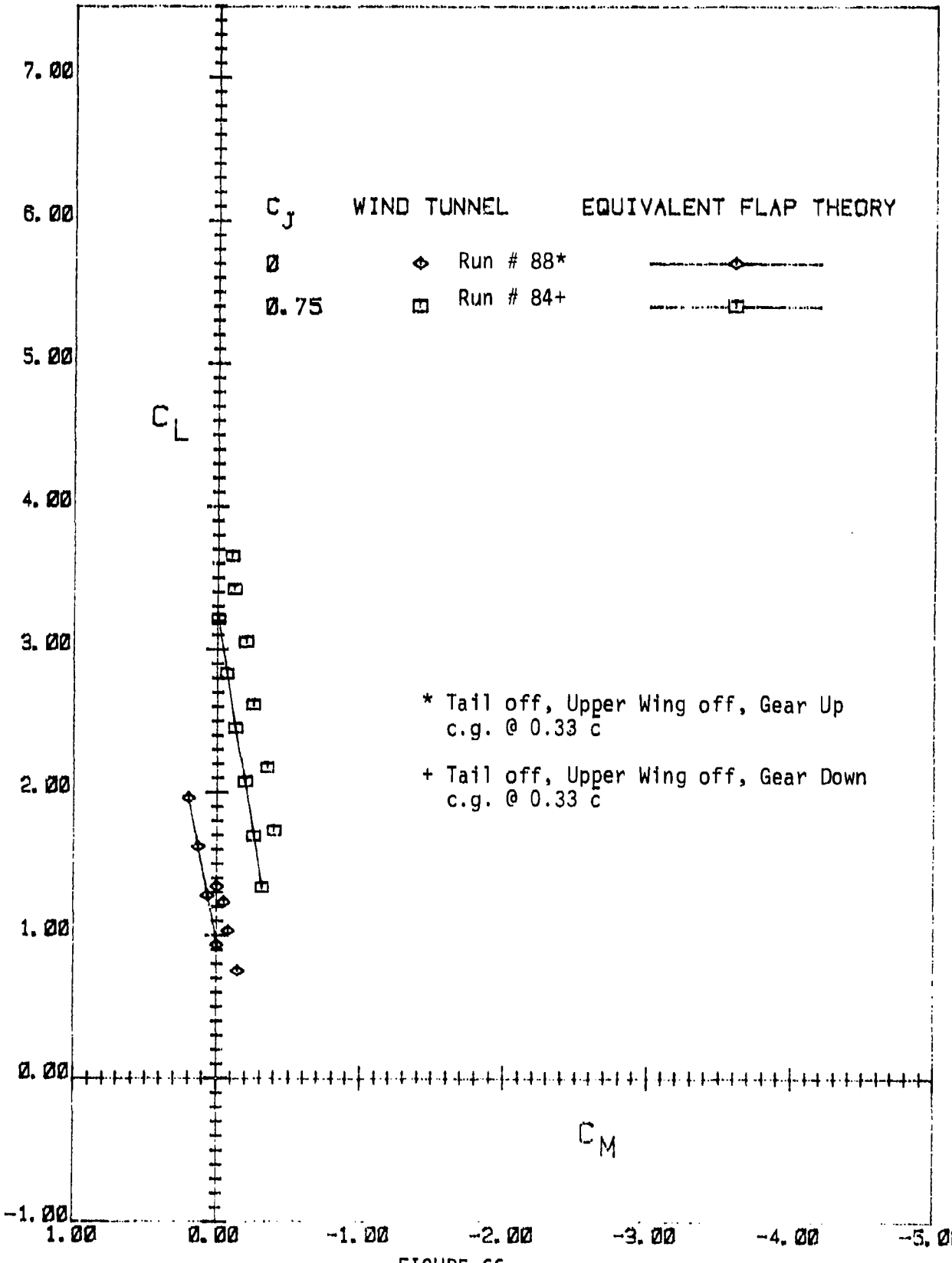

FIGURE 66

COMPARISON OF JACOBS METHOD THEORETICAL C_L vs α RESULTS AND NASA FULL SCALE WIND TUNNEL DATA ON JETWING JW-1 FOR δ_F = 30°, UPPER WING REMOVED

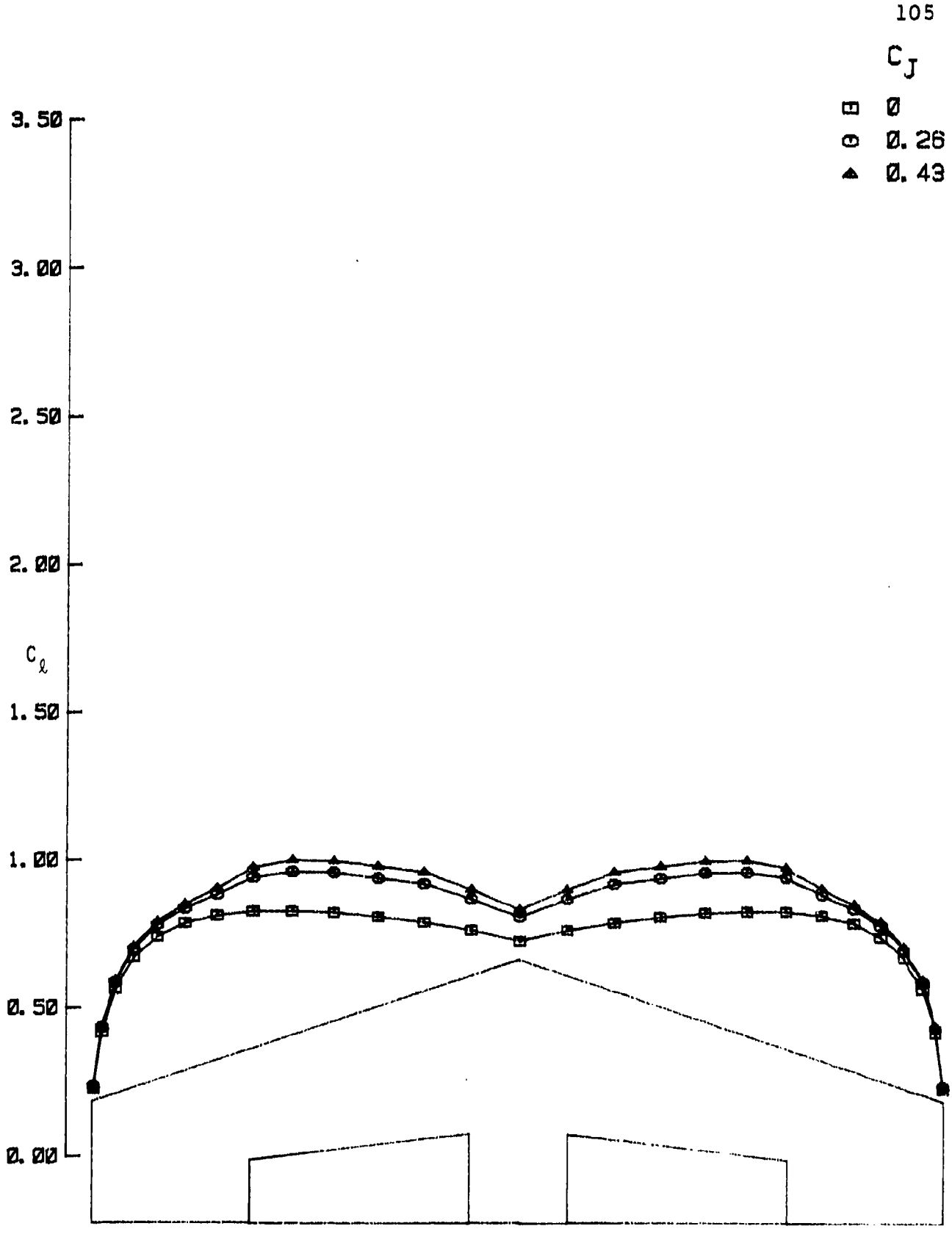

FIGURE 67

SPANWISE DISTRIBUTION OF C_ℓ ON JETWING JW-1 PLANFORM FOR α = 10° AND δ_F = 0°, UPPER WING REMOVED, CALCULATED BY JACOBS METHOD

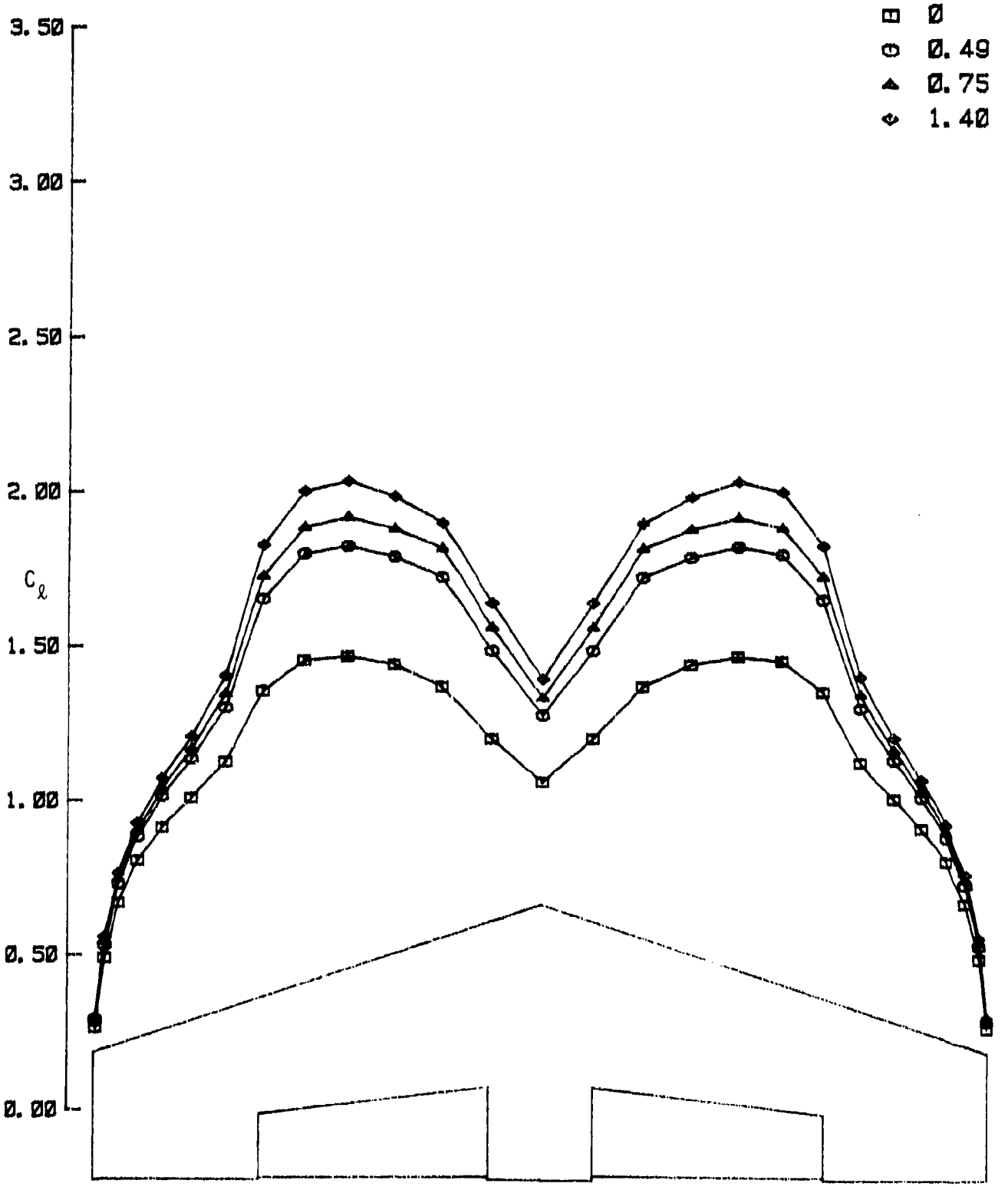

FIGURE 68

SPANWISE DISTRIBUTION OF C_ℓ ON JETWING JW-1 PLANFORM FOR α = 10° AND δ_F = 15°, UPPER WING REMOVED, CALCULATED BY JACOBS METHOD

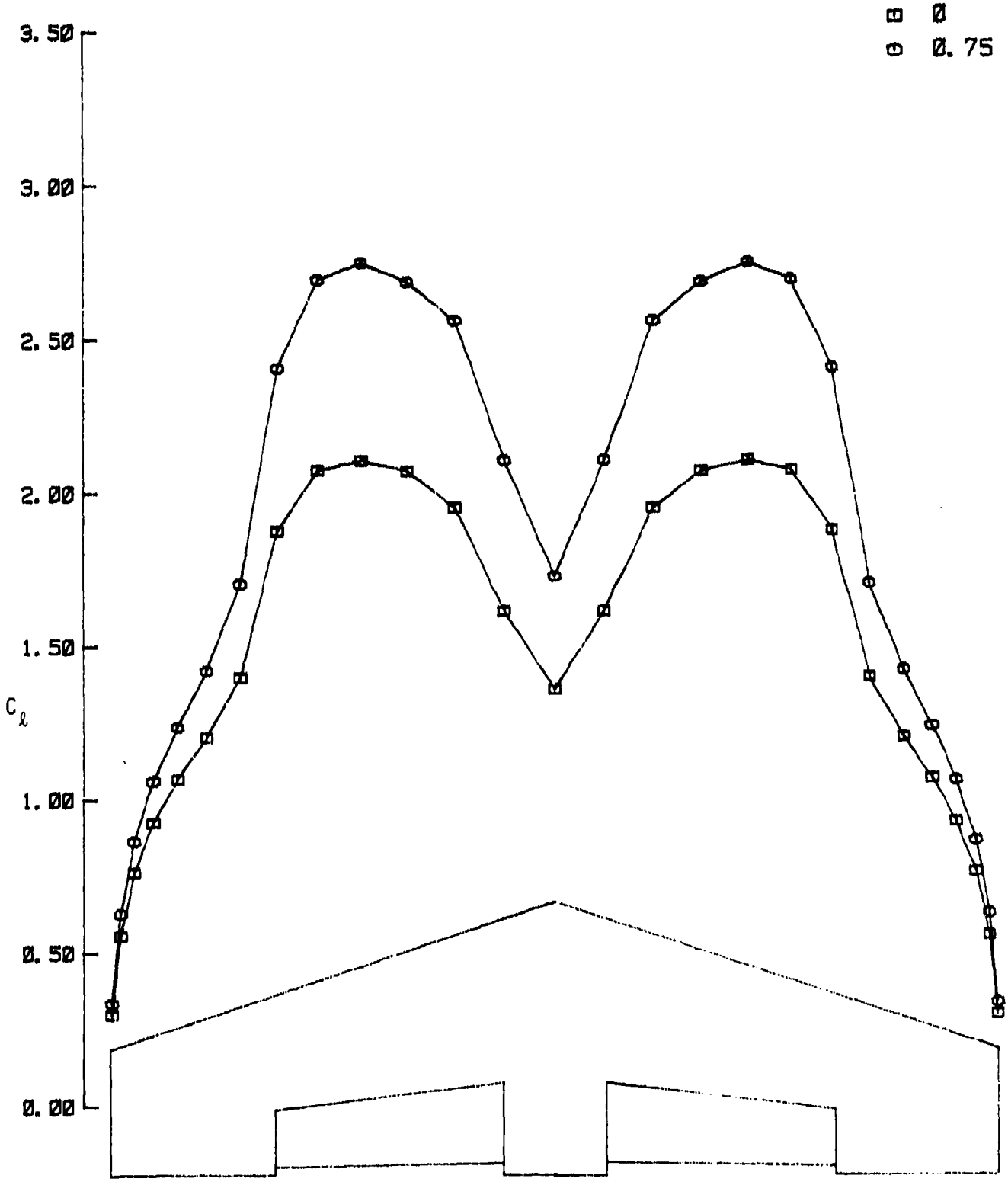

FIGURE 69

SPANWISE DISTRIBUTION OF C_ℓ ON JETWING JW-1 PLANFORM FOR α = 10° AND δ_F = 30°, UPPER WING REMOVED, CALCULATED BY JACOBS METHOD

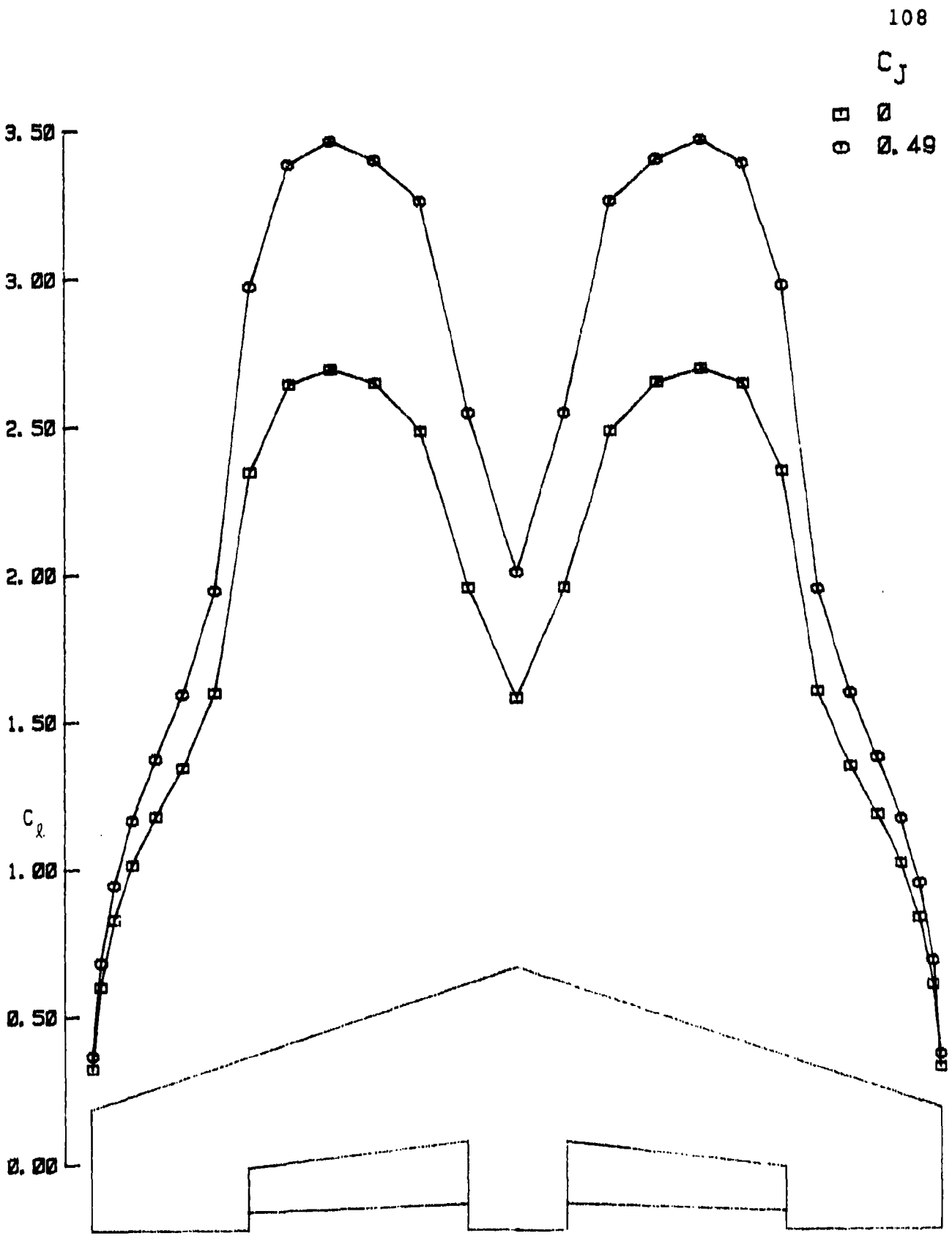

FIGURE 70

SPANWISE DISTRIBUTION OF C_ℓ ON JETWING JW-1 PLANFORM FOR α = 10° AND δ_F = 45°, UPPER WING REMOVED, CALCULATED BY JACOBS METHOD

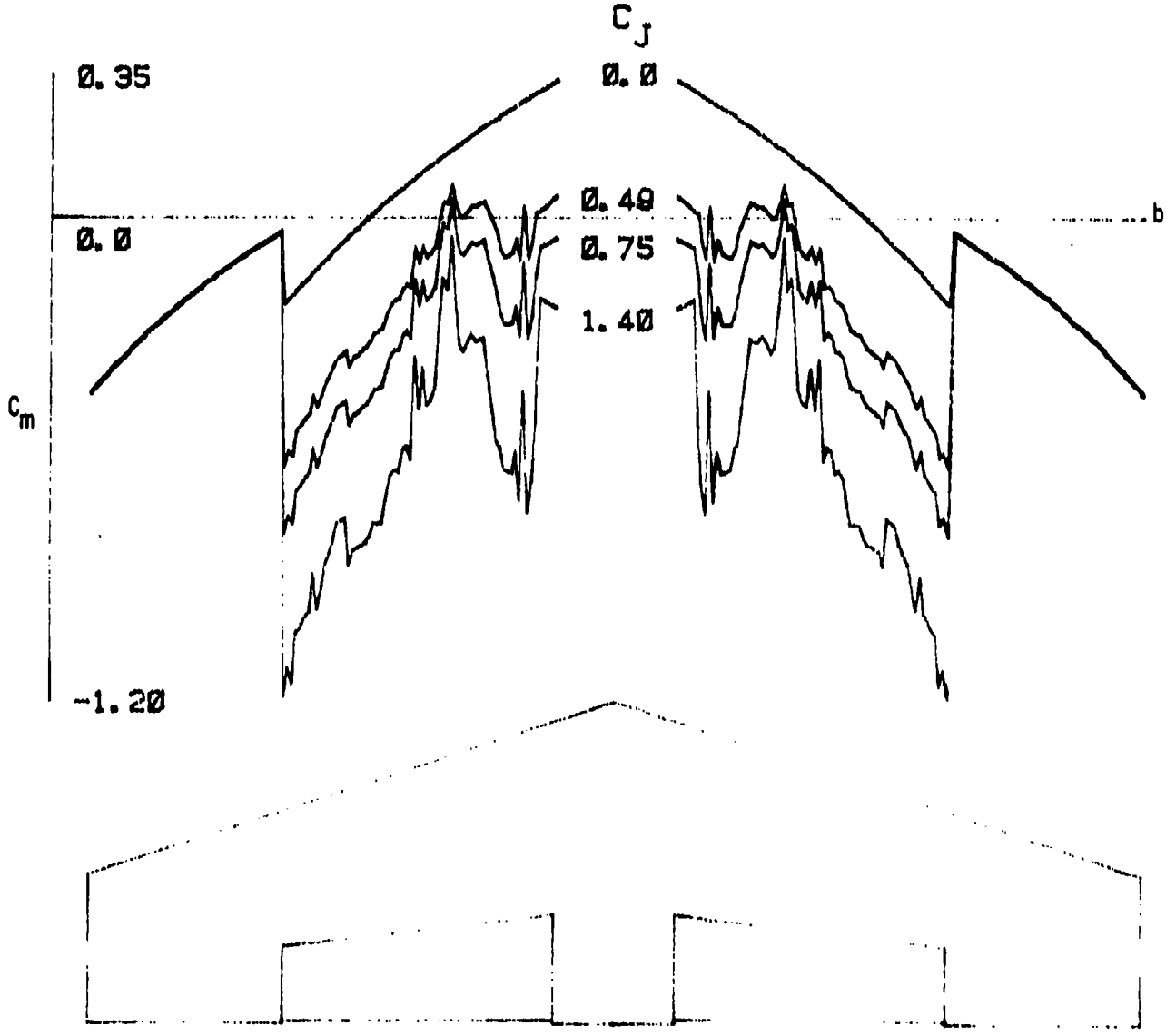

FIGURE 71

SPANWISE DISTRIBUTION OF C_m ON JETWING JW-1 PLANFORM FOR α = 10° AND δ_F = 15°, UPPER WING REMOVED, CALCULATED USING JACOBS METHOD (MOMENT CENTER @ 33% OF M.A.C.)

SECTION V

DISCUSSION OF RESULTS

METHOD 1 (Williams). As figures 44 thru 47 show, this method matches the experimental data reasonably well, the errors being less than 10 per cent for all conditions except low blowing coefficients and high angles of attack ($\alpha > 15^{\circ}$).

In these cases the losses of lift shown by nonlinearities in the wind tunnel data, are obviously due to flow separation, which cannot be predicted by this method. Separation effects and incomplete turning of the jet sheet also account for the lower values of experimental data versus the theoretical curves in the case of high flap deflection ($\delta_F = 45^{0}$), figure 47.

An inherent flaw of the method is, that for blowing coefficients $C_J = 0$, it is insensitive to flap deflection, leading to large errors for no blowing, flaps down configurations.

The slopes of the theoretical curves are throughout slightly steeper than the experimental curves. Therefore, the method tends to underpredict at low angles of attack and overpredict in the high α-range. A better slope matching can obviously be achieved by improving the $G(\nu C_{L\alpha})$ term in equation ($II - 12$). This improvement is currently being investigated.

Figures (48-51) show the lift coefficient plotted against excess thrust coefficient. Again the theory tends to overpredict the experimental data, particularly for higher flap deflections and blowing coefficients. This can largely be explained by the fact that the ram drag in the theoretical prediction method has not been accounted for. For low speed and small C_L (result of small α and/or small δ_F), ram drag can be approximated as the product of density, inlet area, and square of true airspeed. This result, when divided by qS, can be considered as a first approximation of ΔC_{D_0} for ram drag. It may be further simplified to twice the inlet area divided by S, a constant for all C_J, α and δ_F. Addition of the ram drag (ΔC_{D_0}) to the theoretical C_L vs. $C_{F_{ex}}$ curves would bring them closer to the experimental curves. However, in the wind tunnel, high C_J was obtained by reducing q (i.e., slowing down the tunnel) while keeping the engine RPM constant. This procedure increases ΔC_{D_0} for ram drag with increase of C_J as is reflected in the comparison plots (figures 48 thru 51).

Further simplifying assumptions in equation ($II - 15$) neglecting losses due to jet turning and non elliptic lift distribution also can partially account for the difference between theoretical results and wind tunnel data.

METHOD 2 (Wortz). As figures 52 thru 59 show, this method generally matches the experimental data even better than method 1, the errors being less than 5 per cent for most conditions. Again, where separation or nonideal turning of the jet sheet occurs, the errors become large since the method cannot predict these effects.

At zero flap deflection this method underpredicts slightly for all blowing coefficients (figure 52). The break up into components of basic aerodynamic pressure lift, supercirculation lift and jet reaction lift (figure 56) shows, that the error stems mainly from an underprediction of supercirculation lift. A possible explanation may be the unaccounting for of some additional circulation lift due to the jet sheet blowing over the top surface of the airfoil. This will be presented in more detail under the discussion of method 3.

As figures 57 thru 59 show, for flaps down and high blowing coefficients, the supercirculation lift is somewhat overpredicted. Again, this may be partly due to separation effects and insufficient turning of the jet sheet. Another cause can be seen in the tail down load, which reduces the lift coefficients of the wind tunnel data. The slopes of all the theoretical curves also compare very well with the wind tunnel data, giving confidence for the $C_{L\alpha}$ terms in equation (*III* — 43).

METHOD 3 (Jacobs). As figures 61 thru 64 show, the differences between the theoretical curves generated by this method and experimental results are greater than in the previous methods.

It is quite obvious that for $C_J = 0$ cases, C_L is being overpredicted for all but when $\delta_F = 0$. A possible cause for this is the nozzle on the upper wing surface, causing the flow to separate, substantially reducing the lift generated. For $\delta_F = 0$, the flow may reattach itself on the upper surface somewhere downstream of a "separation bubble". In this case there would be practically no loss of lift. Again, for $C_J > 0$ cases, C_L is consistently being underpredicted for all δ_F. Also, this shortfall in C_L increases with increasing α and increasing C_J. This can be explained by the fact that Jacob's Equivalent Flap Theory assumes the jet being issued at the trailing edge of the mechanical flap, whereas in reality the nozzle exit is situated somewhere around 33% of the chord back from the wing leading edge.

This leads to two opposing effects: First, the actual lift is lower than the theoretical lift due to scrubbing losses of the jet sheet on the upper surface. Hence, equivalent flap length and resulting theoretical lift should have been smaller if the jet velocity at the trailing edge was used instead of actual nozzle exit velocity. Second, the actual lift is higher than the theoretical value. This is due to the increase in velocity on the upper surface of the wing, induced by the jet, which also causes circulation to increase. This additional circulation is directly proportional to the velocity difference between the upper and lower wing surface, and should more than offset the loss due to scrubbing. Again, it is easy to see that with increasing C_J this additional lift will also increase. This additional supercirculation lift is produced in the rear portion of the wing which generates an additional negative pitching moment. Hence, if this lift is accounted for, the predicted C_L should be more positive and C_M more negative than the present values. This change would bring the theoretical C_L vs. C_M plots closer to the experimental plots.

One possible disadvantage of the method is that the jet blowing velocity distribution as a function of thrust or engine RPM is needed as an input. For the JETWING this was measured by means of the laser velocimeter as reported in [1]. Together with thrust measured by dynamometer, it provided the required input data. But, for the design team at the conceptual design stage, this information would not be available. So this method would be more suitable to analyze the existing aircraft based on the USB concept.

Another problem for the Equivalent Flap Theory Method is that for high C_J, particularly if coupled with high δ_F, computer convergence on the induced angle of attack may be unreasonably time consuming. However, as far as computer time is concerned, it has been found to be satisfactory up to approximately $C_J = 1$ and $\delta_F = 30°$. For lower δ_F, higher values of C_J can be used in order to achieve comparable run time.

Multhop's Lifting Line Theory is used here because of its simplicity. Another method can be used in its place if better accuracy is desired.

Work is presently underway to predict the unaccounted for jet induced supercirculation lift.

COMPARISON OF THE METHODS.

Method 1 (Williams) is conceptually the simplest and requires the least computer time. It permits computation of C_L vs. α as well as C_L vs. $C_{F_{es}}$.

Method 2 (Wertz) requires only a little more calculation and programming than method 1 and permits the total lift to be broken down into components of basic aerodynamic pressure lift, supercirculation lift and vectored thrust lift. It shows the overall best accuracy for the JETWING C_L vs.α plots.

Method 3 (Jacobs) requires the highest computational effort of the three. However, it can still be considered simple conceptually and from an analytical standpoint when compared to other sophisticated methods [6,7], which require much more computer storage space and time. The predicted C_L values do not match the JETWING wind tunnel data as well as the two other methods do. However, this method does give pitching moments and their slopes (figures 65 and 66).

REFERENCES

1. Kimberlin, Ralph D., "A Flight Test Evaluation of the Ball-Bartoe Jetwing Propulsive Lift Concept," UTSI Report 81-1, The University of Tennessee Space Institute, Tullahoma, Tennessee, 1 July 1981.

2. "Jetwing from Colorado," Air International, 14 (No.2): 69-71, Fine Scroll Limited, London, England, February, 1978.

3. Anon: "Precision Sound Level Meters," International Electrotechnical Commission Publication No. 179., Bureau Central de la Commission Electrotechnique Internationale, Geneva, Switzerland, 1973.

4. Anon: "Noise Standards: Aircraft Type and Airworthiness Certification," Federal Aviation Regulation Part 36, Department of Transportation, Federal Aviation Administration, Washington, D.C., June, 1974.

5. Nichols, J. H. Jr. and Englar, R. J., "Advanced Circulation Control Wing System for Navy STOL Aircraft," David W. Taylor Naval Ship Research and Development Center, Bethesda, MD; published in Journal of Aircraft, Volume 18, No. 12, pp. 1044-1050, December, 1981.

6. Mendenhall, M. R. and Spangler, S. B., "Calculation of the Longitudinal Aerodynamic Characteristics of Upper-Surface-Blown Wing-Flap Configurations," Nielsen Engineering & Research, Mountain View, CA; presented in 17th Aerospace Sciences Meeting, New Orleans, LA, January 15-17, 1979. (AIAA Paper No: 79-0120)

7. Shen, C. C., Lopez, M. L. and Wasson, N. F., "Jet-Wing Lifting-Surface Theory Using Elementary Vortex Distributions," Douglas Aircraft Company, McDonnell Douglas Corporation, Long Beach, CA; published in Journal of Aircraft, Volume 12, No. 5, pp. 448-456, May, 1975.

8. Maskell, E. C. and Gates, S. B., "Preliminary Analysis for a Jet-Flap System in Two-Dimensional Inviscid FLow," A. R. C. C. P. 359, June, 1955.

9. Spence, D. A., "The Lift-Coefficient of a Thin, Jet-Flapped Wing," Proc. Roy. Soc. A. Vol. 238, pp. 46-68, 1956.

10. Spence, D. A., "The Lift on a Thin Aerofoil with a Jet-Augmented Flap," Aero. Quart. Vol. 9 pp. 287-299, August, 1958.

11. Maskell, E. C. and Spence, D. A., "A Theory of the Jet Flap in Three Dimensions," Proc. Roy. Soc. A. Vol. 251, pp. 407-425, 1959.

12. Jacobs, W. F., "Theory of the Jet-Augmented Flap in Two Dimensions," Report No. LG72ER0083, Lockheed-Georgia Company, November 1, 1972.

13. Williams, J., Butler, S. F. J. and Wood, M. N., "The Aerodynamics of Jet Flaps," Aeronautical Research Council Reports and Memoranda No. 3304, Her Majesty's Stationary Office, London, England, 1963.

14. Wertz, R. D., "Application of Spence's Method and Data to Prediction of Lift Coefficients of the JETWING," unpublished internal report of Ball-Bartoe Aircraft Company, 1976.

15. Jacobs, W. F., "Theory of the Jet-Augmented Flap in Three Dimensions," Report No. LG73ER0023, Lockheed-Georgia Company, December 1, 1972.

16. Woolard, H. W., "A Review of Some Air Force STOL Aircraft Aerodynamic Prediction Methods," Air Force Flight Dynamics Laboratory, Wright-Patterson Air Force Base, Ohio. AIAA Paper No. 74-992, presented at AIAA 6th Aircraft Design, Flight Test and Operations Meeting, Los Angeles, CA, August 12-14, 1974.

17. Sheela, B. V. and Ramamoorthy, P., "SWIFT-A New Constrained Optimization Technique," Aerodynamics Division, National Aeronautical Laboratory, Bangalore, India; published in Computer Methods in Applied Mechanics and Engineering 6 (1975), pp. 309-318, North-Holland Publishing Company.

18. Perkins, C. D. and Hage, R. F., "Airplane Performance, Stability and Control," John Wiley and Sons, Inc., New York, 1963.

19. Bartoe, P., "Jetwing Design Notes," Unpublished.

CONCLUSIONS

Part I

1. With exception of lift coefficient versus angle of attack data, there is excellent agreement between the wind tunnel and flight test performance results for this configuration.

2. The agreement between wind tunnel and flight test results for lift coefficient versus angle of attack is probably as good as can be expected considering the measurement accuracies and data reduction technique required.

3. The NASA Ames Research Center wind tunnel data, as verified by this and the previous flight test, [1] is of sufficient validity to use for extrapolation to other flight vehicles employing the Jetwing concept.

4. The performance difference between the upper wing installed and upper wing removed configurations pose some interesting questions concerning the thickness of the blowing jet.

5. Longitudinal handling qualities, particularly longitudinal stability are improved by removal of the upper wing. Other handling qualities are essentially unchanged.

6. Flyover noise levels for the Jetwing aircraft are very low and disappear into the background noise levels in light wind conditions.

Part II

1. Simple analytical methods to reasonably predict lift and excess thrust coefficients for other aircraft employing the Jetwing concept have been demonstrated in this report.

2. Accurate prediction of pitching moment coefficient for Jetwing configuration is more difficult. However, a method is shown in this report which will give reasonable estimates of the longitudinal stability parameter dC_M/dC_L.

3. Accurate prediction of pitching moment coefficient for Jetwing configurations appears to require the use of the more complex vortex lattice methods which were beyond the scope of this effort.

RECOMMENDATIONS

Part I

1. On future programs using the Jetwing aircraft a more accurate method for measuring angle of attack should be devised.

2. The NASA Ames Research Center wind tunnel data on the Jetwing Aircraft should be used for extrapolation to other aircraft designs employing the Jetwing concept.

3. The reasons for performance and handling qualities differences of the Jetwing airplane with and without the upper wing require further investigation since they may have implications for all Upper Surface Blowing configurations.

Part II

1. Since lift and excess thrust coefficients can be reasonably predicted for Jetwing configurations (using the simple methods described in this report) future effort should be concentrated upon predicting stability and control parameters such as pitching moment coefficient and downwash.

APPENDIX I

SOME REMARKS ON BLOWING COEFFICIENT

A key parameter in the theoretical and experimental treatment of powered lift is the blowing coefficient

$$C_J = \frac{\dot{M}_J V_J}{qS}$$

where $\dot{M}_J V_J = J$ is the jet momentum, which can be measured experimentally and represents the product of actual values of mass flow $\dot{M}_J$ and jet velocity V_J. For design purposes these two quantities are usually determined theoretically by assuming nonviscous isentropic flow. The ideal values $\dot{M}_\mu$ and V_μ can be used for the definition of the blowing coefficient

$$C_\mu = \frac{\dot{M}_\mu V_\mu}{qS}$$

This theoretical blowing coefficient C_μ is usually higher than the corresponding actual blowing coefficient C_J, since viscous effects reduce nozzle exit areas, result in scrubbing losses, etc. Therefore, for accurate predictions, appropriate corrections have to be made.

Another problem occurs through the use of the wing reference area S for partially blown wings. Basic theoretical prediction methods like Spence [9] are based on a lifting surface with full span blowing and do not consider fuselage cut-out or part-span blowing. The overall three-dimensional blowing coefficient C_J of a part-span blown wing does not represent the same blowing per unit span as the blowing coefficient C_J of the full-span blown wing.

If we compare, for example, two wings with the same reference areas, one full-span blown and the other half-span blown, then for the same blowing coefficient C_J the sectional blowing intensity per unit span J/b would be twice as high for the half-span blown wing.

In using the theoretical formulae that were derived from full-span blown wings, it is important to use similar blowing intensities for calculation of derivatives etc. Therefore the blowing coefficient has to be modified for part-span blown wings by defining a "mean sectional blowing coefficient"

$$C_j = \frac{\dot{M}_J V_J}{qS'}$$

where S' is the wing reference area corresponding to the spanwise extent of blowing.

In our example

$$S' = \frac{1}{2}S$$

and

$$C_j = 2C_J$$

Then the blowing intensity $\dot{M}_J V_J/b$ is the same for both wings. This correction is used by Williams in Method 1.

Others also consider the "carry over effect" that the blown portion of a part-span blown wing has on the unblown areas, by defining

$$S'' = S' + \frac{1}{2}S_{CO}; \qquad S_{CO} = S - S'$$

Then the modified sectional blowing coefficient becomes

$$C_j = \frac{\dot{M}_J V_J}{qS''} = \frac{S}{S''}C_J$$

This correction is used by Wertz in Method 2. He uses as symbols C_j and C''_μ, which he calls the three-dimensional configuration factor.

To avoid confusion we have used only overall three-dimensional blowing coefficients C_J and corrected two-dimensional "sectional" blowing coefficients C_j in this report. It is understood that C_J refers to experimentally measured values of the jet momentum J or properly corrected theoretical values. The sectional coefficients C_j are defined by means of reference areas S' or S'' under the particular methods.

APPENDIX II

PROCEDURE FOR EVALUATION OF SECTIONAL BLOWING COEFFICIENT IN METHOD 3

In equivalent flap theory, the following procedure has been adopted for the evaluation of spanwise variation of two-dimensional "sectional" blowing coefficient C_j from the input data of jet velocity and nozzle area distribution :

From the definition of three-dimensional blowing coefficient $C_J = \frac{F_G}{qS}$, true airspeed can be written as :

$$V_T = \sqrt{\frac{F_G}{\frac{1}{2}\rho C_J S}}$$

As laser velocimeter data of jet velocity distribution for $55\%N_1$ were thought to be most reliable, these data were used as input. Correspondingly, F_G was obtained as a function of V_T at that particular RPM (i.e., $55\%N_1$) from the thrust calibration plot (figure 40 [1]). Finally, F_G and V_T were obtained, for the desired value of C_J, as the result of an iteration between the expression of V_T and the data from the thrust calibration plot. Since the laser velocimeter data were obtained at static condition, it was felt necessary to translate that data to any airspeed which was determined as a result of aforesaid iteration. Then C_j for unit spanwise distance at any spanwise section was obtained as :

$$C_j = \frac{\dot{M}_j V_j \frac{F_a}{F_{a0}}}{\frac{1}{2}\rho V_T^2 c} = \frac{\rho_j a_j V_j^2 \frac{F_a}{F_{a0}}}{\frac{1}{2}\rho V_T^2 c}$$

where F_{a0} = static thrust at $55\%N_1$
and a_j = area of the nozzle.

DISTRIBUTION LIST FOR

JETWING FLIGHT TEST EVALUATION FINAL REPORT

Department of the Navy
Naval Air Systems Command
Washington, D.C. 20361

CODE	COPIES
AIR-00D4	14
AIR-03E	1
AIR-03PA3	2
AIR-03P3A	1
AIR-310	1
AIR-320D	1
AIR-320F	1
AIR-330	1
AIR-528	2
AIR-5301	1
AIR-536	1

Office of Naval Research
800 N. Quincy Street
Arlington, VA 22217

Attn: CAPT M. A. Howard, Code 210	1
Attn: Dr. R.E. Whitehead, Code 438	1

David Taylor Naval Ship Research
& Development Center
Bethesda, MD 20084

Attn: Dr. H. R. Chaplin, Code 16	3

Naval Air Development Center
Warminster, PA 18974

Code 60	2
Code 605C	1

Naval Air Propulsion Center
Trenton, N. J. 08628

Attn: Mr. A. A. Martino, Code PE4	2

Naval Weapons Center
China Lake, CA 93555

Code 324	1

	COPIES
Department of Aeronautics Naval Postgraduate School Monterey, CA 93940	
Attn: Professor Max Platzer, Code 67 Pl	2
Air Force Wright Aeronautical Laboratories Wright-Patterson AFB Dayton, OH 45433	
Attn: Col. J. R. Chevalier; AFWAL/FIM	1
Attn: Mr. R. Jeffries; AFWAL/FIMM	3
Attn: Mr. V. Hoehne; AFWAL/FIGC	1
NASA Ames Research Center Moffett Field, CA 94035	
Attn: Mr. John Cochrane; Code FHQ Mail Stop 237-10	1
Attn: Mr. David Koenig; Code FHA Mail Stop 247-1	2
NASA Headquarters Washington, D.C 20546	
Attn: Mr. G. G. Kayten; Code RJ-2	1
Mr. C. William Clay Mail Stop 9H-41 Boeing Commerical Airplane Company P.O. Box 3707 Seattle, WA 98124	1
Dr. Frank Aschenbrenner Vice President for Research & Development The Ball Corporation 345 South High Street Muncie, Indiana 47302	1
TOTAL	50